DOI. No. 10.1109/MAES.2016.160071

Tutorial

Overview of Radar Waveform Diversity

Shannon D. Blunt, **University of Kansas, Lawrence, KS, USA**
Eric L. Mokole, **Private Consultant, Burke, VA, USA**

Radar waveform diversity has received considerable attention in recent years due to increasing spectral congestion and the burgeoning capabilities of digital waveform generation. The promise of waveform diversity is far greater utilization of available degrees of freedom to enhance sensing performance and to even facilitate new operating modes. This tutorial provides an overview of this very broad topic, from the basic principles upon which it is founded to the myriad different areas being explored in research for practical sensing applications.

I. INTRODUCTION

The term waveform diversity (WD) [1–3] was coined by Dr. Michael C. Wicks of the Air Force Research Laboratory (AFRL) Sensors Directorate in 2002 [4]. He raised the notion of jointly pursuing a long-term roadmap for research, development, and manufacturing in the broad area of WD with representatives from the U.S. Army (Dr. Robert W. McMillan) and the U.S. Navy (Dr. Eric L. Mokole). Because this group felt that technology was sufficiently mature for extending and implementing the waveform research of the preceding 60 years across all pertinent scientific and engineering disciplines, they began a concerted effort to foster programs in this area. The main goals of the ensuing research have been 1) to address the ever-increasing competition for radar spectrum and encroachment into what have historically been radar bands [5] and 2) to leverage the rapid advances that are being made in digital signal generation (e.g., see [6–8]) and adaptive signal processing. The purpose of this tutorial is to provide the context in which WD has arisen, a sense of the tremendous breadth of the subject, and a sufficient starting point from which to explore WD further.

A good point of reference for a survey of WD is to state the IEEE Standard 686-2008 definition [9], which reads as follows:

> **Waveform Diversity:** Optimization (possibly in a dynamically adaptive manner) of the radar waveform to maximize performance according to particular scenarios and tasks. May also jointly exploit other domains, including the antenna radiation pattern (both on transmit and receive), time domain, frequency domain, coding domain and polarization domain.

The pending update to this definition adds the following: "Also used to denote adaptive receive processing that is applicable to such waveforms. *See also:* waveform; pulse compression; ambiguity function."

This rather broad definition provides the general sense that WD can involve the modulation and/or exploitation of any aspect of the radar signal structure on both transmit and receive. Furthermore, the design, processing, and evaluation of the waveform clearly play key roles.

Fundamentally, a waveform comprises the modulation of an emitted signal such that, via appropriate filtering of the subsequent echoes at the receiver, desired aspects of the illuminated environment can be accurately measured [10]. Most often, the radar generates this waveform, though there has been considerable work on passive radar that exploits the waveforms emitted by other spectrum users (e.g., frequency-modulated [FM] radio) [11–14]. In general, research in WD can be categorized according to the areas delineated in Table I, though it is not uncommon for two or more categories to be considered jointly.

Diverse waveforms have been present in nature well before the information and technological explosions in the latter part of the 20th century. For example, echo-locating mammals (bats, dolphins, and whales) have been exploiting WD for more than 50 million years [15, 16]. Recent technology has permitted replication and characterization of naturally occurring waveforms from such creatures [17], and this newly acquired understanding is being used to improve methods in manmade sensing systems like radar and sonar, which have been in existence for roughly a century. For example, bats emit dynamically adaptive acoustic waveforms that

Table I

General WD Research Categories
Waveform design and optimization
Interference rejection and avoidance
Multidimensional waveforms and processing
Biomimetic and bioinspired operation
Multifunctional operation
RF spectrum utilization

Authors' current address: S. D. Blunt University of Kansas, EECS, 2335 Irving Hill Rd, Lawrence, KS 66045, USA, E-mail: (sdblunt@ittc.ku.edu). E. L. Mokole, 5816 Fitzhugh St, Burke, VA 22015-3625, USA.
Manuscript received March 18, 2016, revised July 21, 2016, and ready for publication July 26, 2016.
Review handled by W. Blair.

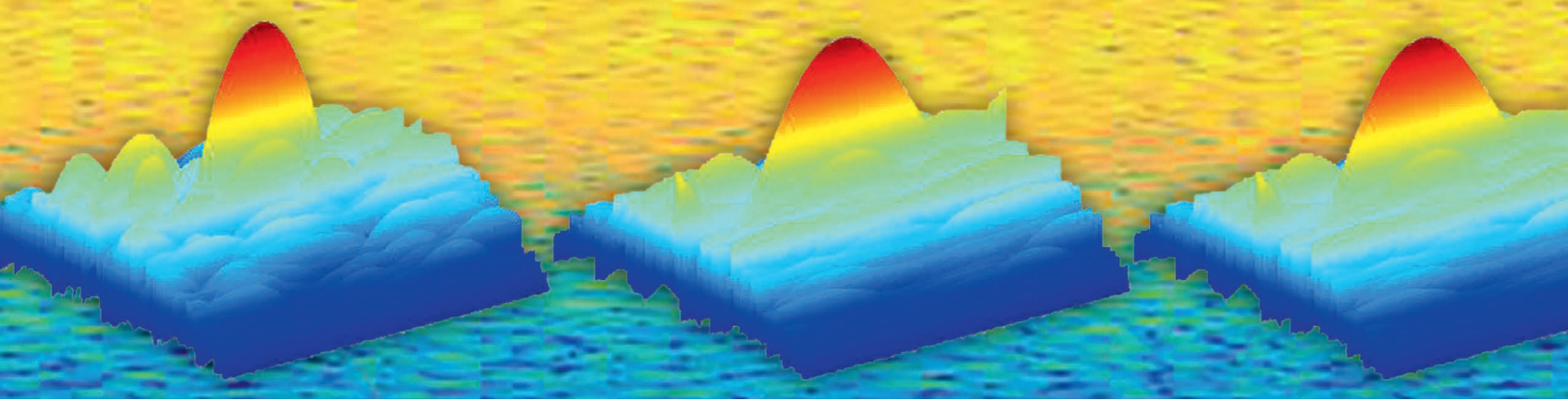

enable autonomous orientation, detection, localization, classification, discrimination, pursuit, and capture of prey. Researchers have shown that bats use a set of different waveforms, such as constant frequency, linear frequency modulation (LFM), hyperbolic frequency modulation (HFM), multiple harmonics, and possibly other nonlinear frequency modulation to meet biological imperatives [18–20]. These investigations suggest that a combination of flight profile, WD, and multialgorithmic processing are crucial factors in a bat's success. Likewise, it has been found that dolphins vary the nature of sequential waveforms to enable discrimination in bubble-rich environments [21–23] and can generally perform sensing tasks far better than one might expect given their "mediocre equipment" [24]. In addition, researchers are trying to characterize how humpback whales use loud acoustic emissions to trap prey within cylindrical walls of bubbles (bubble nets) of their creation [25, 26].

What is currently called WD can be thought to have originated conceptually in 1933, when Edwin Armstrong invented FM radio to improve audio signals conveyed via radio by controlling the noise static generated by electrical equipment and earth's atmosphere. This invention led to the development of theoretical and experimental techniques for FM radar applications [27]. Before the 1990s, WD activities occurred as parts of other investigations such as the high-power microwave efforts of the 1950s and 1960s, waveform design for clutter rejection, electromagnetic compatibility, and spread spectrum techniques for communication and radar systems.

For traditional high-power radar, Klauder et al. [28] published a seminal paper on LFM radar, which was followed by investigations on optimum transmit waveforms (e.g., Barker, polyphase, and complementary codes) to tailor range sidelobes without suffering mismatch loss or mainlobe broadening [29–42]. In the 1970s and 1980s, new theoretical waveform designs were developed to improve the detection performance of radar [43]. Specifically, subcomplementary sequences and a new class of polyphase codes were found to improve pulse compression [44, 45], and studies using Costas codes as detection waveforms yielded nearly ideal properties of the range-Doppler ambiguity function [46].

Since these seminal contributions, research in WD has truly experienced what Dr. Joe Guerci, in his 2014 IEEE Radar Conference keynote address, articulated as a "Cambrian explosion" [47]. Given that, a disclaimer is in order: this survey is intended to provide context (phylum–genus–species cataloging, if you will) for how the myriad forms of WD may be applicable to radar. Despite our best efforts, it is possible that we missed or insufficiently detailed some salient features. Hopefully, however, this tutorial serves as an adequate starting point for further, deeper investigations into WD.

The next section serves an introduction to the fundamentals of radar waveforms and their filtering, along with discussion of pertinent practical considerations. Section III provides an overview of the different areas of research in radar WD, including waveform optimization and environmentally adaptive waveforms, multiple-input multiple-output (MIMO) and distributed aperture radar, waveform agility, and polarization diversity.

II. RADAR PULSE COMPRESSION

Before delving into the various topics with WD, it is first instructive to consider the essentials of radar pulse compression, which plays a pivotal role in WD. The concept of pulse compression was developed independently in Germany, Britain, and the United States during World War II to address the problem of how to attain high-range resolution, such as provided by a short pulse, while ensuring sufficient "energy on target" to provide detectable signal-to-noise ratio (SNR) in the receiver despite the peak power limitation on transmit [28]. The pulse compression solution entails the modulation of a longer pulse that, after application of appropriate receive filtering to the reflected version of the waveform (for now, assume a point scatterer), yields a response (Fig. 1) that has a mainlobe with resolution commensurate with what the short pulse would have provided, along with the addition of range sidelobes.

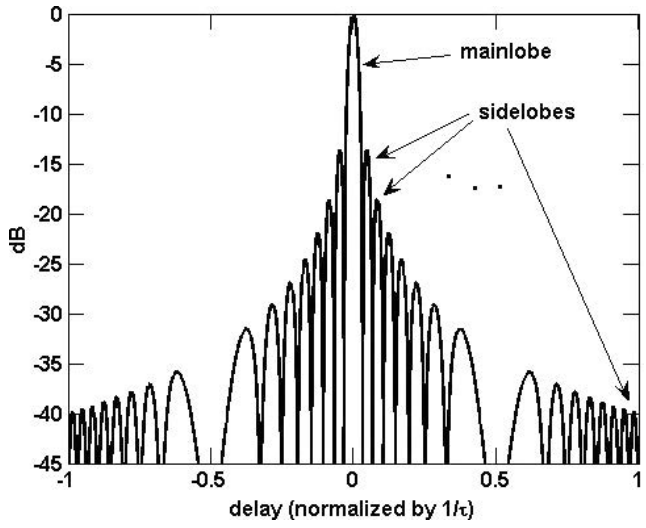

Fig. 1.
Pulse compression response to stationary point scatterer at delay = 0.

Specifically, the range resolution (mainlobe width) is inversely proportional to the waveform bandwidth.

Much of the work in this area [10] involves the design of the waveform (the modulation scheme) and the subsequent receive filtering to suppress the range sidelobes while minimizing degradation to the mainlobe in terms of range resolution (widening of the mainlobe) and SNR loss at the mainlobe peak. Sufficient radial motion also induces a Doppler shift that must likewise be considered.

To illustrate why it is desirable to minimize the sidelobes, consider the result when two point targets have a range separation that is less than the pulsewidth T and whose received powers are considerably different. Fig. 2 depicts the matched filter (MF) response to an LFM waveform used to illuminate these two point targets. Given that standard radar detection methods [48] rely on how much a prospective target stands out relative to the immediate surroundings, it is likely that the smaller target would not be detectable because of the sidelobes induced by the pulse compression response to the larger target.

This section explains the general principles of radar pulse compression, the classes of waveforms that are used, how receive filtering is performed, and the metrics employed to evaluate the goodness of a waveform–filter pair. Practical considerations for pulse compression are also explained. These general principles establish the operational sensing framework from which the larger study of WD has emerged.

A. PULSED VS. CONTINUOUS WAVE

It is common for a waveform to be modulated repeatedly onto multiple segments of the transmitted signal so that the echoes from these segments can be combined on receive (usually coherently) for enhanced gain and as a means to enable discrimination in the Doppler domain. If the transmitted segments are interleaved with the receive intervals, this scheme is called a pulsed mode, where the pulsewidth T is less than the pulse repetition interval (PRI), denoted T_{PRI}, and T/T_{PRI} is called the duty cycle. Because of the variety of radar applications and implementations, the duty cycle could be as low as 0.1% or 25% or more [5]. For a pulsed mode, $1/T_{\text{PRI}}$ is the pulse repetition frequency (PRF).

In contrast to pulsed operation, a continuous wave (CW) radar is one in which the emission of waveform-modulated segments does not alternate with the receive operation but instead performs transmission and reception simultaneously. Frequency-modulated continuous wave (FMCW) is the most common form of CW in use, where the frequency is swept as a function of time. FMCW is used by high-frequency (HF) over-the-horizon (OTH) radars [49], as well as for short-range applications such as automotive radar [50] and is being explored as a means of onboard sense and avoid for small unmanned air systems (UASs) that require low size, weight, and power (SWaP) [51].

The CW mode can be thought of as a special case of pulsed operation in which the duty cycle is 100%. As such, the different types of waveforms are generally applicable to either mode. Pulsed operation is far more prevalent than CW in modern radar systems. Therefore, in the following, we use terminology appropriate to pulsed operation, with the understanding that the same is generally applicable to each repeated interval of a CW mode.

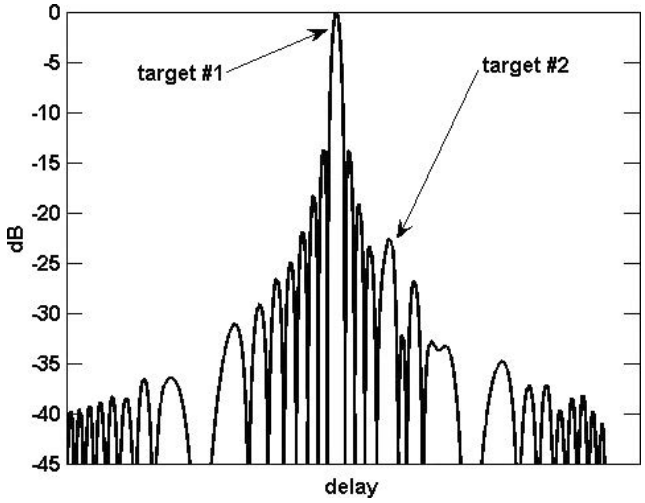

Fig. 2.
Pulse compression response to two nearby targets with disparate receive powers.

B. WAVEFORM CLASSES

There exist myriad varieties of waveforms, though they can generally be sorted into just a few categories. These categories are FM waveforms, phase codes, frequency codes, and random noise waveforms. While arguably not a separate class of waveform, one may also consider various forms of modulation across a set of pulses (to be coherently combined on receive) as a waveform attribute as well (further discussed in Section II.E). Of these categories, the most commonly used in operational radar systems are FM waveforms and the subset of phase codes denoted as binary codes.

Of the FM waveforms, the most prevalent is LFM [10, Chap. 4] because it is easy to implement in hardware, has attractive Doppler properties (see Section II.D), and for wideband operation is amenable to computationally efficient stretch processing [52] on receive. The complex baseband representation of an arbitrary FM waveform of pulsewidth T (normalized to unit energy) is

$$s_{\text{FM}}(t) = \frac{1}{\sqrt{T}} \exp\left(j\theta(t)\right) \tag{II.B1}$$

where $\theta(t)$ is the instantaneous phase, and its scaled derivative

$$\frac{1}{2\pi}\frac{d\theta(t)}{dt} = f(t) \tag{II.B2}$$

is the instantaneous frequency.

The LFM waveform $s_{\text{LFM}}(t)$, commonly called a chirp, thus has the phase function

$$\theta_{\text{LFM}}(t) = \pm\pi B t^2 / T \quad \text{for } 0 \le t \le T \tag{II.B3}$$

where B closely approximates the 3 dB power bandwidth for practical waveforms, and the ± indicates either an up-chirp (increasing frequency) or a down-chirp (decreasing frequency) [10, Chap. 4]. The product BT is called the time–bandwidth product, which is also the coherent processing gain (or compression ratio) of the

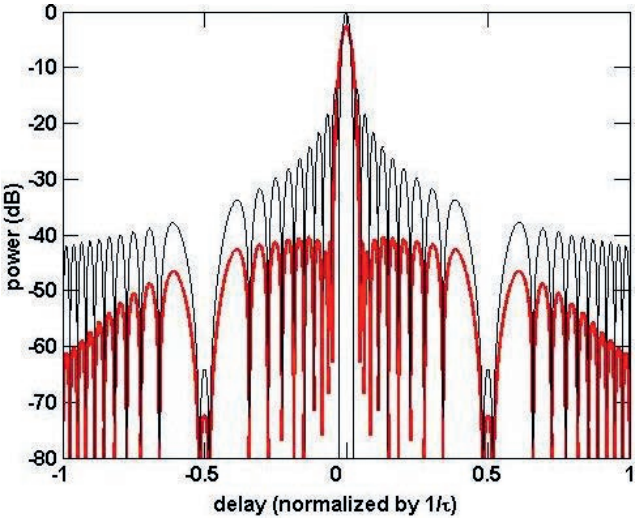

Fig. 3.
Pulse compression response for LFM (black) and square-root Hamming-weighted LFM (red).

waveform when applying the MF (see Section II.C). Upon substituting (II.B3) into (II.B2), the instantaneous frequency for LFM is found to be $f_{\text{LFM}}(t) = \pm Bt/T$, which is clearly a linear function of frequency. Taking another derivative yields the rate at which the frequency changes with time, otherwise known as the chirp rate, and is the constant $\pm B/T$ for LFM. In other words, LFM linearly sweeps over the bandwidth B during the pulsewidth T.

The primary limitation of LFM is the high-range sidelobes it produces (depicted in Fig. 1), the largest of which is generally only about 13 dB below the mainlobe. One way in which these sidelobes can be reduced is by applying an amplitude taper as

$$s_{\text{Tapered-LFM}}(t) = a(t)\, s_{\text{LFM}}(t) \tag{II.B4}$$

where $0 \le a(t) \le 1$ for $0 \le t \le T$ is commonly one of the window functions otherwise used for digital filter design or antenna beampattern design (e.g., Taylor, Hamming, etc.) [10, Chap. 4]. The tradeoff for sidelobe reduction in this manner is a broadening of the mainlobe (degraded range resolution) and SNR loss relative to the absence of tapering. The mainlobe is broadened because the amplitude weighting of an LFM produces a "rounded off" spectral content, as opposed to the relatively flat LFM spectrum, which in turn reduces the 3 dB bandwidth. Because the LFM waveform defined in (II.B1) and (II.B3) has unit energy, the loss due to amplitude tapering on transmit can be determined as

$$\text{SNR Loss}_{\text{transmit taper}} = -10\log_{10}\left[\int_0^T a^2(t)\,dt\right] \tag{II.B5}$$

where $a(t)$ is a real function and bounded between 0 and 1.

For example, Fig. 3 shows the pulse compression response for a square-root Hamming-weighted LFM, where the largest sidelobe has been reduced to just below −40 dB, with an SNR loss of 2.7 dB and a resolution degradation (increase) by a factor of 1.5 (measured 3 dB below the peak of the mainlobe). Such amplitude control also tends to limit operation to lower-power radar applications,

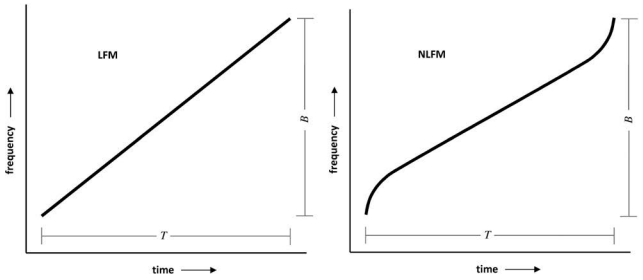

Fig. 4.
Time–frequency relationship for LFM waveform (left) and generic NLFM waveform (right).

because a high-power transmitter generally operates in saturation, thus necessitating the emission of a constant-amplitude waveform [53, Chap. 10]. An alternative that alleviates the transmitter limitation is to taper only at the receive filter, which becomes in this case a form of mismatched filter (MMF; see Section II.H), though resolution degradation and SNR loss still occur to some degree.

Besides LFM, many varieties of nonlinear frequency modulation (NLFM) have been developed [53–58]. The general premise behind the development of NLFM waveforms is that the inherent spectral shaping performed by amplitude tapering in (II.B4) can also be achieved via determination of a time-varying chirp rate function, which avoids the need for amplitude control via tapering (Fig. 4). Put another way, the instantaneous frequency is a nonlinear function of time (hence the name) or, comparing with (II.B3), the instantaneous phase is no longer a quadratic function of time. As such, NLFM can reap the sidelobe reduction benefit of tapered LFM without the associated transmitter limitations and SNR loss discussed earlier, though NLFM still incurs resolution degradation from the spectral shaping (Figs. 5 and 6).

Amplitude tapered LFM waveforms and NLFM waveforms are generally designed such that their overall time–frequency response achieves a desired power spectral density (PSD) because of the Fourier relationship between PSD and the waveform autocorrelation (see Section II.C). For NLFM design, the stationary phase principle was proposed [55], which says the spectral density at a given frequency is inversely related to the rate of frequency change (chirp rate) at that frequency. Thus, one can determine the phase function in (II.B1) that provides a PSD whose corresponding autocorrelation has low sidelobes (known to occur when the spectrum tapers toward the band edges [59]). For example, the Fourier transform of a Gaussian shape is another Gaussian. As such, if the PSD is designed to be Gaussian, the associated autocorrelation would, in theory, exhibit a mainlobe that rolls off with no sidelobes. In addition, just as with the tapered LFM in (II.B4), the NLFM can be amplitude tapered, which is called hybrid FM [60–62].

Another class of waveforms that has received significant attention is that of phase-modulated codes (or simply phase codes), in which the pulsewidth T is temporally subdivided into a set of constant-amplitude subpulses (or chips) of duration $T_C = T/N$, with each chip being modulated by a fixed phase value θ drawn from a discrete set called the phase constellation. Phase codes are generally classified as binary (or biphase) codes, in which the phase constellation is composed of only $\theta = 0°$ and $\theta = 180°$, or as polyphase codes, in which the set of phase values may only be limited by numerical pre-

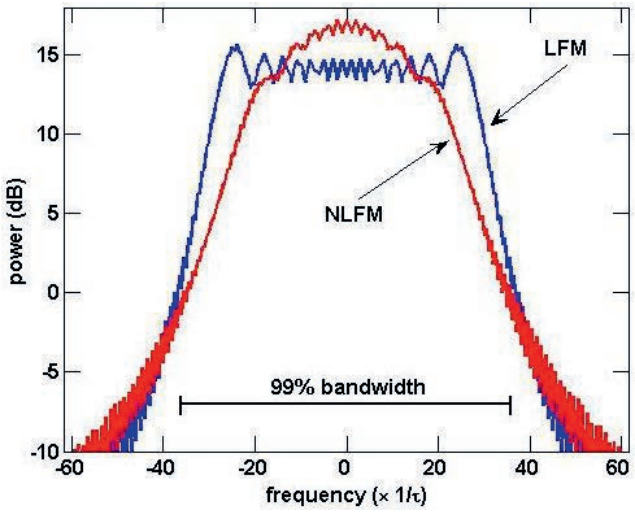

Fig. 5.
PSDs of LFM and NLFM waveforms with same 99% power bandwidth (but different 3 dB power bandwidths).

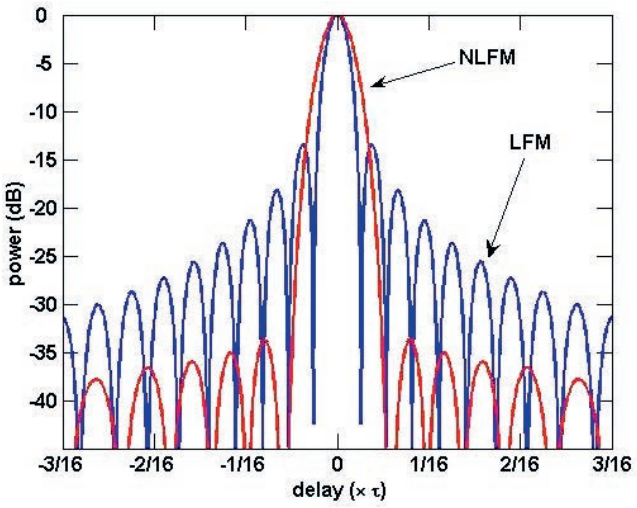

Fig. 6.
Pulse compression responses for LFM and NLFM waveforms.

cision (or $360°/2^{(\#\text{ of bits})}$). Fig. 7 illustrates the structure for a phase-coded (PC) waveform, which can be expressed mathematically as

$$s_{\mathrm{PC}}(t)=\frac{1}{\sqrt{T}}\sum_{n=1}^{N}\exp\left(j\theta_n\right)\mathrm{rect}\left[\frac{t-(n-1)T_{\mathrm{C}}}{T_{\mathrm{C}}}\right]\quad\text{for } 0\le t\le T \qquad \text{(II.B6)}$$

where the nth of N chips is modulated by the phase θ_n that is drawn from a constellation of P possible values. Like the LFM waveform, the energy of the PC waveform is normalized to unity.

Myriad phase codes have been developed, because the determination of "good codes" can be achieved through various optimization approaches that permit searching over the set of P^N possible codes. Well-known examples of binary codes include Barker codes, minimum peak sidelobe (MPS) codes, and maximal length sequences [63–66]. Likewise, well-known polyphase codes include Frank codes, P codes, and polyphase Barker codes [38, 45, 67, 68]. See [10, Chap. 6] and [53, Chap. 20] for further details.

Clearly, the number of possible codes becomes tremendously large as the number of chips N increases (which approximates the time–bandwidth product, based on 3 dB power bandwidth). Because the construction of a PC waveform inherently involves an abrupt phase transition every T_{C} seconds (yielding poor spectral containment because of the resulting $sin(x)/x$ spectral roll-off), it is also important to consider how to implement codes in a manner that is physically amenable to the radar transmitter (discussed in Section III.A).

In contrast to phase coding, a frequency-coded (FC) waveform structure can be defined as

$$s_{\mathrm{FC}}(t)=\frac{1}{\sqrt{NT}}\sum_{n=1}^{N}\exp\left(j\theta_n\right)\exp\left[j2\pi\left(n-\frac{N+1}{2}\right)\frac{t}{T}\right]\quad\text{for } 0\le t\le T \qquad \text{(II.B7)}$$

which amounts to a phase weighting (via the first exponential term of each summand) of a set of complex sinusoids with frequency separation $\Delta f = 1/T$ (thus, the sinusoids are orthogonal). This FC waveform possesses the same 3 dB bandwidth (and therefore the same $T_{\mathrm{C}} = BT \approx N$) as the PC waveform structure from (II.B6) and is likewise normalized to unity energy. The combination of these complex sinusoids (also called the multiple carrier frequencies), introduces a time-varying amplitude that inhibits high-power operation through the use of a saturated power amplifier, with the peak-to-average power ratio (PAPR) [69] providing a measure of how much the power must be backed off from the peak power to avoid distortion because of amplitude clipping. Thus, PAPR also directly implies the loss in SNR one could expect for a FC waveform relative to a constant-amplitude waveform. This formulation is a single symbol interval of orthogonal frequency division multiplexing (OFDM), which is widely used in cellular communications [69]. Furthermore, because this form is already nonconstant amplitude, one may relax the restriction of using a constant-amplitude code (the first exponential term in (II.B7)) by replacing it with a constellation that employs both amplitude and phase, such as quadrature amplitude modulation (QAM), to provide greater design freedom.

A more general scheme that incorporates both phase coding and frequency coding is the multicarrier phase-coded (MCPC) structure [70]. For the same time–bandwidth product N as for the PC and FC structures in (II.B6) and (II.B7), respectively, in this case N_{MC} sub-codes with N_{PC} chips each are modulated onto N_{MC} carriers such that the total dimensionality remains as $N_{\mathrm{MC}}N_{\mathrm{PC}} = N$. The N_{PC} chips in each sub-code have a duration of $T_{\mathrm{MC}} = T/N_{\mathrm{PC}}$. The MCPC structure is thus [10, Chap. 11]

$$s_{\mathrm{MCPC}}(t)=\frac{1}{\sqrt{N_{\mathrm{MC}}T}}\sum_{m=1}^{N_{\mathrm{PC}}}\sum_{m=1}^{N_{\mathrm{MC}}}\exp\left(j\theta_{n,m}\right)\times\exp\left[j2\pi\left(m-\frac{N_{\mathrm{MC}}+1}{2}\right)\frac{t}{T_{\mathrm{MC}}}\right]\mathrm{rect}\left[\frac{t-(n-1)T_{\mathrm{MC}}}{T_{\mathrm{MC}}}\right] \qquad \text{(II.B8)}$$

where the frequency difference between each pair of adjacent carriers is now $\Delta f = 1/T_{\mathrm{MC}}$ to maintain orthogonality of the carriers. Because (II.B8) is a PC generalization of (II.B7), the MCPC structure can likewise be viewed as multiple symbol intervals of an OFDM

signal. In addition to the PAPR issue and the potential for a more general amplitude or phase coding, as discussed for the FC scheme, the MCPC structure has the same issue with spectral containment as was mentioned for the PC scheme because of the abrupt changes in the code values across all M carriers every T_{MC} seconds.

The last general waveform class that is based on pulse-compression processing is noise radar [71–75], in which the waveform is made to appear as noise, for which a bandpass representation can be expressed as [72]

$$s_{\text{noise}}(t) = a(t)\cos\left[\omega_0 t + \theta(t)\right] \tag{II.B9}$$

for a Rayleigh distributed amplitude $a(t)$ and a uniformly distributed phase $\theta(t)$. The random, and otherwise unstructured, nature of this emission scheme gives it an inherently low probability of intercept (LPI) [76]. Noise radar is generally implemented as a form of nonrepeating CW and used as an ultrawideband (UWB) waveform to facilitate high-range resolution. This emission scheme can also be filtered such that the resulting spectral shape yields a PSD that has an associated autocorrelation with low range sidelobes [75]. Because of significant amplitude modulation (AM), combined with the amplitude being predominantly near zero (PAPR could exceed 10 dB), noise radar tends to be limited to lower-power, short-range applications.

Finally, there is a distinctly different class of pulsed UWB waveforms characterized by short temporal durations and broad instantaneous bandwidths. A primary objective of radar is to achieve a large enough SNR to detect targets of interest, with sufficiently high-range resolution to separate the different targets. To achieve very high resolution, the notion of impulse radar has been pursued, subsequently leading to new UWB waveforms of shorter duration than standard radar signals. The major demonstrated benefit that UWB radar provides is ultrahigh resolution, which can be used for object characterization and identification. In particular, such waveforms and their associated radar systems were initially developed for forestry applications [77, 78], for characterizing sea scatter [79], and for detecting underground utilities, land mines, and unexploded ordnance (ground penetrating radar [GPR]) [80–86]. More recent systems have been designed for through-structure detection in urban areas [87], for imaging in search and rescue operations, and for obstacle avoidance in automobiles and micro–air vehicles [88]. As the technology for UWB radar has developed and improved over the last 50 years, the sophistication and performance of these radars have increased. Nonetheless, several crucial issues remain that are problematic to UWB radar: spectral availability, hardware limitations in the transmission chain, electromagnetic interference and compatibility, difficulties with waveform control and shaping, and unreliability of high-power sources for sustained use above 2 GHz. Consequently, UWB radar will probably be limited to short-range, low-power, directive, niche applications. To overcome these deficiencies, recent systems have taken advantage of increased memory, throughput, and computational speed to build stepped-frequency UWB radars for sensing through walls [89]. Because a significant body of literature exists on UWB and this venue has insufficient space to cover it adequately, this interesting field is not discussed further. The authors suggest that interested readers avail themselves of the voluminous literature on UWB waveforms and systems.

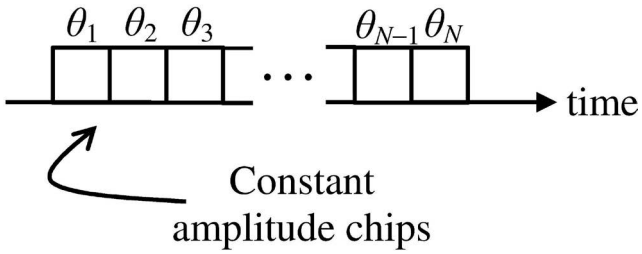

Fig. 7.
PC waveform structure.

To summarize the discussion of different waveform classes, Table II lists the different waveforms and provides a brief synopsis of their attributes.

C. MATCHED FILTERING

Denote $s(t)$ as the complex baseband representation of an arbitrary waveform with temporal extent T (pulsewidth for a pulsed waveform). For this waveform, there exists a matched filter $h_{\text{MF}}(t)$ such that the SNR after filtering is maximized. This filter, originally derived by North [90], has the form $h_{\text{MF}}(t) = Cs^*(T-t)$, where $(\bullet)^*$ denotes complex conjugation and C is an arbitrary constant. For the purpose of comparison among different waveform classes and with the MMFs in Section II.H, it is convenient to define C such that $\left(\int_0^T \left|h_{MF}(t)\right|^2 dt\right)^{1/2} = 1$, thus yielding a normalized MF that produces a unity noise-power gain regardless of the waveform.

The MF response to the waveform (without appreciable Doppler shift during the pulsewidth and for the waveform energy assumed to be unity) is the convolution

$$h_{\text{MF}}(t) * s(t) = \int_{t=0}^{T} s(t)s^*(t+\tau)\,dt \tag{II.C1}$$

which is also the autocorrelation of the waveform. If the energies of both $s(t)$ and $h_{\text{MF}}(t)$ are normalized to unity, (II.C1) likewise pro-

Table II

Waveform Classes and Attributes

Waveform class	Attributes
LFM	Easy to generate and process wideband, high-peak sidelobes
NLFM	Trade LFM resolution for lower sidelobes
Phase codes	Easy to optimize, binary or polyphase subclasses
Frequency codes	Modulate onto different subcarriers, high AM effects
Noise radar	Nonrepeating form of CW, high AM effects, LPI
UWB	Very short pulse, very wide band, ultrahigh resolution

duces a unity magnitude at $\tau = 0$ (peak of the mainlobe). As mentioned in Section II.B, the sidelobes of the autocorrelation can be minimized through proper design of the waveform PSD.

For $x(t)$ the scattering response of an illuminated environment that consists of an unknown number of targets and ubiquitous clutter, the received signal at the radar can be expressed as

$$y(t) = s(t) * x(t) + v(t) \tag{II.C2}$$

where $v(t)$ is additive noise and the influence of Doppler during the pulsewidth is neglected. The MF response for this received signal is therefore

$$\hat{x}_{\mathrm{MF}}(t) = h_{\mathrm{MF}}(t) * y(t) \tag{II.C3}$$

in which the $\hat{x}_{\mathrm{MF}}(t)$ term is the MF estimate of the true scattering $x(t)$. It has become increasingly common to perform this filtering operation in the digital domain, which is discussed in Section II.G.

For most radar systems, the MF response of (II.C3) is collected over a set of pulses for subsequent filtering over this set of responses via Doppler processing (possibly including clutter cancellation) or by synthetic aperture radar (SAR) processing (possibly including additional image focusing). The time interval for this set of pulses is called the coherent processing interval (CPI). These next-stage processes after pulse compression rely on the slow time Doppler shift that occurs between successive pulses, as opposed to the fast time Doppler shift during a pulsewidth.

D. DELAY-DOPPLER AMBIGUITY FUNCTION

Thus far, we have only considered the response to scattering that exhibits no Doppler shift during the pulsewidth. When there is radial motion between the radar platform and a given scatterer, a Doppler frequency shift is induced and may not be negligible. With regard to pulse compression, this Doppler shift imparts a time-varying phase change to the reflected waveform, thereby changing the response of the MF. Specifically, the MF response of (II.C1) for a pulsed waveform of pulsewidth T can be generalized to arbitrary delay τ and Doppler frequency f_{D} as

$$\chi(\tau, f_{\mathrm{D}}) = \int_{t=0}^{T} e^{j2\pi f_{\mathrm{D}} t} s(t) s^*(t+\tau)\, dt \tag{II.D1}$$

which is known as the delay-Doppler ambiguity function as formulated by Woodward [91]. Note that (II.D1) is plotted as $20\log_{10}(|\chi(\tau, f_{\mathrm{D}})|)$ vs. τ and f_{D}.

For example, Fig. 8 depicts the ambiguity function for the well-known LFM waveform. Observe that the mainlobe is part of a delay-Doppler ridge that exhibits a gradual roll-off from the peak at ($\tau = 0, f_{\mathrm{D}} = 0$). The existence of this ridge is why LFM is also called a Doppler-tolerant waveform, because an appreciable Doppler shift induces little SNR loss relative to the peak. The sidelobes of the autocorrelation of the LFM waveform in Fig. 1 are part of a larger Doppler-dependent pattern known as Fresnel lobes (the lobing pattern surrounding the large delay-Doppler ridge).

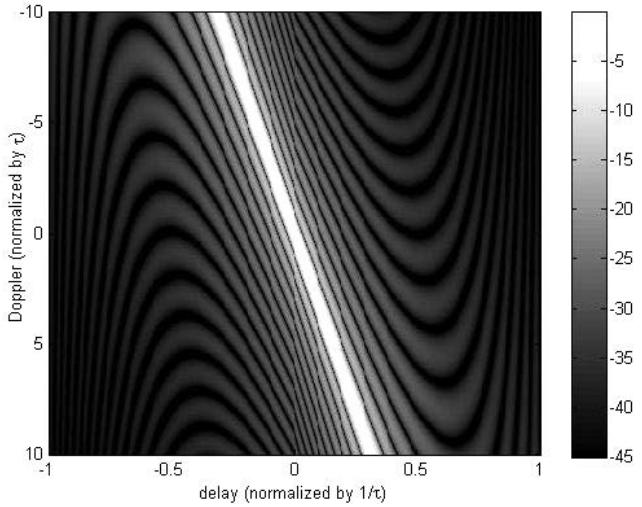

Fig. 8.
Delay-Doppler ambiguity function for LFM waveform (brightness in decibels).

An important property of the ambiguity function is that the maximum value occurs at ($\tau = 0, f_{\mathrm{D}} = 0$) [10, Chap. 3]. It can likewise be shown [10, Chap. 3] that

$$\int_{f=-\infty}^{+\infty} \int_{\tau=-\infty}^{+\infty} \left|\chi(\tau, f_{\mathrm{D}})\right|^2 d\tau\, df_{\mathrm{D}} = 1 \tag{II.D2}$$

for arbitrary waveform structure, assuming the waveform energy is normalized to unity. In other words, there exists a conservation of ambiguity such that if a waveform has lowered sidelobes in one location (say on the $f_{\mathrm{D}} = 0$ axis), then a commensurate increase must occur elsewhere in delay-Doppler space. Finally, the 3 dB resolution in range (the distance between the peak and first null) for useful waveforms is approximately the reciprocal of the 3 dB bandwidth B of the waveform, while the Doppler resolution (peak to first null) is $1/T$ for pulsewidth T.

E. COHERENT PROCESSING OF MULTIPLE PULSES

For a single pulse, the Doppler resolution is $1/T$. However, for a CPI of M identical pulses with constant T_{PRI}, the Doppler resolution is greatly improved to $1/(MT_{\mathrm{PRI}})$. Furthermore, the ambiguity function for a single waveform-modulated pulse via (II.D1), for a CPI of identical pulses [10, Chap. 7], is now scaled as

$$\left|\chi_{\mathrm{CPI}}(\tau, f_{\mathrm{D}})\right| = \left|\chi(\tau, f_{\mathrm{D}})\right| \left|\frac{\sin(M\pi f_{\mathrm{D}} T_{\mathrm{PRI}})}{M \sin(\pi f_{\mathrm{D}} T_{\mathrm{PRI}})}\right| \quad \text{for } |\tau| \le T\,. \tag{II.E1}$$

Recalling from Section II.A that an FMCW waveform can be viewed as a set of pulses for which the duty cycle is 100% ($T_{\mathrm{PRI}} = T$), it is thereby evident that (II.E1) is likewise applicable to the processing of M segments of FMCW.

The coherent processing of multiple pulses also provides a mechanism for the inclusion of additional degrees of freedom for design of the overall delay-Doppler response. For example, greater control of the Doppler sidelobes can be achieved via interpulse (and intrapulse) weighting over the CPI (see [10, Chap. 7]). Like-

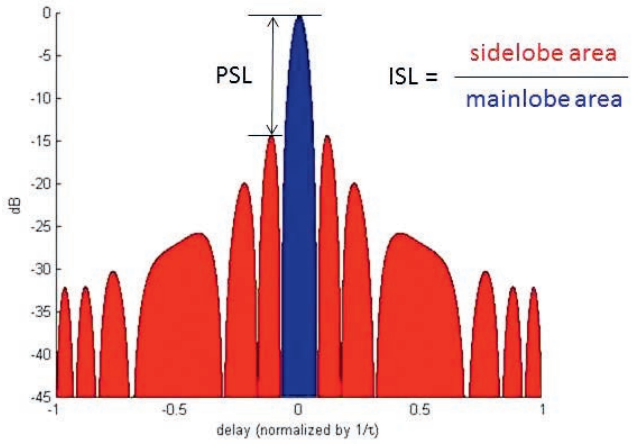

Fig. 9.
Conceptual definition of PSL and ISL measured on zero-Doppler ambiguity function response of a waveform.

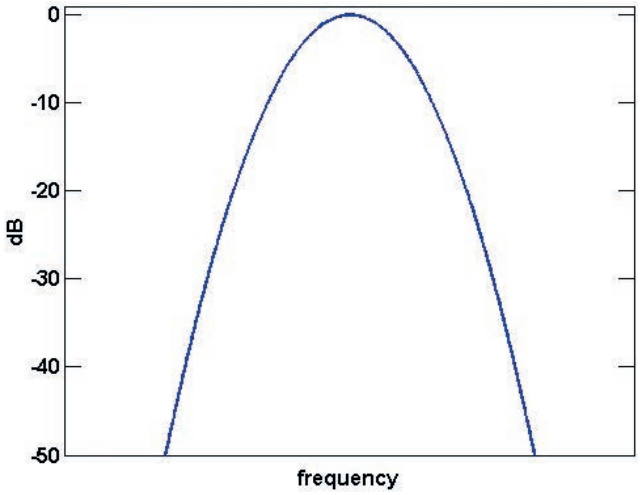

Fig. 10.
Gaussian PSD in decibels.

wise, changing the PRI during the CPI (known as PRI/PRF staggering or jittering) can address the problem of blind speeds for moving target indication (MTI) radar [92, 93] (also see [10, Chap. 8]). One can even employ different waveforms over the set of pulses in a CPI, which is generically called pulse agility or waveform agility and is discussed in greater detail in Section III.C.

F. WAVEFORM METRICS

The determination of goodness of a waveform is generally dependent upon the evaluation of attributes of the delay-Doppler ambiguity function from Section II.D, along with consideration of practical characteristics such as time–bandwidth product (waveform dimensionality), spectral containment, and amenability to the transmitter (see Section II.H). Here, we focus on the attributes that relate to the ambiguity function defined in (II.D1) for a single pulse.

Perhaps the most common metric for waveform range sidelobes is the peak sidelobe level (PSL), or peak sidelobe ratio (PSR) [53, Chap. 20], here denoted Φ_{PSL} and typically defined using the delay-Doppler ambiguity function of (II.D1) as

$$\Phi_{\text{PSL}}\left[\chi(\tau,f_{\text{D}})\big|_{f_{\text{D}}=0}\right]=\max_{\tau}\left|\frac{\chi(\tau,0)}{\chi(0,0)}\right| \quad \text{for } \tau\in\left[\tau_{\text{main}},T\right]. \tag{II.F1}$$

Only the zero-Doppler cut ($f_{\text{D}} = 0$) is considered, which amounts to neglecting the effect of radial motion during the pulsewidth. Accounting for symmetry of $|\chi(\tau,0)|$ about $\tau = 0$, the interval $[0,\tau_{\text{main}}]$ corresponds to the time (range) mainlobe such that the interval $[\tau_{\text{main}},T]$ contains sidelobes. The PSL metric indicates the largest degree of interference that one point scatterer can cause to another at a different delay offset (for both having zero Doppler).

For the class of waveforms known as linear period modulation (LPM) [94], which is also called hyperbolic FM (HFM) and is employed in sonar and by some species of bats, the value [61]

$$\text{PSL}_{\text{LPM bound}}=\left[-20\log_{10}(BT)-3\right]\text{dB} \tag{II.F2}$$

serves as a lower bound on PSL for the waveform time–bandwidth product BT, as defined in Section II.B. Although this PSL bound only holds for LPM (HFM) waveforms, it is nonetheless a useful benchmark with which to compare the performance of untapered FM waveforms (i.e., a fixed measuring stick for optimization purposes).

Another important metric is the integrated sidelobe level (ISL) [53, Chap. 20], which for the zero-Doppler cut ($f_{\text{D}} = 0$) of the ambiguity function can be defined as

$$\Phi_{\text{ISL}}\left[\chi(\tau,f_{\text{D}})\big|_{f_{\text{D}}=0}\right]=\frac{\int_{\tau_{\text{m}}}^{T}\left|\chi(\tau,0)\right|^2 d\tau}{\int_{0}^{\tau_{\text{m}}}\left|\chi(\tau,0)\right|^2 d\tau}\ . \tag{II.F3}$$

The ISL metric is particularly useful for establishing the susceptibility to distributed scattering such as clutter. Conceptual depictions of PSL and ISL are shown in Fig. 9. Consideration of a Doppler interval could be included in the PSL and ISL metrics by generalizing the mainlobe and sidelobe regions to correspond to the interior and exterior, respectively, of a delay-Doppler ellipse.

Finally, given the Fourier relationship between a waveform's autocorrelation (zero-Doppler cut of the ambiguity function) and PSD, it is useful to define a PSD-based metric as well. In this case, it is necessary first to establish a desired PSD $|W(f)|^2$ that corresponds to some desired autocorrelation response (with a sufficiently narrow mainlobe and sufficiently low sidelobes). A good example is a Gaussian PSD that is scaled to have the same energy as a constant-amplitude pulse of duration T (Fig. 10). A metric in this context would then permit measuring how close (in some sense) the actual frequency response of the waveform is to this desired PSD.

For instance, the frequency template error (FTE) metric [95] is defined as

$$\Phi_{\text{FTE}}\left[S(f),W(f)\right]=\left(\frac{1}{f_{\text{H}}-f_{\text{L}}}\right)\int_{f_{\text{L}}}^{f_{\text{H}}}\left|\left|S(f)\right|^p-\left|W(f)\right|^p\right|^q df \tag{II.F4}$$

where f_{L} and f_{H} demarcate the edges of the frequency interval of interest (which should include enough of the spectral roll-off region to provide sufficient fidelity). The positive real values p and q define the degree of emphasis placed on different frequencies. For $p = 1$ and $q = 2$, the FTE metric defines a form of frequency-domain mean-square

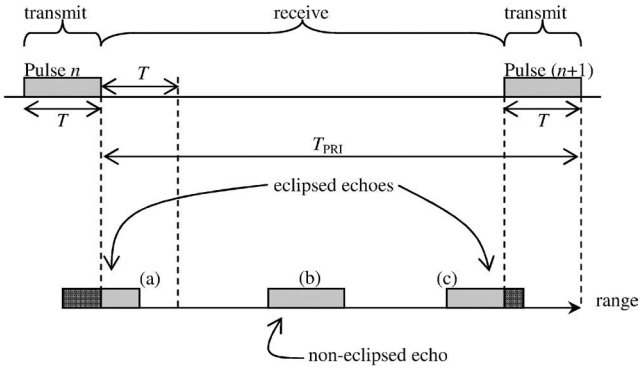

Fig. 11.
Echoes (a) and (c) are eclipsed because they arrive at the receiver when the radar is transmitting. More echoes will be eclipsed if duty cycle T/T_{PRI} is increased.

error (MSE). Alternatively, $p > 1$ overly emphasizes frequencies with higher in-band power, and $p < 1$ overly emphasizes frequencies with lower out-of-band power. Only the spectral envelope (magnitude) is used in (II.F4) so that the phase response remains free for design.

G. PRACTICAL CONSIDERATIONS

There are several practical aspects one must consider when designing or selecting a pulse compression waveform. From an operational perspective, the bandwidth and pulsewidth (and thus the time–bandwidth product) are selected to be suitable to the application (MTI, SAR, etc.) and, combined with the selection of PRF, to achieve an acceptable maximum ambiguous range and Doppler values. For a pulsed mode, in which the receiver and transmitter operation are interleaved, the notion of pulse eclipsing also arises.

Pulse eclipsing [96, 97] (Fig. 11) occurs when the receiver turns on or off during the reception of a waveform-induced echo. Reflected echoes experience reduced SNR, because a portion of the reflected pulse is not captured at the receiver. For frequency-swept waveforms such as LFM and many useful forms of NLFM, pulse eclipsing also translates into degraded range resolution because part of the received bandwidth is lost.

For example, Fig. 12 illustrates a comparison between the MF response of a complete LFM echo and the MF response for an LFM echo that is eclipsed by 50%. Compared to the former, the latter suffers a 6 dB SNR loss and degradation in range resolution by a factor of 2. Thus, while a longer pulse provides greater energy on target, and therefore higher received SNR in the absence of eclipsing, one must decide whether the subsequent increase in the occurrence of eclipsing is worth the trade.

Another attribute that must be considered is the impact of the radar transmitter upon the waveform one wishes to emit. The purpose of the transmitter is to generate and amplify the waveform to a degree that the reflected echoes of lower power can be adequately captured by the receiver relative to the noise and interference. The most common ways to generate a waveform are as follows:

1. A frequency-swept local oscillator (LO), which is often used to produce an LFM chirp
2. A surface acoustic wave (SAW) device, which can be used to generate either LFM or NLFM waveforms
3. A digital arbitrary waveform generator (AWG), which is becoming increasingly popular because of its tremendous flexibility

Following waveform generation, the transmitter high-power amplifier (HPA) then produces the necessary emitted power, typical values that could be ~100 W up to several megawatts depending on the application [5]. While vacuum-tube HPAs such as klystrons, traveling wave tubes (TWTs), and crossed field amplifiers (CFAs) are still in widespread use because of their high power efficiency, achievable transmit power, and reliability [98], solid-state HPAs continue to make advances and have begun to be used in radars that employ active electronically scanned array (AESA) antennas [99]. Advances in tube technology [100, 101] likewise continue.

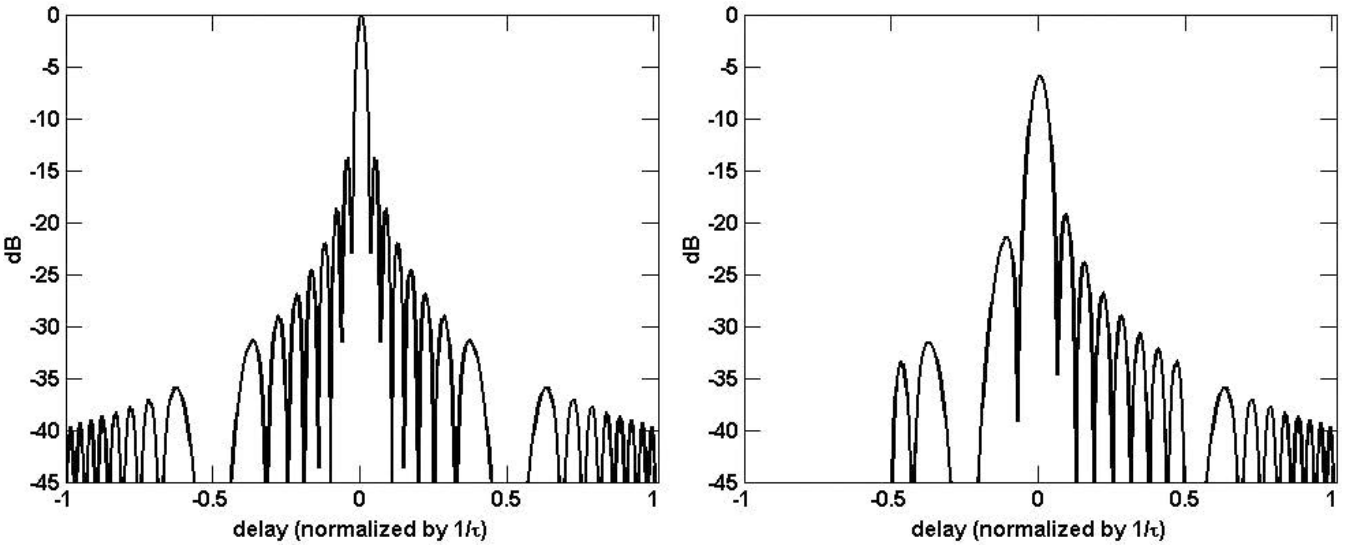

Fig. 12.
Matched filter response to (left) complete LFM echo and (right) 50% eclipsed LFM echo.

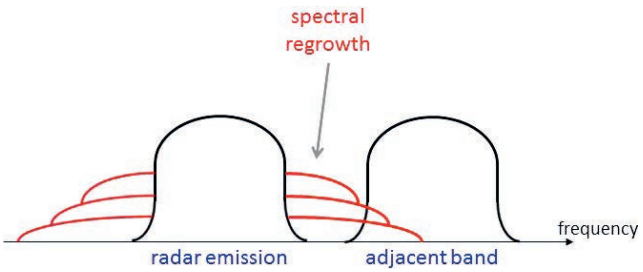

Fig. 13.
Spectral regrowth can create interference for adjacent spectral users.

The overall transmit chain introduces two forms of distortion on the intended waveform: linear and nonlinear. Linear distortion is a direct result of the spectral shaping that arises from the finite bandwidths of the individual transmitter components, and its impact is that the waveform may experience amplitude ripple and phase distortion (dispersion). Nonlinear distortion is primarily caused by the typical HPA operation in saturation (particularly for tube-based HPAs), thereby creating the formation of intermodulation products (harmonics) from the pairwise multiplication of different frequency components in the waveform [102]. These intermodulation products introduce leakage into the surrounding spectrum, an effect generally known as spectral regrowth (Fig. 13), which should be avoided as spectral congestion continues to increase [5].

The presence of transmitter distortion is arguably the main reason the use of certain forms of coded waveforms (i.e., polyphase codes) has thus far been limited. Specifically, the abrupt transitions between adjacent chips in a code correspond to out-of-band spectral content that cannot pass the bandlimited transmitter. Furthermore, this linear distortion introduces AM that is subsequently further distorted if the HPA is operated in saturation.

For example, Fig. 14 shows the spectral content of a $N = 64$-chip P4 code [103], which represents a complex baseband sampled version of an LFM waveform, and the spectral content of an LFM waveform with the same BT for comparison. Using the form described in (II.B5) for the coded waveform, both P4 and LFM have been implemented on an AWG and driven into an S-band radar testbed that includes a mixer, preamplifier, bandpass filter, and a class AB solid-state gallium arsenide (GaN) HPA. The resulting emissions were captured by a receiver in a loopback configuration (i.e., not emitted into free space) in which each is downconverted to baseband, analog lowpass filtered, and then sampled at a rate of 150 samples/chip interval (the same rate as the version of each waveform that was loaded onto the AWG).

For each waveform, Fig. 14 compares the spectrum of the original AWG waveform and the resulting captured loopback emission, thereby representing a before-and-after perspective on the impact of transmitter distortion. The inherent spectral shaping of the transmitter clearly exhibits significant distortion for the coded waveform but far less distortion for LFM. This result is to be expected, because unlike the coded waveform, LFM contains no abrupt phase changes. For these examples, spectral regrowth is rarely observed because of the use of a Class AB solid-state HPA, compared to what one could expect from a tube-based HPA that can produce greater output power (and distortion).

Examination of the pulse shape of each waveform after transmitter distortion (Fig. 15) also reveals that the abrupt chip transitions in the code translate into amplitude nulls commensurate with the amount of phase change. Because a P4 code exhibits larger phase changes near the beginning and end of the code, deeper nulls are present near the ends of the transmitter-distorted pulse shape. In contrast, the loopback-measured LFM shows only a small amount of amplitude ripple that is expected from any real system. As an aside, both pulse shapes in Fig. 15 exhibit rapid pulse rise and fall times, which are additional contributors to broader radar spectral content.

To help explain why these amplitude nulls occur, Fig. 16 illustrates the unit circle on which the phase constellation of a code is defined (here with just eight equally spaced phase values). Whereas an FM waveform moves around this circle continuously accord-

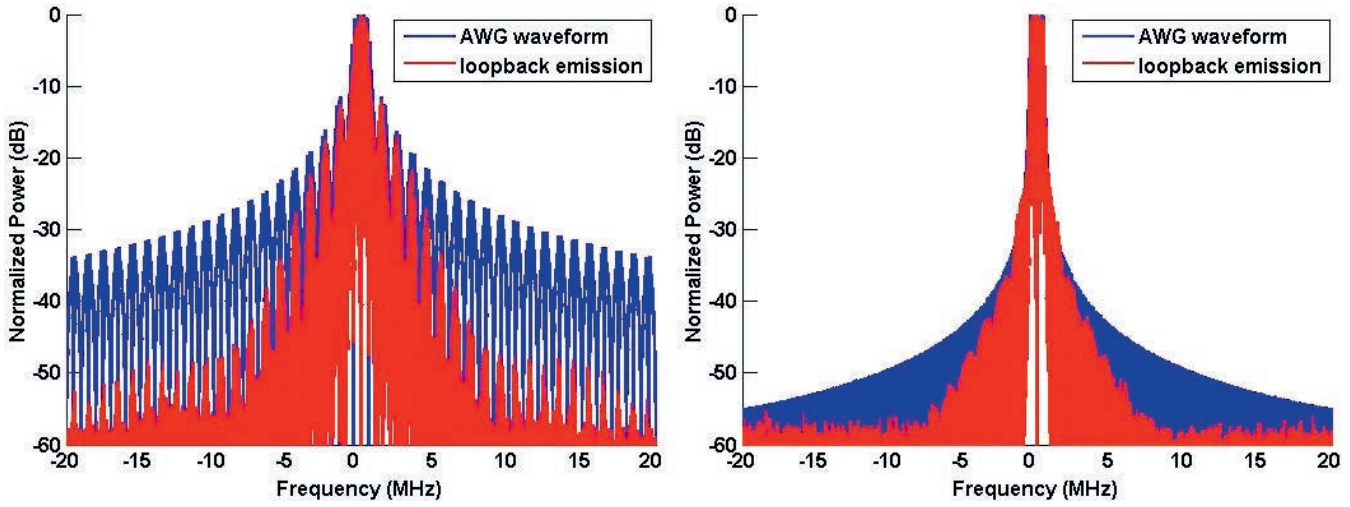

Fig. 14.
Spectral content of (left) P4 code before and after transmitter distortion and (right) LFM waveform before and after transmitter distortion.

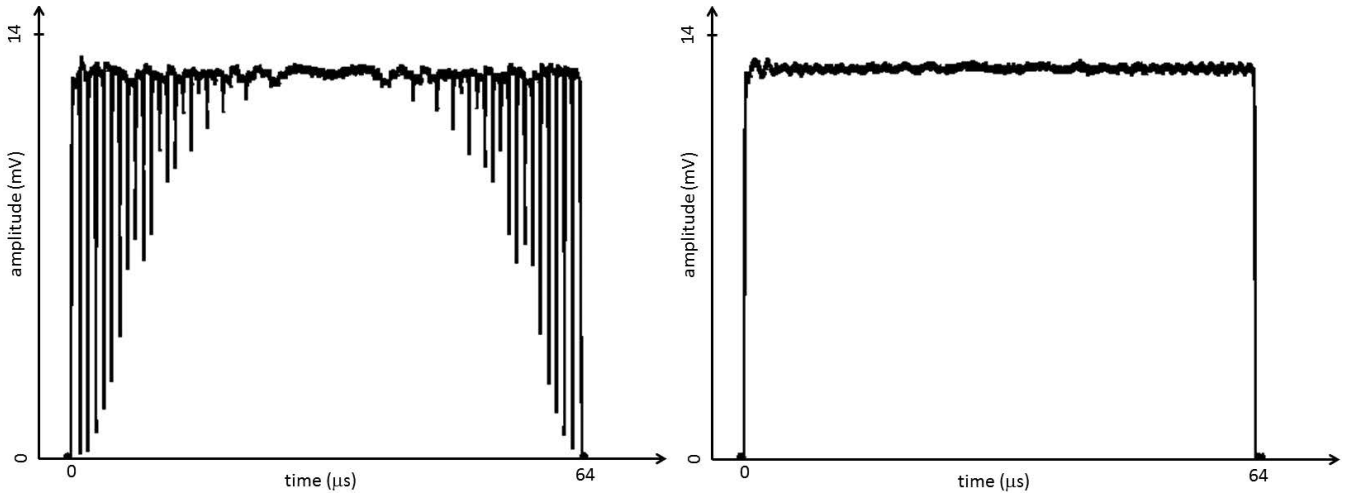

Fig. 15.
Pulse shape after transmitter distortion for (left) P4 code and (right) LFM waveform.

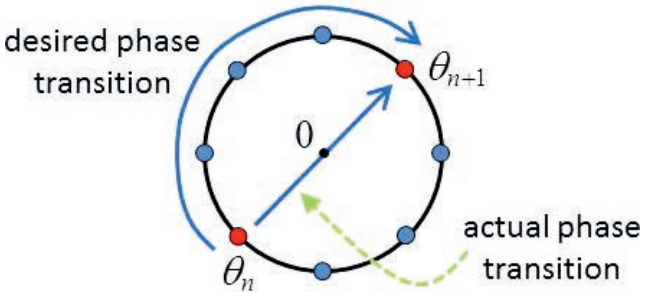

Fig. 16.
Desired and actual phase transitions for phase code because of transmitter effects.

ing to the instantaneous frequency (i.e., instantaneous rate of phase change), a PC waveform makes abrupt jumps from one phase value to another (here from θ_n to θ_{n+1}). While we would wish these phase transitions to move around the unit circle, the high spectral content required to do so is suppressed by the inherent bandlimiting of the transmitter so that the transition instead moves through the interior of the unit circle, thus producing an amplitude null.

Distortion of the waveform is problematic because the considerable time and effort put into designing a code that is optimal in some sense (e.g., minimal PSL) may have been wasted if the distorted version of the coded waveform deviates from this optimality condition (which is rather likely). An additional problem that arises from the amplitude nulls observed earlier is that the saturated HPA is still generating power even though a low-amplitude value is occurring at the output. As such, this generated power is effectively reflected back into the system as a time-varying spike in the voltage standing wave ratio (VSWR) that produces intermittent increases in the operating temperature of the system. At best, such temperature increases translate into higher phase noise; at worst, these temperature fluctuations could potentially damage the system.

The limitations discussed earlier do not imply that phase codes are necessarily a poor option for waveform modulation. For lower-power systems in which AM effects can be well controlled or for operating modes or environments in which distortion and spectral regrowth effects are acceptable (particularly if an accurate replica of the actual emitted waveform can be captured after the HPA for use in matched filtering), the design freedom provided by phase codes may still be an attractive option. Furthermore, as discussed in Section III.A, there are existing methods to convert binary codes into waveforms that are amenable to an HPA (which is why binary codes are commonly used for high-power systems), and recent work has shown that a well-known scheme from communications can likewise convert arbitrary polyphase codes into new kinds of HPA-ready NLFM waveforms.

There are practical aspects to be considered for the FC waveforms from (II.B7) and (II.B8) as well, because they involve the weighted combination of multiple carriers, which subsequently induces significant AM effects [104]. While such waveforms are attractive from a design freedom perspective, the AM effects require significant power backoff to avoid distortion (discussed in Section II.B), thereby leading to a substantial SNR loss as determined by (II.B5) for the AM envelope $\alpha(t)$. To demonstrate why the power backoff is so important, Fig. 17 illustrates the autocorrelation of an $N = 64$ optimized FC waveform from [105] using (II.B7), along with the autocorrelation of the same waveform after undergoing distortion by a saturated power amplifier. In terms of PSL, as defined in (II.F1), the distorted waveform experiences a PSL degradation of 14.7 dB relative to the ideal case. The amplitude envelopes for these before-and-after distortion cases are also shown in Fig. 18. Because linear amplification is a necessity to avoid this distortion, such waveforms are thus restricted for use in lower-power radar applications.

A final practical consideration for all waveforms occurs when performing pulse compression (receiver matched filtering) digitally. In this case, after the anti-aliasing filter and analog-to-digital conversion, the continuous baseband received signal from (II.C2) can be expressed in discrete notation as

$$y(n) = \mathbf{x}^T(n)\mathbf{s} + v(n). \tag{II.G1}$$

Here the length-N vector $\mathbf{s} = [s_1\, s_2 \ldots s_{N-1}]^T$ is the discretized version of the waveform for $N \approx BT$, the vector $\mathbf{x}(n) = [x(n)\, x(n-1) \ldots x(n-N+$

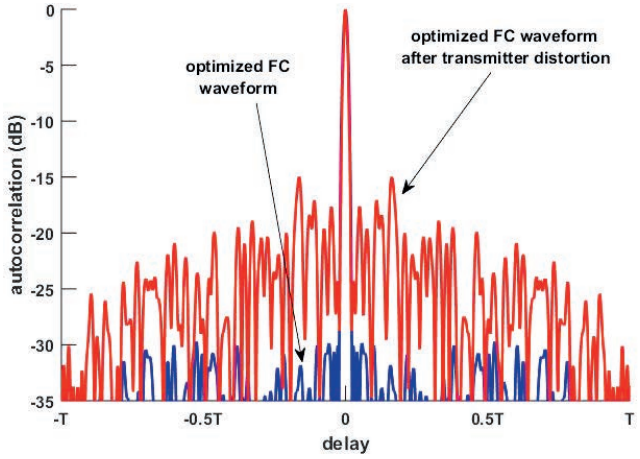

Fig. 17.
Autocorrelation of optimized FC waveform before and after distortion by saturated power amplifier.

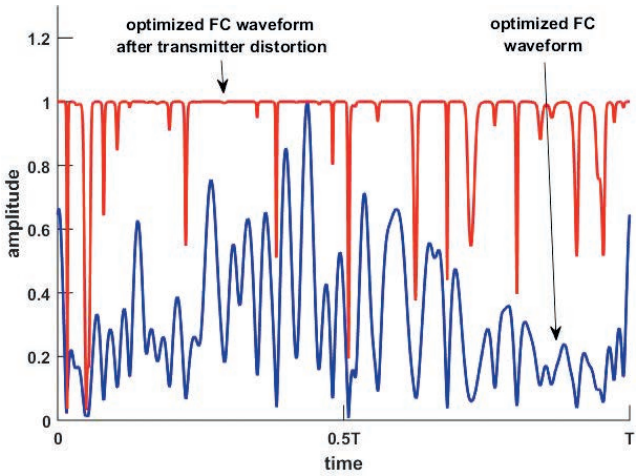

Fig. 18.
Amplitude envelope of optimized FC waveform before and after distortion by saturated power amplifier.

1)]^T is the collection of N contiguous samples of the unknown illuminated scattering, $v(n)$ is a sample of additive noise, $(\bullet)^T$ is the transpose operation, and the influence of Doppler shift during the pulsewidth is neglected. Collecting N contiguous samples of $y(n)$ from (II.G1) to form the vector $\mathbf{y}(n)$, the MF response from (II.C3) thus becomes

$$\hat{x}_{\mathrm{MF}}(n) = \mathbf{h}_{\mathrm{MF}}^H \mathbf{y}(n) = C\mathbf{s}^H \mathbf{y}(n) \qquad \text{(II.G2)}$$

in which $(\bullet)^H$ is the complex-conjugate transpose (Hermitian) operation and the scalar C is again selected to provide unity noise-power gain ($\|\mathbf{h}_{\mathrm{MF}}\| = 1$).

The implication of discretizing the waveform into N samples (for $N \approx BT$ with B the 3 dB bandwidth) is that the receiver sampling rate is likewise defined according to the waveform 3 dB bandwidth. While the 3 dB bandwidth is intrinsically related to the range resolution of the MF, which is itself generally measured by the autocorrelation 3 dB mainlobe width, the actual spectral content of the waveform and subsequent echo are considerably greater. If one performs (complex) receiver sampling at a rate corresponding to the 3 dB bandwidth, which is likewise approximately the chip rate for phase codes, then there is a possibility that the relative delay of a reflected echo may be offset by an amount that introduces a mismatch loss when applying the MF. In other words, for sampling period T_S, the received reflected echoes may arrive with a delay offset of as much as $\pm 0.5T_S$ relative to the sampled structured of the MF. Generally called range straddling or scalloping, this effect occurs because the received signal and the associated MF (obtained from the waveform) are undersampled according to Nyquist. Thus, there exists a continuum of possible delay-shifted versions of the waveform, some of which differ enough from $\mathbf{h}_{\mathrm{MF}} = C\mathbf{s}$ that an appreciable loss occurs (as much as a couple decibels) [106]. Furthermore, for a transmitter-distorted phase code, the presence of abrupt phase changes (even after transmitter bandlimiting) means certain delay-shifted versions coinciding with these transitions may be considerably different from the nominal versions that are well matched to the code (because the phase is constant during a chip for a phase code).

There is a simple way to minimize the mismatch loss because of range straddling: use a higher receiver sampling rate. In doing so, (II.G1) does not change, aside from the discretized version of the waveform $\mathbf{s} = [s_1\ s_2\ \ldots\ s_{NK-1}]^T$ and the oversampled collection of scatterers $\mathbf{x}(n) = [x(n)\ x(n-1)\ \ldots\ x(n-NK+1)]^T$, which are both now length-NK. Likewise, NK samples of the oversampled received signal $y(n)$ are now collected to form $\mathbf{y}(n)$ for subsequent application of the (now) length-NK matched filter $\mathbf{h}_{\mathrm{MF}}$, which is still normalized such that $\|\mathbf{h}_{\mathrm{MF}}\| = 1$.

The tradeoff for operating at a higher rate is an increase in the computational cost to perform pulse compression, which already tends to be a bottleneck because of the need to process a large amount of data rapidly (usually in real time). This computational burden may be alleviated somewhat by performing pulse compression filtering in the frequency domain [107, Chap. 7], which is already commonly done. Continued improvements in computing speed are also helping to ease this bottleneck.

H. MISMATCHED FILTERING

As discussed in Section II.B, an amplitude-tapered version of LFM can significantly reduce range sidelobes at the cost of degraded range resolution and SNR loss. Furthermore, the need for amplitude control prevents the transmitter from operating in saturation, thereby inducing additional SNR loss relative to what could be achieved if the HPA were operated in saturation. Besides NLFM, another alternative is to transmit an untapered LFM with a receive filter that is different from the MF, that is, a mismatched filter (MMF).

The simplest MMF involves tapering of the MF as follows:

$$h_{\mathrm{MMF}}(t) = a(t)h_{\mathrm{MF}}(t)\ . \qquad \text{(II.H1)}$$

For example, where the response shown in Fig. 3 involves a square-root Hamming-weighted LFM and associated MF (which thus also contains a square-root Hamming taper), Fig. 19 depicts the response of a Hamming-weighted MMF via (II.H1) to an untapered LFM waveform. Where the former distributes the weighting equally over the waveform and filter via the square root, the latter employs the entire weighting only at the receive filter. The MMF

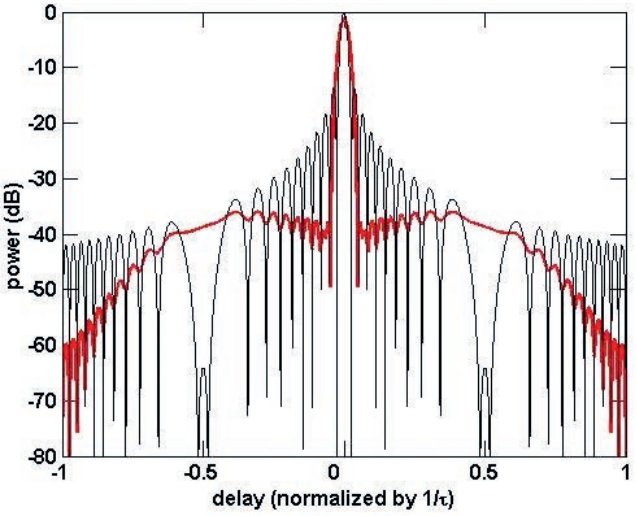

Fig. 19.
LFM pulse compression response for matched filter (black) and Hamming-weighted MMF (red).

yields the same resolution degradation of a factor of 1.5 relative to the use of untapered LFM with a MF. The largest sidelobe is now about −36 dB, while the SNR loss is about 1.4 dB.

While the tapered LFM with matched filtering and untapered LFM with mismatched filtering exhibit SNR losses of 2.7 and 1.4 dB, respectively, these losses are for different reasons. The amplitude-tapered LFM clearly exhibits SNR loss because of the deviation from a constant-amplitude waveform (see (II.B5)), yet the subsequent (normalized) MF still maximizes the received SNR (with unity noise-power gain). In contrast, untapered LFM maximizes the transmit power, while the subsequent receive MMF accepts a mismatch loss as a tradeoff for lower sidelobes. By likewise normalizing the MMF to produce unity noise-power gain via scaling such that $\left(\int_0^T \left|h_{MMF}(t)\right|^2 dt\right)^{1/2} = 1$ (or $\|\mathbf{h}_{\text{MMF}}\| = 1$ from a digital perspective), one can surmise that the mismatch loss, as the name suggests, is a result of the filter not being exactly matched to the waveform; therefore, the received echo signals do not experience the maximum coherent processing gain provided by the waveform time–bandwidth product.

In general, the loss in SNR because of mismatched filtering is

$$\text{SNR Loss}_{\text{mismatch}} = -10\log_{10}\left(\frac{\text{SNR}_{\text{MMF}}}{\text{SNR}_{\text{MF}}}\right) \tag{II.H2}$$

where SNR_{MMF} and SNR_{MF} are defined at the mainlobe peaks of the respective filter responses and, if the filters are normalized to produce unity noise-power gain as discussed earlier and in Section II.C, the noise-power terms cancel out such that the ratio is between achievable signal powers after filtering. For the amplitude-weighted MMF, assuming the weighting is a real function, the mismatch loss can be expressed as follows:

$$\text{SNR Loss}_{\text{mismatch (weighted)}} = -10\log_{10}\left(\frac{\left(\int_0^T a(t)\,dt\right)^2}{T\int_0^T a^2(t)\,dt}\right). \tag{II.H3}$$

Likewise, the discretized representation of (II.H3) is

$$\text{SNR Loss}_{\text{mismatch (weighted)}} = -10\log_{10}\left(\frac{\left(\sum_{n=1}^{NK} a(n)\right)^2}{NK\sum_{n=1}^{NK} a^2(n)}\right) \tag{II.H4}$$

for $N \approx BT$ and the receive oversampling factor K relative to 3 dB bandwidth. While (II.H3) and (II.H4) provide a way to compute the mismatch loss for the specific form of MMF based on amplitude tapering of the MF, (II.H2) is the more general formulation that is useful for all manner of mismatched filtering.

Another prominent MMF instantiation arises from least squares (LS) estimation [108]. For arbitrary receive oversampling K and filter-length increase-factor b (typically on the order of 2 to 4), the length-bNK LS-MMF formulation is posed as

$$\mathbf{A}\mathbf{h}_{\text{LS-MMF}} = \mathbf{e}_m \tag{II.H5}$$

where $\mathbf{e}_m$ is the length $(b+1)NK - 1$ elementary vector with a 1 in the mth element and 0 elsewhere and

$$\mathbf{A} = \begin{bmatrix} s_1 & 0 & \cdots & 0 \\ \vdots & s_1 & & \vdots \\ s_{NK} & \vdots & \ddots & 0 \\ 0 & s_{NK} & & s_1 \\ \vdots & & \ddots & \vdots \\ 0 & \cdots & 0 & s_{NK} \end{bmatrix} \tag{II.H6}$$

is a $((b+1)NK - 1) \times bNK$ Toeplitz matrix. If $K = 1$ (not oversampled), the optimal MMF in the LS sense is thus

$$\mathbf{h}_{\text{LS-MMF}} = \left(\mathbf{A}^H\mathbf{A} + \varepsilon\mathbf{I}\right)^{-1}\mathbf{A}^H\mathbf{e}_m \tag{II.H7}$$

where the diagonal loading term $\varepsilon\mathbf{I}$, for real and positive ε and identity matrix $\mathbf{I}$, has been added to the LS solution to provide further control over MMF performance. Once determined, the filter is subsequently scaled such that $\|\mathbf{h}_{\text{LS-MMF}}\| = 1$.

If $\varepsilon = 0$, the true LS-MMF is obtained, though the resulting mismatch loss determined via (II.H2), which is waveform dependent, may be unacceptable. In contrast, if δ is made large, the LS-MMF in (II.H7) effectively becomes a scaled version of the MF with surrounding zeros. While the MF may not provide acceptable sidelobe performance, it yields no mismatch loss, straddling effects notwithstanding. Thus, the $\varepsilon\mathbf{I}$ term enables determination of an acceptable tradeoff between sidelobe reduction and mismatch loss.

If the received signal is oversampled ($K > 1$) to combat mismatch loss from range straddling, the LS-MMF in (II.H7) produces a superresolution condition that, while yielding a narrower mainlobe for the pulse compression filter response, also suffers from considerable mismatch loss (several decibels) and increased sidelobes [109]. This effect can be remediated by replacing $\mathbf{A}$ with $\tilde{\mathbf{A}}$, for which some number of rows above and below the mth row are replaced with zeros to provide a beam-spoiling effect. The precise number of zeroed rows to achieve the nominal resolution (same as the MF) depends on the waveform and the value of K [110].

Besides mismatch loss, an additional effect arises when range straddling occurs for the LS-MMF. Because this filtering scheme is constructed from the waveform via (II.H6) and (II.H7) to suppress sidelobes to the greatest degree possible (for a given acceptable mismatch loss and resolution), the LS-MMF is particularly sensitive to model mismatch effects such as occurs in a range straddling condition. When the sampled version of the received waveform differs from the version used to construct the LS-MMF, the degree of sidelobe suppression is hindered. Thus, there is a need to continue exploring MMF robustness measures, such as the filter averaging approach considered in [110].

In addition to the earlier LS-MMF, which is based on minimization of the L_2 norm, many other MMF formulations have been developed. These approaches include the use of different L_p norms with convex optimization [111–114], iterative reweighting of LS [115, 116], inverse filtering [117], the two-sample sliding window adder [118, 119], linear programming [120], minimax optimization [121, 122], and even alternative signal representations such as the Laurent decomposition of the waveform [123].

Adaptive forms of MMF have also been developed in which the pulse compression response from the initial matched or mismatched filtering is used as prior knowledge to enable further sidelobe suppression. The earliest of these approaches [124], which eventually became commonly known as the CLEAN algorithm [125, 126], sequentially subtracts the estimated sidelobe responses generated by large scatterers. A more recent approach, adaptive pulse compression (APC) [127], performs adaptive nulling in the range domain by using the current estimate of the measured pulse compression response to generate an updated adaptive filter specific to each particular range cell. Subsequent variants of APC address fast-time Doppler [128–130], pulse eclipsing [97, 131], postmatched filter processing [132, 133], the application to FM waveforms [110], and multistatic [134, 135] and dual-polarized [136] operation. More computationally efficient versions have likewise been developed [137, 138].

I. BANDWIDTH CONSIDERATIONS

One means for characterizing a signal, device, or system in a meaningful way is to use some measure of the bandwidth B of the spectral density of its transfer function to define a categorization scheme. Consequently, defining a signal, device, or system unambiguously is a two-step process: 1) clearly specify the notion of bandwidth and 2) categorize the signal, device, or system in terms of its bandwidth. This process begs the following questions: What is bandwidth? And what is an appropriate categorization scheme? The answers to these questions are neither obvious nor unambiguous [139, 140], because numerous definitions of bandwidth exist in the literature and various standards [9, 141, 142], and these definitions are influenced by differing needs and viewpoints of communities of interest (radar, communication, directed energy, electromagnetic interaction, high-power electromagnetics, etc.). Even though many of these communities are related, no codified definition across them exists. So when using the term bandwidth, the user should clearly define what is meant and how the bounding frequencies are selected. In addition, because well-known standard definitions for narrowband signals and hardware either do not apply or are not easily extendable to UWB signals and hardware, it is imperative that the meaning of bandwidth be clearly stated and well formulated. Issues with understanding and classifying UWB short-pulse and signals and devices for radar and communication applications led to the categorization schemes by the U.S. Office of the Secretary of Defense/Defense Advanced Research Projects Agency (OSD/DARPA) Panel [143], the International Electrotechnical Commission (IEC) [144], and the U.S. Federal Communications Commission (FCC) [145].

In general, there are three common ways in which to measure bandwidth; root mean square (RMS), power level, and energy level, albeit with many variations thereof. For the time-domain signal $s(t)$ with finite energy and its frequency-domain representation $S(f)$ determined by the Fourier transform pair

$$s(t) = \int_{-\infty}^{\infty} S(f) e^{j2\pi ft}\, df \tag{II.I1}$$

$$S(f) = \int_{-\infty}^{\infty} s(t) e^{-j2\pi ft}\, dt \tag{II.I2}$$

these bandwidth measures are as follows.

In radar signal theory, the RMS bandwidth B_{RMS} is often used. IEEE Standard 686-2008 [9] now defines B_{RMS} according to [146, Chap. 2] as the second moment of the square magnitude of $S(f)$ about a designated frequency. Specifically,

$$B_{\text{RMS}} = \sqrt{\frac{\int_0^{\infty} \left[2\pi\left(f - f_{\text{mp}}\right)\right]^2 \left|S(f)\right|^2 df}{\int_0^{\infty} \left|S(f)\right|^2 df}} \tag{II.I3}$$

where the denominator is half of the signal energy and the mean frequency f_{mp} over positive frequencies is given by:

$$f_{\text{mp}} = \frac{\int_0^{\infty} f \left|S(f)\right|^2 df}{\int_0^{\infty} \left|S(f)\right|^2 df} \tag{II.I4}$$

Relative to f_{mp}, the high end of the band is $(f_{\text{mp}} + 0.5B_{\text{RMS}})$, while the low end of the band is set as $\max\{0, (f_{\text{mp}} - 0.5B_{\text{RMS}})\}$ because $(f_{\text{mp}} - 0.5B_{\text{RMS}})$ could be negative. For well-behaved spectra, f_{mp} is usually near the frequency associated with the maximum value of the energy density, which is usually the carrier frequency for radiated narrowband signals.

The X dB power-level bandwidth $B_{X\text{dB}}$ is [139]

$$B_{X\,\text{dB}} = f_{\text{high}} - f_{\text{low}} \tag{II.I5}$$

where the lowest f_{low} and highest f_{high} frequencies are solutions of

$$20\log_{10}\left|S(f)\right| = 20\log_{10}\left|S\left(f_{\max}\right)\right| - X \tag{II.I6}$$

for positive X, where $f_{\max}$ is the frequency at which the PSD $|S(f)|^2$ achieves its maximum value. For example, $B_{3\text{dB}}$ corresponds to values of f at which $|S(f)|^2$ is half its maximum value. Power-level bandwidths are used in a variety of applications. Filter design and control theory traditionally use $B_{3\text{dB}}$, the FCC employs $B_{10\text{dB}}$ to de-

fine UWB signals, and the spectrum-management community uses $B_{20\text{dB}}$ and $B_{40\text{dB}}$.

Finally, for each value X in (0,1], let A_X be the collection of nonnegative pairs $\{f_{\text{low}}, f_{\text{high}}\}$ of real numbers that satisfy:

$$\int_{f_{\text{low}}}^{f_{\text{high}}} \left|S(f)\right|^2 df = X \int_0^{\infty} \left|S(f)\right|^2 df \quad . \tag{II.I7}$$

The X fractional energy bandwidth is thus [139, 140]:

$$B_{X\,\text{EB}} = \inf\left\{\left(f_{\text{high}} - f_{\text{low}}\right) : \left\{f_{\text{low}}, f_{\text{high}}\right\} \text{ in } A_X\right\} \quad . \tag{II.I8}$$

Although A_X may contain more than a single pair of frequencies, $B_{X\text{EB}}$ is unique. For example, if the spectral magnitude is a rectangular function, the X fractional bandwidth is a single value, even though A_X contains an infinite number of distinct pairs. The fractional energy bandwidth provides good information on how the signal energy is distributed in the frequency domain. This quality makes $B_{X\text{EB}}$ a useful measure for characterizing signals in terms of their spectral occupancy (spectrum management) and their electromagnetic interference on other sources (directed-energy systems and electromagnetic hardening).

Where the preceding measures provide different definitions of bandwidth, it is likewise useful to classify the nature of a signal or system as narrowband, wideband, or UWB according to its fractional bandwidth, which is defined as

$$B_{\text{F}} = \frac{\left(f_{\text{pass,high}} - f_{\text{pass,low}}\right)}{\left(f_{\text{pass,high}} + f_{\text{pass,low}}\right)/2} \times 100\% \tag{II.I9}$$

where $f_{\text{pass,high}}$ and $f_{\text{pass,low}}$ denote the upper and lower edges of the passband, respectively. As such, a signal, component, or system is categorized in terms of its fractional bandwidth as follows [140, 147]:

- narrowband if $0\% \le B_{\text{F}} \le 1\%$
- wideband if $1\% \le B_{\text{F}} \le 25\%$
- UWB if $25\% \le B_{\text{F}} \le 200\%$

The 1% demarcation between narrowband and wideband is not used in the IEEE Radar Standard [9] and should be taken as one possible summary of the literature. Some references suggest that a 10%–20% fractional bandwidth could effectively be considered narrowband. For example, Engler [148] states that "a typical narrowband signal will have 10% bandwidth or less" and Urkowitz et al. [149] denote a signal as narrowband if $B_{\text{F}} < 20\%$ because in such case the "range and range rate (have) no dependence upon the bandwidth of the transmitted signal." Likewise, according to Richards [150] "Few radars achieve 10% bandwidth. Thus, most radar waveforms can be considered narrowband, bandpass functions."

One could also consider the point at which group delay dispersion become noticeable or VSWR exceeds a specified value. Clearly, there are various definitions of bandwidth and means of categorizing bandwidth. The takeaway here is that one must be careful to specify which definition is being used and to remember that the notion of spectral content is more complicated than the statement of a single number.

III. WAVEFORM DIVERSITY

Because of the combination of increasing RF spectrum pressure, an increasingly complex interference environment, and the continued desire for improved radar sensitivity and discrimination capability, research in WD has flourished. Therefore, it is not feasible to survey all developments. Instead, we take a general view of the different types of WD, with a focus on the practical problems and attributes. Specifically, while one could argue that WD research is largely arising from a signal processing and waveform design perspective, the RF system and electromagnetics effects play crucial roles in what is physically achievable. These effects become particularly important when considering the impact of coupling among the various dimensions of fast time (range), slow time (Doppler), space, polarization, and coding (modulation). When operating frequency is included, this set has been called the transmission hypercube or transmission hyperspace [151].

A. PRACTICAL WAVEFORM OPTIMIZATION

The properties of a waveform that are the most conducive to its emission from a radar are 1) constant amplitude and 2) sufficient spectral containment. The former helps to avoid some of the nonlinear distortion that would otherwise be imparted to AM waveforms by the HPA and facilitates maximization of power-added efficiency (PAE) and subsequent "energy on target" for detection sensitivity. The spectral containment property helps to minimize the spectral shaping imposed by the transmitter that can produce additional AM effects leading into the HPA, subsequently compounding distortion and potentially creating additional problems (see Section II.G).

As discussed in Section II.B, FM waveforms are attractive because they are constant amplitude and inherently well contained spectrally, thus making them amenable to a physical radar transmitter, particularly the distortion induced by the HPA. However, binary codes have also been widely used, due in large part to the existence of implementation schemes through which the code structure can be converted into a transmitter-appropriate physical waveform. The two most common implementation schemes are derivative phase shift keying (DPSK) [152] and biphase-to-quadriphase (BTQ) transformation [153], the latter being a form of minimum shift keying (MSK). For example, specifying $s_{\text{BC}}(t)$ as the binary coded version of (III.B6) with $\theta = 0°$ or 180°, the resulting DPSK-implemented waveform can be expressed as [152]

$$s_{\text{DPSK}}(t) = s_{\text{BC}}\left(t - T_{\text{C}}/2\right)\left|\cos\left(\pi t/T_{\text{C}}\right)\right| - j s_{\text{BC}}(t)\left|\sin\left(\pi t/T_{\text{C}}\right)\right| \tag{III.A1}$$

thereby ensuring that the phase is continuous by avoiding the abrupt chip transitions (see DPSK implementation of a length-5 Barker code in Fig. 20). Likewise, the BTQ transformation [153] causes any transition from 0° to 180°, or vice versa, first to transition to ±90°, thus forcing the phase to traverse the unit circle instead of going through its center (such as we observed in Figs. 15 and 16). While widely used, the main limitation for binary-coded waveforms is a lack of design freedom because of the $P = 2$ phase constellation.

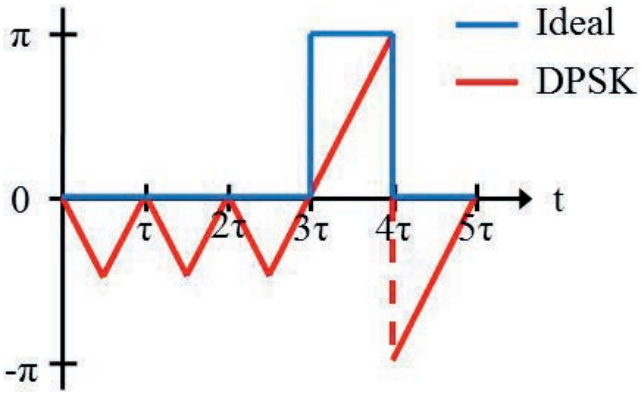

Fig. 20.
Phase trajectory of binary code (ideal) and its DPSK implementation.

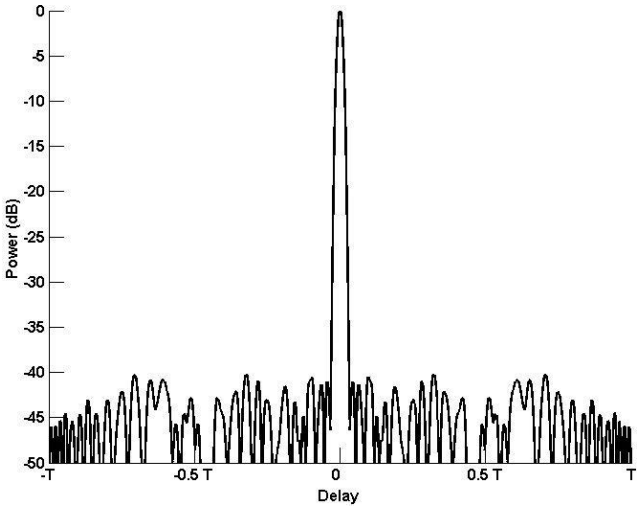

Fig. 21.
Autocorrelation of optimized PCFM waveform with $BT = 64$.

Just as DPSK or MSK can be used to implement binary codes, it has recently been shown that arbitrary polyphase codes can likewise be implemented using a modified form [103, 154] of continuous phase modulation (CPM) [155] that is otherwise commonly employed in aeronautical telemetry [156], deep space communications [157], and the Bluetooth wireless standard [158]. The resulting waveform is a form of FM and thus is denoted as polyphase-coded frequency modulation (PCFM). For this formulation, a train of N impulses is formed that have time separation T_p and thus a total time support of $T = NT_p$. The nth impulse is weighted by $-\pi \le \alpha_n \le \pi$, which is the phase change occurring over a T_p interval and thus can be viewed as a discretized representation of the instantaneous frequency in (II.B2)). From a design standpoint, it is possible either to determine the α_n values directly or to obtain them from a standard length $N+1$ polyphase code via

$$\alpha_n = \begin{cases} \tilde{\alpha}_n & \text{if } |\tilde{\alpha}_n| \le \pi \\ \tilde{\alpha}_n - 2\pi \operatorname{sgn}(\tilde{\alpha}_n) & \text{if } |\tilde{\alpha}_n| > \pi \end{cases} \tag{III.A2}$$

where

$$\tilde{\alpha}_n = \theta_n - \theta_{n-1} \quad \text{for } n = 1, \ldots, N, \tag{III.A3}$$

sgn(•) is the sign operation, and θ_n is the phase value of the nth chip in the length $N+1$ polyphase code.

Given the phase-change code $\mathbf{x} = [\alpha_1\ \alpha_2\ \ldots\ \alpha_N]^T$ and arbitrary starting phase θ_0, the resulting PCFM waveform is generated as [103]

$$s_{\text{PCFM}}(t;\mathbf{x}) = \exp\left\{ j\left(\int_0^t g(\tau) * \left[\sum_{n=1}^{N} \alpha_n \delta\left(\tau - (n-1)T_p\right) \right] d\tau + \theta_0 \right) \right\} \tag{III.A4}$$

where the shaping filter $g(t)$ must integrate to unity over the real line and have time support on $[0,T_p]$, for * denoting convolution. For example, a rectangular filter meets these requirements and, upon inclusion in (III.A4), serves as a linear interpolation of phase that can be viewed as a first-order hold representation of the phase function. By comparison, the standard phase-code structure of (II.B6) can be viewed as a zero-order hold representation, because the phase is constant between the abrupt transitions. Fig. 21 depicts an optimized PCFM waveform from [95] that has a time–bandwidth product of 64. Compared to the LPM bound from (II.F2), for which the PSL value can be computed to be −39.1 dB, this optimized FM waveform realizes an improved PSL of −40.2 dB.

The phase component of the first-order representation of (III.A4) can be written as

$$\theta_{1\text{st}}(t;\mathbf{x}_1) = \int_0^t \left[\sum_{n=1}^{N} \alpha_n g_1\left(\tau - (n-1)T_p\right) \right] d\tau + \theta_0 \tag{III.A5}$$

where the notation $g_1(t)$ and $\mathbf{x}_1 = [\alpha_1\ \alpha_2\ \ldots\ \alpha_N]^T$ are used to explicitly denote this shaping filter and phase-change code as corresponding to first-order. Higher-order phase functions can also be defined [159]. For example, a second-order coded representation can be defined as

$$\theta_{2\text{nd}}(t;\mathbf{x}_2) = \int_0^t \int_0^\tau \left[\sum_{n=1}^{N} b_n g_2\left(\tau' - (n-1)T_p\right) \right] d\tau'\, d\tau + \int_0^t \omega_0\, d\tau + \theta_0 \tag{III.A6}$$

and likewise, a third-order coded representation as

$$\theta_{3\text{rd}}(t;\mathbf{x}_3) = \int_0^t \int_0^\tau \int_0^{\tau'} \left[\sum_{n=1}^{N} c_n g_3\left(\tau'' - (n-1)T_p\right) \right] d\tau''\, d\tau'\, d\tau + \int_0^t \int_0^\tau \beta_0\, d\tau'\, d\tau + \int_0^t \omega_0\, d\tau + \theta_0 \tag{III.A7}$$

and so on, for higher orders, where $\mathbf{x}_2 = [b_1\ b_2\ \ldots\ b_N]^T$ and $\mathbf{x}_3 = [c_1\ c_2\ \ldots\ c_N]^T$ are therefore frequency-change (chirp rate) and chirp-rate-change (chirp acceleration) codes, respectively, with associated shaping filters $g_2(t)$ and $g_3(t)$. In addition, θ_0 is the starting phase, and ω_0 and β_0 are the starting frequency and chirp rate, respectively. These coding structures in (III.A5), (III.A6), and/or (III.A7) may even be combined [159] to permit multiorder coding for even greater freedom in FM waveform design. This increased freedom means there are more ways in which to represent the continuum of possible phase trajectories, thus enabling the potential to obtain waveforms whose pulse compression response yields even lower sidelobes for the zero (or at least small) Doppler regime of the ambiguity function. For example, again using a time–bandwidth product of 64, Fig. 22 depicts the autocorrela-

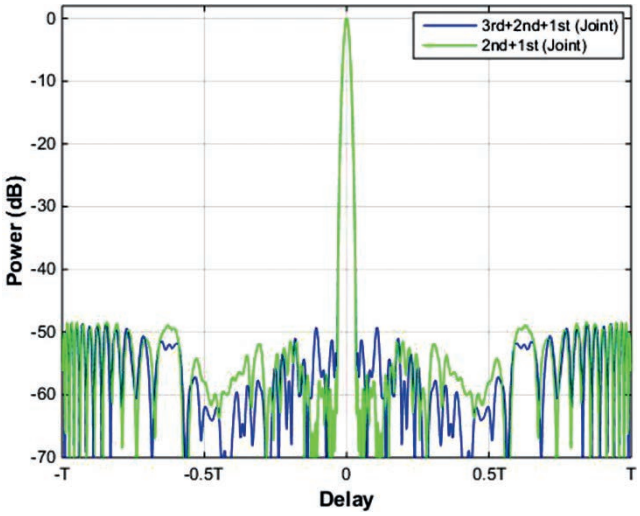

Fig. 22.
Autocorrelation of optimized higher-order PCFM waveforms for $BT = 64$.

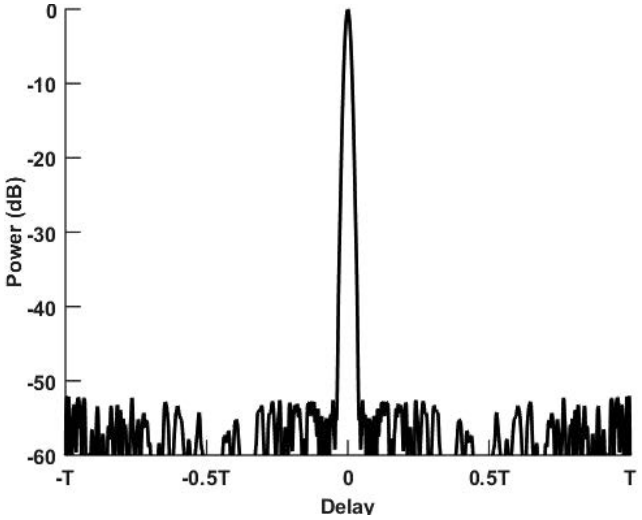

Fig. 23.
Autocorrelation of optimized overcoded PCFM waveform for $BT = 64$.

tions of waveforms obtained via joint optimization of the first- and second-order components, as well as the first-, second-, and third-order components. These waveforms realize PSL values of −48.4 and −48.7 dB, respectively.

Besides higher-order phase functions, the PCFM implementation of (III.A4) can be expanded to accommodate what has been called overcoding [160]. In the overcoded formulation, 1) the phase-change intervals of T_p are subdivided into smaller intervals, and 2) the amount of phase change over the interval of T_p, which in (III.A2) was limited to $|\alpha_n| \leq \pi$ because of extraction from traditional polyphase coding, is now allowed to exceed this limit as long as the aggregate spectral containment is maintained. Thus, even more different continuous phase functions may be realized, thereby enabling waveforms such as the one demonstrated in Fig. 23, in which a PSL value of −52.0 dB is attained, again for a time–bandwidth product of 64.

One may also consider how structures such as these higher-order and overcoding formulations could be combined, potentially to yield even greater sidelobe reduction. Furthermore, because the continuum of possible continuous phase functions supports a theoretically infinite number of possibilities, other coding implementation structures could be developed. Other examples include the recent design of FM waveforms based on the use of Bézier curves [161], polynomial function design [58] (which inspired the preceding higher-order form), the Zak transform [57], and various forms of piecewise NLFM [62]. In addition, recent work on hybrid FM (amplitude-tapered NLFM) discussed in Section II.B has experimentally demonstrated a PSL better than −83 dB (−108 dB in simulation) with only a quarter dB of SNR loss [162]. Clearly there is significant room for improvement in operational systems with regard to sidelobe-limited sensitivity.

These various forms of FM waveforms, along with DPSK/MSK implemented binary codes, provide different ways to parameterize a continuous, constant-amplitude waveform that is amenable to a high-power radar transmitter. However, one should not infer that such waveforms experience no distortion. If the goal is to achieve very low sidelobes that are many tens of decibels below the mainlobe peak, then even a small degree of distortion can become the limiting factor on performance. Consequently, it becomes necessary to consider the impact of the transmitter on the generation of the emitted waveform. In so doing, we introduce a stratified nomenclature in which the *code* (if one exists) comprises a discrete set of parameters that, via some subsequent implementation scheme (such as those discussed earlier), then realizes the *waveform* that is subsequently injected into the transmitter for amplification, thereby ultimately producing the physical *emission* that is launched into the environment.

With the HPA generally representing the most significant source of transmitter distortion because of its inherent nonlinearity, many different linearizing transmit architectures have been developed, including the Kahn technique, envelope tracking, various outphasing methods, the Doherty technique, etc. (see [163] for a review of such methods). Likewise, predistortion techniques (see [164] for an overview) rely upon a variety of models such as a lookup table (LUT), Volterra model, polynomial model, Wiener model, Hammerstein model, and variations thereof to parameterize and subsequently estimate the nonlinear nature of the HPA so as to undo such effects upon the waveform. Collectively, all these approaches seek to avoid the top scenario in Fig. 24 (where the waveform and emission are different) in favor of the bottom scenario, in which the actual radar emission is a close approximation to the intended waveform.

An alternative perspective was recently proposed in [95]. By denoting $s(t;\mathbf{x}) = T_{C2W}\{\mathbf{x}\}$ as some arbitrary code-to-waveform implementation operation followed by the operation $u(t;\mathbf{x}) = T_{Tx}[s(t;\mathbf{x})]$ that represents the distortion imposed by the transmitter, a holistic waveform design formulation can be posed as shown in Fig. 25, in which $\Phi[u(t;\mathbf{x})]$ corresponds to the application of some metric such as those described in Section II.F. As opposed to the preceding linearization approaches that seek to compensate for transmitter distortion, this transmitter-in-the-loop paradigm instead seeks to optimize the final emission inclusive of the transmitter distortion effects. These distortion effects could leverage known mathematical models for the transmitter via a model-in-the-loop (MiLo) framework or by directly using the actual radar system via

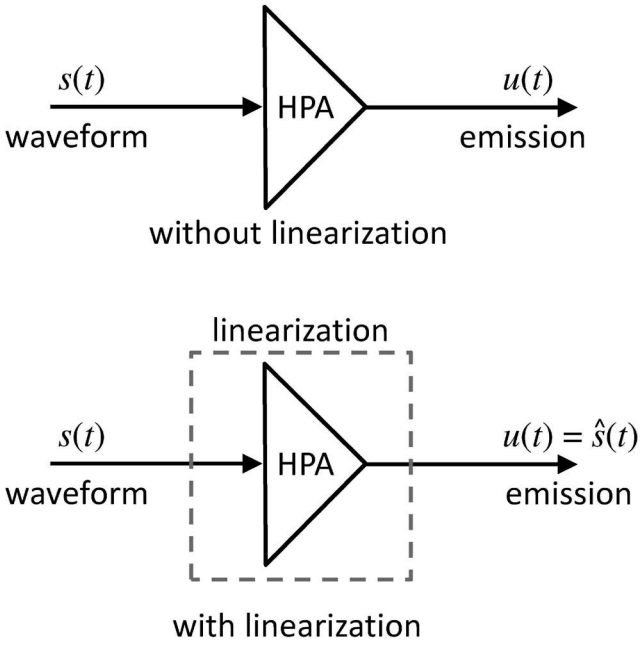

Fig. 24.
Transmitter generation of (top) distorted version of intended waveform and (bottom) near approximation to intended waveform via linearization.

a hardware-in-the-loop (HiLo) framework. The tradeoff between these is faster convergence for the former and greater accuracy for the latter. Some form of hybridization of MiLo and HiLo would likewise yield the best speed vs. accuracy tradeoff in practice.

An interesting feature of the transmitter-in-the-loop design paradigm is that the linearization methods discussed previously can still be incorporated into the transmitter architecture as a means of facilitating greater design freedom. This notion of joint transmitter and waveform optimization, which was inspired by observations of sensing performance by dolphins despite their "mediocre equipment" [24], has been suggested [165] as a promising direction to explore to address the expected continued erosion of radar spectrum [5] combined with increased "network densification" of interferers expected from future wireless systems [166]. Leveraging previous "spectrally clean" emission schemes [152], such joint design approaches have already begun to emerge [167, 168]. Specifically, [168] proposes the Smith tube concept as an extension to the well-known Smith chart used in RF systems engineering, whereby the vertical component (making it a tube) can be some other optimizable parameter such as waveform bandwidth. Moreover, Fellows et al. [168] envision further extension to a veritable Smith hypertube composed of multiple optimizable waveform parameters while maintaining transmitter PAE.

Finally, given the high-dimensional solution space for waveform design, further complicated if one considers the emission induced by transmitter distortion like that in Fig. 25, one can surmise that numerous local minima exist. Though it is not necessary to determine the global minimum as long as a predetermined performance specification is met (multiple "good enough" solutions could be beneficial from an operational flexibility perspective), the determination of the sufficiently good waveform(s) may still be a challenge. Thus, although myriad search strategies exist that one could take [169], some general observations about waveform design are useful to consider: 1) per (II.D2) the delay-Doppler ambiguity function integrates to a constant, thereby establishing a conservation of ambiguity; 2) as depicted in Fig. 8 for LFM, the ambiguity function for a chirp-like waveform exhibits a delay-Doppler ridge so that, by using the previous observation, a significant portion of the total ambiguity is already "absorbed"; and 3) metrics such as PSL (II.F1) and ISL (II.F3), and even PSD-based metrics such as FTE (II.F4), are complementary measures of the same delay-Doppler ambiguity function. Based on these observations, the recently emerged performance diversity paradigm [95] uses an LFM signal as an initialization to start with a well-consolidated ambiguity ridge and then alternates between different metrics during a greedy search to help avoid local minima, because each complementary metric still exhibits a different performance surface. One could even consider various combinations of these metrics to provide even more different performance surfaces upon which to search. Refer to [95, 103] as a starting point for further reading on the optimization of physical waveforms.

B. ENVIRONMENT-SPECIFIC WAVEFORMS

The RF environment in which radar operates continues to become more congested, which conflicts with the radar community's sustained need for ever-better detection, discrimination, and tracking. Thus, whereas Section III.A discussed the optimization of physically realizable waveforms in a general context, this section considers the impact of the radar environment on waveform design.

Section II.F discussed how the PSD, because of its Fourier relationship with the autocorrelation, is useful for waveform design. For example, one could determine a desired autocorrelation, determine the associated PSD, and then optimize a waveform to match that PSD (e.g., the FTE metric defined in (II.F4)). It is known for NLFM waveform design that to achieve low range sidelobes, the signal spectrum should decrease toward the band edges

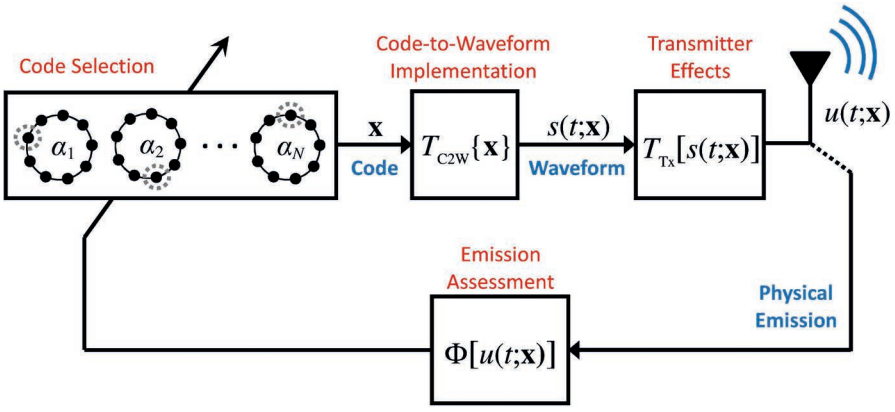

Fig. 25.
Transmitter-in-the-loop optimization of radar emissions.

[59]. However, growing spectral congestion driven by the demands for commercial cellular [5] has motivated research into how radar and communications could share spectrum [170–173]. For example, one could insert notches into the radar spectrum to avoid other in-band or near-band spectrum users, both as a means to facilitate more efficient use of the spectrum via sharing [174] and to remediate the associated degradation to radar performance [175]. Doing so in a manner that involves listening to the spectral environment [176] and modifying one's emissions accordingly [177] is considered a form of cognitive sensing [178, 179]. Because they collectively operate in the congested HF, VHF, and UHF bands, the modalities of OTH radar [148], foliage penetration (FOPEN) radar [180], GPR [181], and urban sensing [89] have been already been contending with this problem for quite some time. A survey of the challenges of radar spectrum engineering can be found in [5, 165].

An early approach to avoid other in-band spectrum users incorporates notches into swept-frequency waveforms [182]. The same could be achieved for a stepped-frequency waveform, for which the center frequency of the mth pulse in the CPI is incremented by $m\Delta f$ (described in Section III.E), either by skipping the pulses for which the associated frequencies are to be avoided [180, Chap. 5] or using an additional within-pulse phase coding to "thin the spectrum" [183]. Many subsequent phase-code and NLFM "sparse frequency" waveform design approaches have been developed [184–193].

An important practical aspect involved with designing waveforms that possess spectral notches is whether the waveform remains constant amplitude for injection into an HPA, or at least to what degree the AM effects are minimized if linear amplification is feasible for the sensing application. Furthermore, because ambiguity is conserved, the presence of in-band spectral notches tends to translate into a broadening of the out-of-band spectrum if constant amplitude is preserved. As spectral congestion continues to grow, one must also be cognizant of the increase in range sidelobes that is incurred as the penalty for spectral notching [194], as well as the prospect of "power struggles" [195] as cognitive systems attempt to outmaneuver one another.

Another form of environment-specific waveform arises when one considers how to design a waveform to emphasize known (or at least hypothesized) attributes of a desired target. In [196], Bell applied information theory to formulate waveform designs that rely on presumed knowledge of a target's impulse response either to maximize probability of detection or to maximize the amount of information gleaned from the target response. Such signals are called matched illumination as coined by Gjessing [197, 198]. Since then, considerable work has appeared (e.g., [199–210]) exploring the ways in which the radar could perform the alternating process of 1) observing the environment with a given waveform and then 2) reformulating a new waveform to capture or enhance some additional salient feature of the environment. For example, successive refinement of the waveform may permit better discrimination between different classes of targets or between targets and the ambient clutter. Because it relies on this query-and-revise strategy, the concept of time reversal has also been investigated for this problem (e.g., [211–213]), albeit with a cautionary note on the electromagnetics provided in [214]. Regardless of the specific approach, this notion of adaptive waveform design can be viewed as a form of cognitive sensing [178, 179]. Such waveforms must still adhere to the physical requirements imposed by the radar transmitter, antenna included, as discussed in Sections II.G and III.A. See [178, 179] as a starting point for further reading on cognitive sensing and adaptive waveform design.

The waveforms used for nonlinear harmonic radar [215–220] generally require particular consideration of their spectral containment to enable adequate discrimination between nonlinear and (typically far stronger) linear scattering. For example, because electronics typically contain diodes and transistors that can produce such a nonlinear response, this form of radar is considered a means to detect, and perhaps even to discriminate, electronics in the illuminated environment. In principle, if one can generate a pure sinusoid at frequency f_0, then a nonlinear response would occur at $2f_0$ and higher integer multiples. The difficulty is that this harmonic response tends to be orders of magnitude smaller than the linear response [221] and could be masked by harmonics generated by the transmitter itself if the emission does not possess sufficient spectral purity [218]. This form of radar has yielded some rather interesting applications, such as a nonlinear junction detector to enable countersurveillance by sweeping for listening devices [220] and the tracking of insects using RF tags composed of Schottky diodes [216].

The related concept of stimulated emissions relies on RF receivers, such as those in cell phones, producing an identifiable signal when illuminated by an appropriate stimulation signal [222]. One can even induce an intermodulation effect within the nonlinear device by using multiple signals to produce a desired emitted waveform [217, 223]. For example, higher-order intermodulation products are produced when a nonlinear device is simultaneously interrogated with tones that have frequencies of f_1 and f_2. These and higher-order mixing products facilitate the "fingerprinting" of different commercial RF devices [217]. From an operational sensing standpoint, the detection or identification of unknown electronic devices could therefore follow the sequential interrogation paradigm discussed earlier for adaptive waveform design, albeit with the inclusion of the nonlinear response [224]. A survey of recent work in this area can be found in [217].

Finally, the clutter response generated by the radar may provide the spectral environment in which other signals could be designed to reside. The resulting notion of radar-embedded communication involves the generation of either interpulse [225–228] or intrapulse [229–232] signals that are designed to be embedded within ambient radar scattering by RF transponders or tags as a means to self-identify friendly targets (blue force tracking), to enable environmental monitoring, or to provide a covert communication link. In general, the interpulse form [225–228] encodes information into the radar backscatter via pulse-to-pulse modulation so that the communication signal resides in the slow-time (Doppler) domain. This form is well tested, with Sandia's Athena tag being a notable example [233]. The data rate, however, is on the order of bits per CPI, which is quite low for any useful communication mode, aside from self-identification.

In contrast, the intrapulse form [229–232] involves the determination of a set of $K = 2^{\#\text{bits}}$ communication symbols $\{c_1(t), c_2(t), \ldots, c_K(t)\}$ that have minimal mutual cross-correlation yet have commensurate correlation with the ambient scattering produced by

the radar waveform $s(t)$. The former requirement maximizes the separability of the symbols on receive, while the latter mitigates receiver bias that could be generated by the radar clutter. This form of radar-embedded communication, while still at the theoretical stage, enables a data rate of bits per pulse, thus scaling with PRF such that data rates commensurate with speech may be possible. Starting points for further reading on interpulse and intrapulse radar-embedded communication are [226] and [229], respectively.

C. COLOCATED MIMO RADAR

The category of WD denoted as MIMO has arguably received more attention than all the rest combined based on the sheer volume of publications. Inspired by the capacity and performance gains enabled by spatial diversity for MIMO communications [234, 235], the early notions of MIMO radar [236–238] sought to generalize the prior concept of ubiquitous radar [239], in which the transmitter illuminates a wide spatial beam combined with multiple narrow receive beams to facilitate spatial diversity on transmit. The terminology was also separately used to refer to joint operation of multiple, widely separated transmitters and receivers [240]. Many of these ideas built on even earlier work, such as multiple simultaneous transmit beams for phased arrays [241], that was realized on the advanced multifunction RF concept (AMRFC) testbed [242], and spatiotemporal coding for radar array processing [243], which were themselves predated by the French Synthetic Antenna and Impulse Radar (RIAS) system [244–246]. The latter was experimentally performing "transmit beamforming on receive" well before the term MIMO was used in the radar context.

A collection of much of the early theoretical work on MIMO radar was compiled in [247]. Today, MIMO radar is generally considered to belong to one of two types: colocated MIMO in which phase coherence can be assumed; and distributed (or statistical) MIMO in which phase coherence typically cannot be assumed, though there are exceptions [248, 249]. The latter can be treated under the umbrella of the more traditional nomenclature of multistatic radar and is discussed in Section III.D, while we will focus here on the notion of colocated MIMO.

In general, colocated MIMO involves the generation of different waveforms from different antenna elements (or subarrays of elements [250–252]). For example, given a linear array of L elements indexed by $\ell = 1,2,\ldots,L$, the set of distinct waveforms $\{s_\ell(t)\}$ can be defined according to the waveform structures from Section II.B. Likewise for a planar array, the MIMO waveforms could be indexed according to the horizontal and vertical antenna elements, thereby providing a spatially diverse emission structure in both azimuth and elevation angles.

For the ubiquitous MIMO emission of a wide transmit beam, these waveforms should be designed to possess a low cross correlation—the term "orthogonal" has been widely used, but it is a misnomer for radar if the waveforms have overlapping spectral support, per the Wiener-Khintchine theorem, because no assumption of synchronicity of radar echoes can be made. This ubiquitous mode could be a means to enable multifunction operation [238, 239] if the tradeoff between the loss in transmit spatial gain and the increased dwell time is feasible for the given operating parameters [253, 254]. Of course there are other means to achieve a multifunctional capability. For example, the AMRFC [242] assigns different functions to different array subapertures. That said, enhanced spatial resolution and reduced spatial sidelobes have been demonstrated for MIMO relative to a non-MIMO mode [255]. Sensing modes such as SAR, in which the transmit beam is intentionally broad so as to capture the long synthetic aperture, could be inherently well suited for the wide beamwidth provided by such a MIMO emission [256].

The notion of partially correlated waveforms has also been proposed [251], in which the set of MIMO waveforms lie somewhere between the extremes of fully coherent (identical aside from a subsumed phase shift for beam steering) and completely independent waveforms that facilitate ubiquitous operation. As such, greater design freedom is available to shape the spatiotemporal structure of the radar emission, thereby providing greater control over the trade between mainbeam gain and spatial diversity.

MIMO radar has also been a source of controversy as some radar systems engineers question the validity of some of the theoretical claims of MIMO [253, 254, 257], going so far as to suggest that it could be "snake oil" [253]. However, there are some clear practical applications of MIMO radar. A case in point is OTH radar [258] in which the transmitted and received signals are reflected off various layers of earth's ionosphere in transit each way. Experimental results in [259] have shown that the transmit-beamforming-on-receive spatial diversity of MIMO radar, which Frazer et al. refer to as "non-causal transmit beamforming," provides greater separability of OTH radar echoes because of the inherent range or angle coupling that exists for the skywave propagation channel.

Another way of looking at the MIMO emission structure is via the far-field fast-time signal as a function of spatial angle, which is intuitively attractive because it is this signal that is physically incident upon a scatterer. Consider a uniform linear array with interelement spacing d and wavelength λ, in which the ℓth antenna element emits the narrowband pulsed waveform $s_\ell(t)$ for $0 \le t \le T$. The far-field emission (baseband representation) at time t for transmit spatial angle $-90° \le \phi_T \le 90°$ can thus be expressed as

$$g\left(t,\phi_T\right) = \frac{1}{L}\sum_{\ell=1}^{L} s_\ell(t) e^{j(\ell-1)\bar{\phi}_T} \tag{III.C1}$$

where $\bar{\phi}_T = 2\pi d \sin\left(\phi_T\right)/\lambda$ is the transmit electrical angle for $\phi_T = 0°$ at array boresight. Integrating (III.C1) over the pulsewidth and dividing by T therefore yields the aggregate beampattern

$$B\left(\phi_T\right) = \frac{1}{T}\int_0^T g\left(t,\phi_T\right) g^*\left(t,\phi_T\right) dt \tag{III.C2}$$

as a function of transmit spatial angle ϕ_T. For the simplified case in which $s_\ell\left(t\right) = s\left(t\right)e^{-j\ell\phi_{look}}$ and the electrical angle ϕ_{look} corresponds to an arbitrary spatial "look" direction, (III.C2) is just the standard array factor beampattern [260].

Where the delay-Doppler ambiguity function developed by Woodward [91] (II.D1) describes the MF response to different Doppler-shifted versions of a waveform, it is likewise useful to define a delay-angle ambiguity function for MIMO operation. For receive spatial angle ϕ_R and the similarly specified receive electrical angle $\bar{\phi}_R$, the unity-gain normalized MF can be defined as

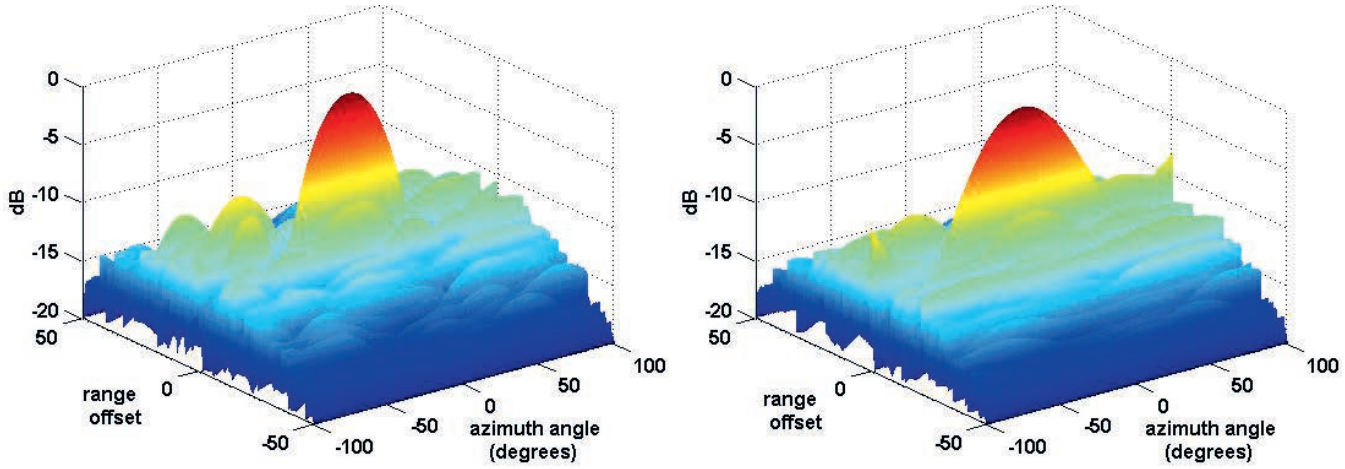

Fig. 26.
Delay-angle ambiguity function for 16 waveforms generated via DPSK implementation of length-50 random binary codes, where (left) no mutual coupling is present and (right) −10 dB nearest-neighbor mutual coupling is present but not accounted for on receive. Result is degraded resolution and 1.1 dB mismatch loss.

$$h\left(t,\phi_{\mathrm{R}}\right)=\frac{g\left(t,\phi_{\mathrm{R}}\right)}{\sqrt{\int_0^T g\left(t,\phi_{\mathrm{R}}\right)g^*\left(t,\phi_{\mathrm{R}}\right)dt}}\quad .\qquad \text{(III.C3)}$$

Thus, the combination of receive beamforming by the L antenna elements in the direction ϕ_{R} and associated pulse-compression matched filtering as a function of receive angle realizes the delay-angle ambiguity function

$$\chi_{\text{delay-angle}}\left(\tau,\phi_{\mathrm{T}},\phi_{\mathrm{R}}\right)=\frac{\int_0^{\infty}\left[\sum_{\ell=1}^{L}g\left(t,\phi_{\mathrm{T}}\right)e^{j(\ell-1)\bar{\phi}_{\mathrm{T}}}g^*\left(t-\tau,\phi_{\mathrm{R}}\right)e^{-j(\ell-1)\bar{\phi}_{\mathrm{R}}}\right]dt}{L\sqrt{\int_0^T g\left(t,\phi_{\mathrm{R}}\right)g^*\left(t,\phi_{\mathrm{R}}\right)dt}}\qquad \text{(III.C4)}$$

that describes the response that a given set of emitted waveforms would produce when reflected by a point scatterer in the environment as a function of angle and relative delay. Using (II.D1), the delay-angle ambiguity function of (III.C4) readily generalizes to a delay-Doppler-angle ambiguity function given by

$$\chi_{\text{delay-Doppler-angle}}\left(\tau,f_{\mathrm{D}},\phi_{\mathrm{T}},\phi_{\mathrm{R}}\right)=\frac{\int_0^T\left[\sum_{\ell=1}^{L}e^{j2\pi f_{\mathrm{D}}t}g\left(t,\phi_{\mathrm{T}}\right)e^{j(\ell-1)\bar{\phi}_{\mathrm{T}}}g^*\left(t-\tau,\phi_{\mathrm{R}}\right)e^{-j(\ell-1)\bar{\phi}_{\mathrm{R}}}\right]dt}{L\sqrt{\int_0^T g\left(t,\phi_{\mathrm{R}}\right)g^*\left(t,\phi_{\mathrm{R}}\right)dt}}\qquad \text{(III.C5)}$$

and likewise incorporates the impact of a coherent pulse train in the same manner as (II.E1). Different forms of the MIMO ambiguity function can be found in [247, 261–263], along with more detailed discussion of the associated properties.

The true discrimination capability of the much increased dimensionality provided by MIMO may also necessitate adaptive receive processing that leverages this high dimensionality, which comes with an additional tradeoff that could involve a significant increase in computation cost. However, just as space–time adaptive processing (STAP) [264] enables an interference suppression capability that could not be achieved using adaptive beamforming or Doppler processing alone, MIMO-oriented adaptive processing may likewise enable such new capabilities. For example, it was recently demonstrated experimentally [265, 266] that a MIMO formulation could be used to generate a joint space-frequency null on transmit to avoid interfering with other nearby spectrum users.

MIMO waveforms possess the same physical requirements and undergo the same transmitter effects as non-MIMO waveforms per Section II.G, therefore necessitating consideration of practical waveform design as discussed in Section III.A. Furthermore, because the physical MIMO emission inherently depends on the interaction between the set of L waveforms and the distributed antenna elements in the array, the electromagnetic effects of the array must likewise be considered. For example, mutual coupling among antenna elements, which involves neighboring antenna elements receiving and reradiating the waveform from a given element, produces a distortion of the far-field delay-angle emission structure relative to the ideal case of no mutual coupling (Fig. 26) [267, 268].

Another practical impact of MIMO arises when attempting to emit wideband signals over a wide beamwidth, such as desired for SAR [269]. For narrowband operation, the wavelength λ of the center frequency is an adequate approximation over the entire bandwidth. Thus, interelement spacing of d (=λ / 2) is the maximum value that avoids grating lobes (though if the MIMO array takes advantage of the virtual array concept to more widely separate the elements for enhanced spatial resolution, phase discontinuity effects must still be considered [270]). In contrast, when the bandwidth becomes sufficiently large that a single wavelength is not a good approximation, one could set $d = \lambda_{\text{min}}/2$, for the shortest wavelength λ_{min} corresponding to the highest in-band frequency to avoid grating lobes for all corresponding frequencies in the passband [271]. However, this choice has the undesired effect of yielding interelement spacing for the longer wavelengths (lower frequencies) such that $d/\lambda \ll 0.5$, which can result in emission of power into the imaginary space (or invisible space) [258] that exists beyond the endfire spatial directions at $\phi_{\mathrm{T}} = \pm 90°$ (Fig. 27). However, this power is not actually

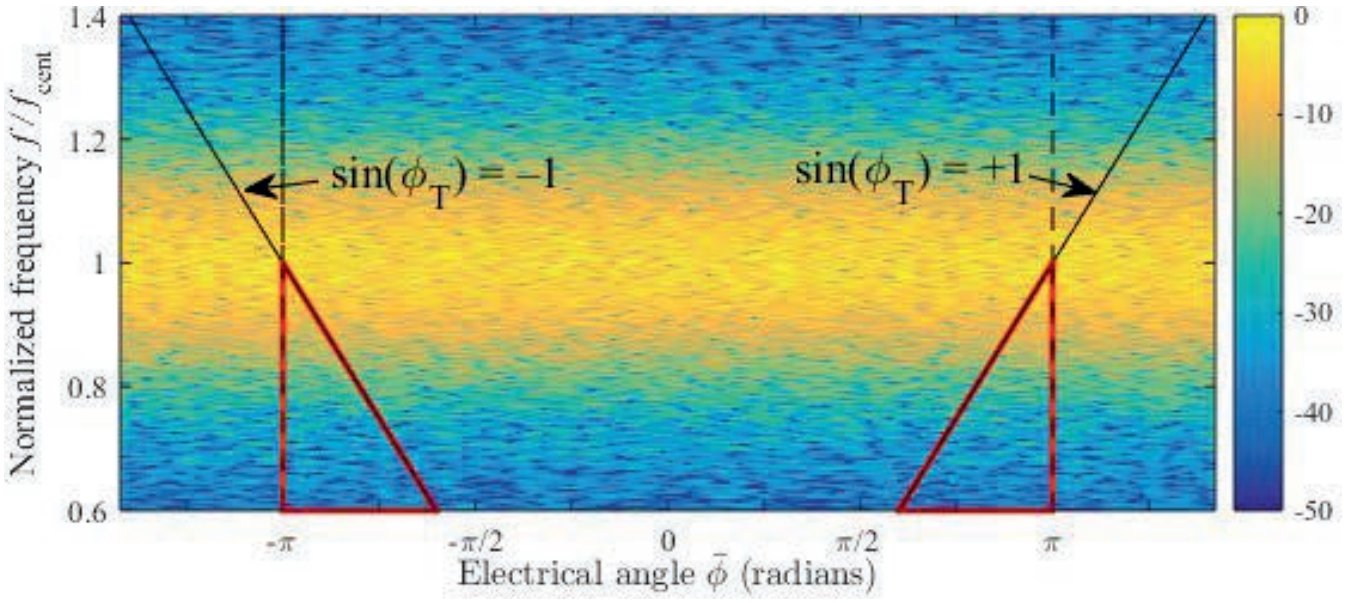

Fig. 27.
Wideband frequency content vs. electrical angle for MIMO emission. Element spacing is half-wavelength for center frequency f_{cent} (so $d = 0.5\ \lambda_{cent}$) and bandwidth is 30% relative to center frequency. Red triangles identify invisible space. Alternatively, setting $d = 0.51\ \lambda_{min}$ would raise location of red triangles in figure so that more of emission would be into invisible space.

emitted as it becomes energy that is stored in the reactive near field of the array and can lead to large amounts of power being reflected back into the transmitter, potentially damaging the radar [253]. The implication for MIMO is that waveform design must account for the relative instantaneous phase difference between waveforms on adjacent antenna elements so as to avoid exceeding the boundaries of real space [272].

Another notable form of MIMO is the frequency diverse array (FDA) [273–277], in which all antenna elements emit the same waveform, aside from a small frequency shift that is incremented across the array. In other words, the carrier frequency for the waveform generated by the ℓth antenna element is $f_C + (\ell - 1)\Delta f$, where f_C is a nominal carrier frequency and Δf is the small frequency increment. As a result, the beamforming look direction varies in fast time and sweeps across space at a rate depending on the value of Δf. Because it maintains a coherent mainbeam (the location of which changes with time), the FDA can be expected to experience less degradation than arbitrary MIMO as a result of mutual coupling effects. The relevant concept of circulating codes [278, 279] provides an alternative perspective to forming such spatially swept beams through the use of small time shifts $t + (\ell - 1)\Delta t$ across the array.

Inspired by fixational eye movement [280, 281], the FDA framework has also recently been subsumed by the notion of spatial modulation [282], which provides the freedom to change the rate and direction of fast-time spatial steering via an extension of the PCFM coding in (III.A4). For example, relative to standard beamforming, Fig. 28 illustrates the aggregate beampattern from (III.C2) when using spatial modulation with a planar array to traverse a circle during the pulsewidth [283].

As is known for STAP [264], the increase in useful degrees of freedom obtained by coupling the antenna's spatial channels with the slow-time (Doppler) channels of the pulses in the CPI is most notably useful when employed adaptively. The same holds true for the increased degrees of freedom afforded by MIMO emissions. Because of the myriad ways in which MIMO can be realized, juxtaposed against the numerous different types of radars, it is not surprising that many different adaptive MIMO receive processing algorithms have emerged (e.g., [284–289]). These approaches all seek to exploit the much increased dimensionality to enhance sensing performance, that is, to improve resolution and discrimination, sidelobe suppression, and interference rejection. As with STAP, MIMO also incurs the "curse of dimensionality" in terms of higher computational cost and possibly higher sample data requirements (depending on the nature of

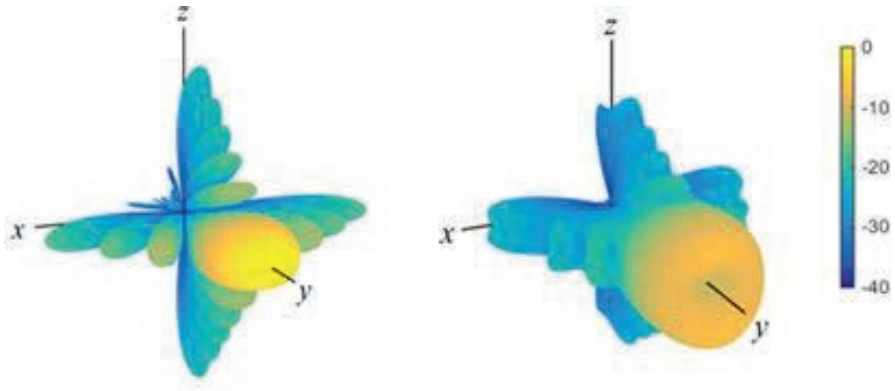

Fig. 28.
2D aggregate beampattern via planar array for (left) standard beamforming and (right) circular spatial modulation.

the algorithm). Furthermore, any such adaptive algorithm must rely on models of physically realizable waveforms that can be transmitted by a radar, if possible even using captured replicas of the actual emissions to ensure maximum fidelity, and must appropriately consider the straddling effect that arises from discretization [110, 263, 288].

Finally, it is worth noting some of the concepts that have emerged from the ubiquitous notion of MIMO radar. As a countermeasure to combat passive bistatic exploitation of the emission of an active radar, the idea of bistatic denial was developed [290], in which a secondary waveform is emitted to mask the spatial sidelobes of the primary waveform. More recently, a counter-countermeasure was proposed [291] that seeks to estimate the primary waveform in the presence of the secondary waveform interference (from the perspective of the bistatic radar). The MIMO-enabled increased degrees of freedom have also been exploited to facilitate the embedding of communications within the radar emission [292–294]. Additional forms of radar-embedded communication are discussed in the next two sections. A good subset of references to begin further reading on colocated MIMO is [238, 247, 253, 256, 258, 276].

D. DISTRIBUTED APERTURE RADAR

While the colocated MIMO formulation in the previous section employs WD to realize delay-angle coupled radar emissions with greater design degrees of freedom, the notion of distributed aperture radar considers multiple antenna apertures with considerable spatial separation. This arrangement has been known by many names, including netted radar [295, 296], statistical MIMO [240, 297–299], and more classically as multistatic radar or multisite radar [300–305]. In this formulation, practical realization of phase coherency may be difficult (though progress continues [306, 307]), thus often necessitating noncoherent combining to perform target detection using the distributed apertures. Furthermore, this arrangement also includes the advantageous exploitation of other emitters in the environment, for which one has no control over the structure of the associated waveforms.

A prospective benefit of this distributed arrangement is a way to address the aspect angle dependence of a target's radar cross section (RCS), which may vary by tens of decibels as the target moves with respect to the radar. The well-known Swerling models [308] can be used to represent how such RCS fluctuations behave statistically as a function of the target decorrelation time (scan to scan or pulse to pulse) [53, Chap. 7]. Frequency diversity has long been used to realize this same fluctuating RCS effect to improve target detection [309–312].

The distributed coherent aperture X-band radar experiments undertaken by MIT Lincoln Lab [248, 249] demonstrated the use of low cross-correlation waveforms to perform time and phase synchronization of the incident waveforms upon a selected target (in this case, the application was ballistic missile defense). Once sufficient synchronization was achieved, the same waveform could be used across the distributed aperture to realize a cohere-on-transmit (or effectively cohere-on-target) mode yielding a 9 dB SNR gain.

The general notion of a distributed aperture dates back to the earliest work in radar, where the waveforms employed were typically CW and the transmit and receive antennas were separated in a bistatic configuration for various operational and technical reasons (see Chaps. 1 and 2 of [11] for a fascinating historical review of the subject). For the bistatic arrangement, it has been shown [313, 314] that the delay-Doppler ambiguity function, referenced to the receiver, can be expressed as follows (modifying the nomenclature for consistency)

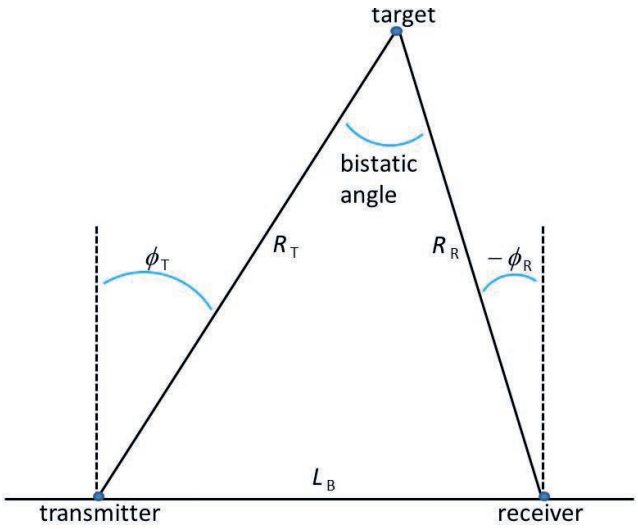

Fig. 29.
Bistatic geometry.

$$\chi_{\text{bistatic}}\left(R_R^{(\text{h})}, R_R^{(\text{a})}, \mathbf{v}^{(\text{h})}, \mathbf{v}^{(\text{a})}, \phi_{\text{R}}, L_B\right) = \int_{-\infty}^{\infty} s\left(t-\tau^{(\text{a})}\left[R_R^{(\text{a})}, \phi_{\text{R}}, L_B\right]\right) s^*\left(t-\tau^{(\text{h})}\left[R_R^{(\text{h})}, \phi_{\text{R}}, L_B\right]\right) \times \exp\left\{-j2\pi\left(f_{\text{D}}^{(\text{h})}\left[R_R^{(\text{h})}, \mathbf{v}^{(\text{h})}, \phi_{\text{R}}, L_B\right] - f_{\text{D}}^{(\text{a})}\left[R_R^{(\text{a})}, \mathbf{v}^{(\text{a})}, \phi_{\text{R}}, L_B\right]\right)\right\} \quad \text{(III.D1)}$$

The superscripts (a) and (h) denote the actual and hypothesized values of delay τ and Doppler frequency f_{D}, which are themselves nonlinear functions of the target velocity vector $\mathbf{v}$ and the bistatic geometry depicted in Fig. 29. The bistatic angle is implicitly defined via the transmitter-to-target, receiver-to-target, and baseline transmitter-to-receiver distances R_{T}, R_{R}, and L_{B}, respectively.

In recent years there has been an explosion of research on many aspects of bistatic radar, particularly the exploitation of illuminators of opportunity such as FM radio, broadcast television, commercial cellular, etc. (see surveys in [13, 315]). This general research area has been called passive radar, hitchhiking, passive coherent location, and more recently commensal radar. While one has no control over the waveforms used by the illuminators of opportunity; and thus, it is fair to assume that such waveforms are generally not optimal for a sensing application, the delay-Doppler ambiguity functions for these signals can be inferred based on the type of signal and its purpose (see [316, 317] and [13, Chap. 6]). For example, analog FM radio has been found to realize an ambiguity function that is highly dependent on the nature of signal content (for example, speech vs. music, as well as the tempo of the latter as shown in Fig. 30) and the signal structure (the chrominance subcarrier of analog television contains a repeating structure

that produces strong ambiguities in range and Doppler per Fig. 31). In contrast, more recent digital modulation schemes produce delay-Doppler ambiguity functions that tend toward a thumbtack response (Fig. 32).

The bistatic ambiguity function of (III.D1) has also been generalized in different ways to account for multiple emitters in a multistatic configuration [318–320]. It then becomes necessary to consider how best to select from among the myriad emitters (and their subsequent echo responses) that may be present [321, 322] and then how to combine the responses in the most advantageous way based on the observed or known signal structures and the multistatic geometry [323–326]. When concerned with image formation, this approach has also been called RF/microwave tomography [327–330]. Surveys of bistatic and multistatic radar techniques can be found in [11–14, 302–304].

E. WAVEFORM AGILITY

Where the previous two sections considered the impact of WD via the spatial dimension, here we consider the implications of changing the waveform pulse to pulse during a CPI. Known as pulse agility, pulse diversity, or waveform agility, this arrangement provides increased degrees of freedom that may be used to suppress range sidelobes, to extend maximum unambiguous range, to enable radar-embedded communication, and potentially to improve robustness to structured interference (e.g., commercial communications).

Complementary codes, originally proposed by Golay in the 1960s [39], are a form of waveform agility in which the pulse compression responses from two or more codes sum to produce an overall response whereby the range sidelobes cancel, leaving only the mainlobe [44, 331–335]. Using (III.C1), the combined responses from a complementary set composed of M waveforms can be expressed as

$$\sum_{m=1}^{M} h_{\mathrm{MF},m}(t) * s_m(t) \approx \delta(t) \tag{III.E1}$$

where $\delta(t)$ is a Dirac delta and the approximation denotes that this ideal response would comprise the pulse compression mainlobe of finite bandwidth waveforms. It was shown in [336] that a similar result could be obtained by modulating a given waveform (e.g., LFM) with a set of orthonormal codes. While the complementary arrangement would seem to solve the range-sidelobe problem, the sidelobe suppression performance for complementary codes is known to degrade when the signal structure deviates from the ideal, such as when generated by a physical transmitter (because of bandlimiting and distortion) or when Doppler is present. That said, continued work is exploring ways in which to improve the Doppler tolerance limitation [335, 337, 338] and practical transmitter effects could be incorporated such as discussed in Section III.A.

Another well-known form of waveform agility is called stepped frequency, synthetic wideband, or frequency jumped burst and essentially involves a center frequency offset of Δf between adjacent pulses [339, Chap. 5]. The benefit of stepped frequency waveforms is that wideband, hence high-range resolution, sensing can be achieved while avoiding the complexity and cost of wide-

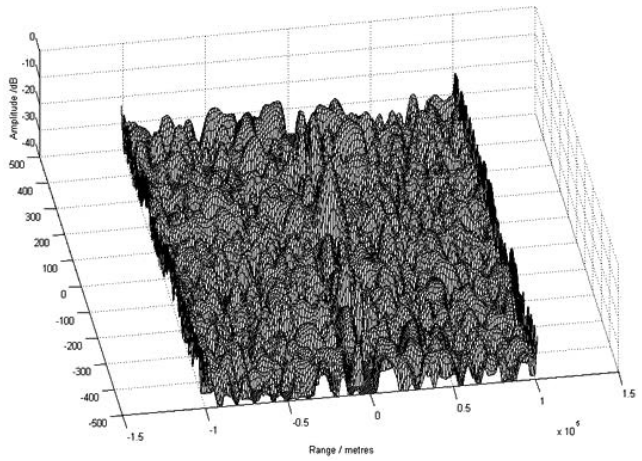

Fig. 30.
Delay-Doppler ambiguity function of fast tempo jazz on FM radio (courtesy of Prof. Hugh Griffiths, University College London).

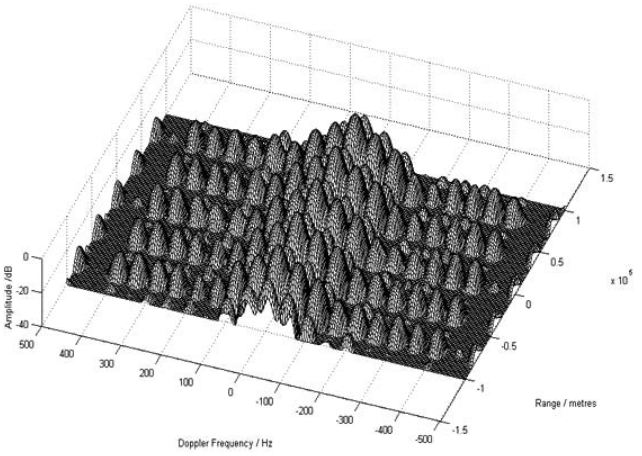

Fig. 31.
Delay-Doppler ambiguity function of chrominance subcarrier of analog TV (courtesy of Prof. Hugh Griffiths, University College London).

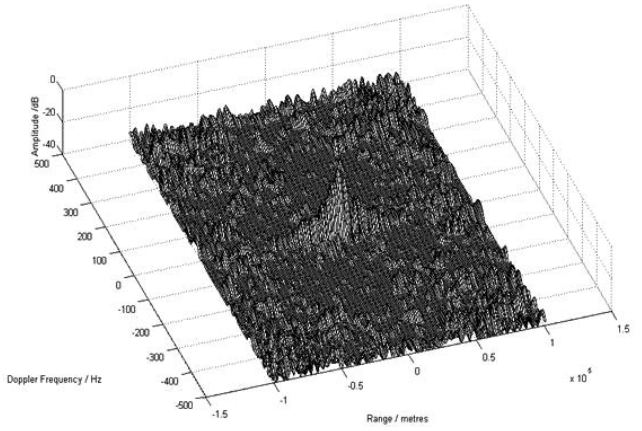

Fig. 32.
Delay-Doppler ambiguity function of digital audio broadcast (courtesy of Prof. Hugh Griffiths, University College London).

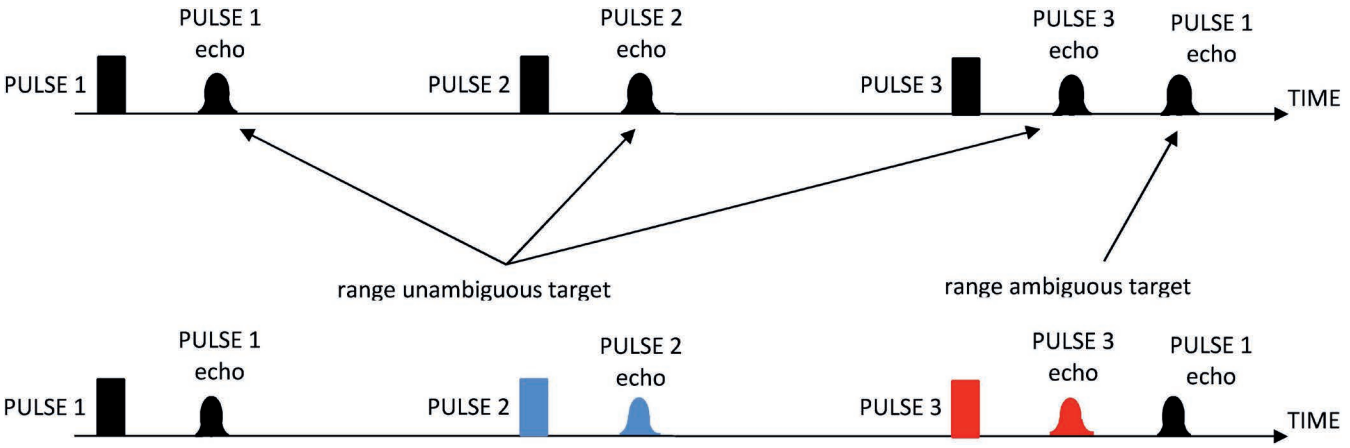

Fig. 33.
Same pulse is repeated throughout CPI (top) so that distant target is range ambiguous, while target could be range ambiguous if different waveforms were used within CPI (bottom).

band hardware. Instead, a burst of narrowband pulses with offset center frequencies is generated, with the resulting received echoes pulse compressed as usual according to each waveform and then coherently combined across the set of pulses (e.g., via inverse fast Fourier transform). Assuming the same waveform is repeated over the set of frequency steps, it was shown in [10] that the delay-Doppler ambiguity function for the overall stepped-frequency emission can be generalized from (II.E1) as

$$\left|\chi_{\mathrm{SF}}\left(\tau, f_{\mathrm{D}}\right)\right| = \left|\chi\left(\tau, f_{\mathrm{D}}\right)\right| \left|\frac{\sin\left(M\pi\left(f_{\mathrm{D}} + k_{\mathrm{s}}\tau\right)T_{\mathrm{PRI}}\right)}{M\sin\left(\pi\left(f_{\mathrm{D}} + k_{\mathrm{s}}\tau\right)T_{\mathrm{PRI}}\right)}\right| \quad \text{for } |\tau| \le T \quad \text{(III.E2)}$$

where $|\chi(\tau,f_{\mathrm{D}})|$ is the ambiguity function of the single waveform and

$$k_{\mathrm{s}} = \pm\frac{\Delta f}{\mathrm{PRI}} \quad \text{(III.E3)}$$

is the LFM ramp applied across the CPI.

A problem with using a constant pulse-to-pulse frequency offset across the CPI is the appearance of grating lobes. Consequently, much of the work on this type of emission scheme has focused on how to design the frequency offsets and the selection of the individual pulsed waveforms so as to reduce these grating lobes [183, 340–345]. As discussed in Section IV.B and [180, Chap. 5], the stepped-frequency emission structure also provides a convenient way in which to avoid other in-band spectrum users, albeit with an expected degradation in sidelobe performance. The related concepts of frequency agility [309–312] and frequency diversity [346, Chap. 12], which provide robustness to frequency-dependent target RCS fluctuations and radar countermeasures, respectively, likewise involve a pulse-to-pulse change of the center frequency, even though generally not in as clearly structured a manner as with stepped frequency. The stepped-frequency scheme bears some similarity in mathematical construction, if not the domain in which it is applied, to the more recent MIMO concept of the FDA of Section III.C. See [10, 53, 346] as a primer for further reading on complementary codes, stepped-frequency, and frequency-diverse operation.

Besides the preceding complementary coding and stepped-frequency concepts, waveform agility may provide an alternative to using multiple PRFs to extend the unambiguous range (Fig. 33) [347, 348, 53, Chap. 17], it may facilitate the embedding of communication or navigation information in radar emissions [349], and may even enable new forms of discrimination. As an example of the latter, a biomimetic form of waveform agility, called twin inverted pulse (TWIP), was recently developed for sonar [23] and radar [350]. TWIP mimics a waveform scheme employed by dolphins to discriminate between linear and nonlinear scattering in bubble-rich underwater environments [351, 352], such as those from the wakes of passing ships. In this formulation, pulse pairs are emitted, with the two pulses having opposite polarity ($s_2(t) = -s_1(t)$). Computing the ratio between the difference and sum of the resulting MF responses to these waveforms then provides a way to emphasize the nonlinear scattering relative to the linear scattering, as demonstrated experimentally in [350].

An earlier idea that arose to address range ambiguities was to incorporate a pulse-to-pulse phase coding [353–357]. Waveform agility can be viewed as a generalization of this idea—instead of phase coding the same waveform across the set of pulses, each pulse could be a different waveform. However, when changing the waveform pulse to pulse, clutter cancellation may be degraded for radar modes on which it is performed. Fig. 34 illustrates the MF response to each of four DPSK-implemented length-100 randomly generated binary codes, in which we can observe that the sidelobe structure is different for each. Clutter illuminated by waveforms such as these would experience a range sidelobe modulation effect over the CPI that in turn would limit the efficacy of clutter cancellation. Thus, if one is to consider waveform agility in the context of clutter cancellation, it is necessary 1) to compensate for the modulation effect, 2) to expand the dimensionality of the receive processing so as to perform fast-time (range) and slow-time (Doppler) processing jointly, or 3) to expand the overall dimensionality of the radar emission so that these sidelobes are simply driven into the noise, because they do not combine coherently.

In the case that only two different waveforms are used, and under the assumption that fast-time Doppler effects are negligible, one can satisfy the sidelobe similarity constraint [349]

$$h_{\mathrm{MF},1}(t) * s_1(t) = h_{\mathrm{MF},2}(t) * s_2(t) \quad \text{(III.E4)}$$

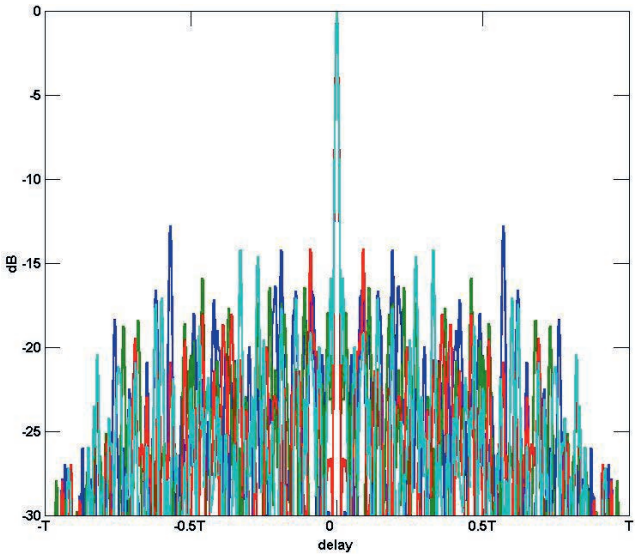

Fig. 34.
MF responses for four length-100 random binary codes implemented with DPSK. The sidelobes are quite different.

by setting $s_2(t) = s_1^*(T-t)$ such that $h_{MF,1}(t) = s_2(t)$ and $h_{MF,2}(t) = s_1(t)$. However, this constraint cannot be met for more than two waveforms because, in general, the frequency response for the mth filter would be

$$H_m(\omega) = \frac{S_1(\omega)H_1(\omega)}{S_m(\omega)} \tag{III.E5}$$

which is an infinite impulse response (IIR) filter because of the term in the denominator. Thus, the similarity constraint can only be met approximately for more than two waveforms by using MMFs of sufficient length. It was shown in [349], and subsequently extended in [358, 359], that a joint formulation of the least-squares-based MMF described in Section II.H provides this capability, with the caveat that the number of waveforms still be relatively small (say 4 or 5) because of the associated tradeoff of a general increase in sidelobes across the (now similar) MMF responses. In [360], this filter design problem was also considered from a convex optimization perspective.

One may also consider performing pulse compression and (slow time) Doppler processing jointly. An adaptive processing formulation for this joint perspective on waveform agility was developed in [361], though the associated computational cost is rather high. A nonadaptive approach was likewise conceived in [362] and subsequently was extended in [363]. While these joint processing schemes are clearly more complex and generally have a higher computational cost than performing pulse compression and Doppler processing separately, the multiplicative increase in adaptive degrees of freedom (not unlike that obtained via STAP [264]) provides the means to address the range-Doppler coupling that arises from range-sidelobe modulation of clutter. Furthermore, these schemes can be extended to incorporate multiple-time-around clutter, also known as range-ambiguous clutter or folded clutter that becomes more prevalent at higher PRF [364, 365, 366, Chap. 9.5].

Finally, an arguably more straightforward approach to addressing range-sidelobe modulation is simply to expand the dimensionality of the radar emission to such a degree that the sidelobes are driven into the noise, because they do not coherently combine. While not necessarily designed for this reason, one could contend that this effect occurs for noise radar [71–75] and the similar concept of chaotic radar [367–369]. For example, for the recently developed FMCW noise radar concept in [370], Fig. 35 illustrates the RMS average sidelobe response computed over 10^4 waveform segments (left) that is reduced by roughly 40 dB when coherently integrating over these segments (right) such as occurs with Doppler processing. Recently, this concept was also examined for a pulsed mode [371] where it was observed that a high PRF (100 kHz in this case) provides performance similar to the FMCW mode, while a lower PRF (1 kHz) necessitates additional receive processing, because the dimensionality is no longer high enough to drive the sidelobes into the noise. See [349, 361, 371] as a starting point for further reading on waveform agility.

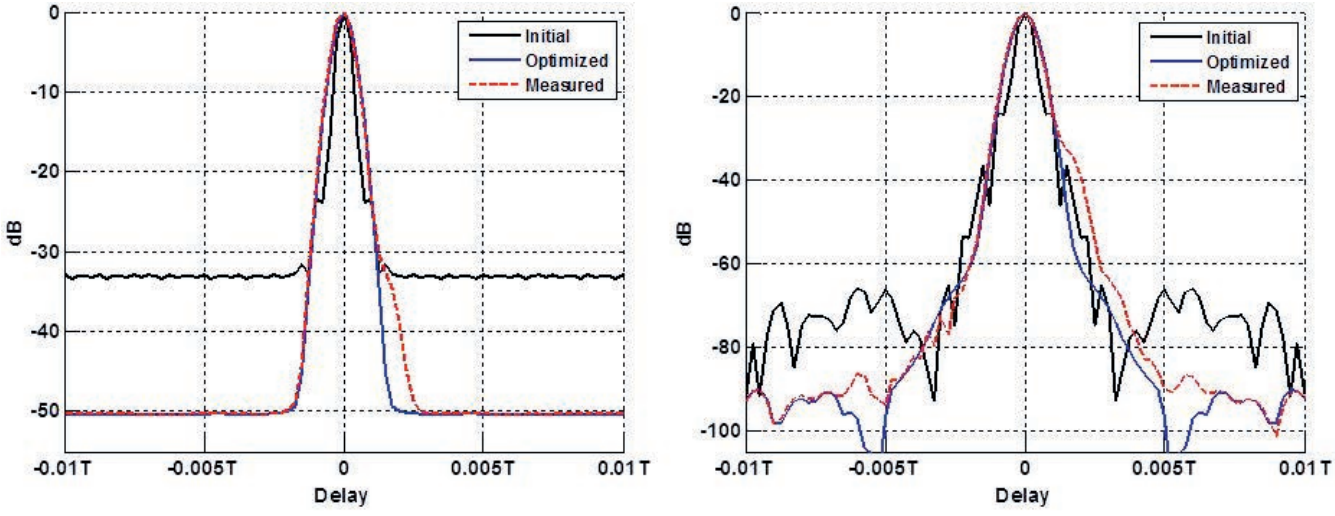

Fig. 35.
Range sidelobes for FM noise radar for (left) RMS average computed over 10^4 waveform segments and (right) coherent integration over these segments.

F. POLARIZATION DIVERSITY

Polarization provides another dimension to utilize for radar detection, tracking, and imaging. In 1986, Giuli [372] provided an excellent survey on polarization diversity. Simply put, a dual-polarized antenna has twice the degrees of freedom as a similar antenna with only one polarization channel, though with the caveat of increased complexity and implementation cost. Assuming each antenna element (if part of an array) has orthogonally polarized channels, such as the simple crossed dipoles depicted in Fig. 36, then the additional freedom on both transmit and receive may provide several advantages. These advantages include enhanced classification, identification, and discrimination between targets and clutter [373–380], measurement of scattering depolarization for remote sensing applications [381–385], dual-polarized generalization of the matched illumination concept discuss in Section III.B [202, 386], dual-polarized SAR [387, 388], and polarization coding on transmit [136, 389].

A useful and well-known way to visualize the polarization state is the Poincaré sphere (Fig. 37), which includes the basic states (horizontal, vertical, and left- or right-hand circular), as well as all variations between. Any two antipodal states on the Poincaré sphere are orthogonal. Thus, it is common to express the received radar scattering at a given instant in time in terms of the linear horizontal and vertical components via the scattering matrix

$$\mathbf{X} = \begin{bmatrix} x_{\mathrm{HH}} & x_{\mathrm{HV}} \\ x_{\mathrm{VH}} & x_{\mathrm{VV}} \end{bmatrix} \tag{III.F1}$$

where the subscripts denote the receive and transmit channel for each component. Therefore, the horizontal (vertical) antenna captures a copolarized (cross-polarized) signal, as well as a cross-polarized (copolarized) signal. Many decompositions of the scattering matrix have been developed to achieve greater understanding of the inherent scattering properties of an object and to develop recognizable features for various scattering environments and target structures [390–393].

Because the copolarized and cross-polarized components of (III.F1) are superimposed at each orthogonal antenna element, accurate estimation of the scattering matrix terms as a function of range is often performed by alternating transmission by each of the orthogonal antenna elements to achieve isolation [394, 395]. However, this isolation comes at the cost of increased ambiguities, because the measurement time is doubled relative to simultaneous dual-polarized operation. It was suggested in [396, 397] that simultaneous operation could be performed if the waveforms emitted by the orthogonal antenna elements are sufficiently separable. According to the Wiener-Khintchine theorem, if these two waveforms have the same spectral support (which is generally desired in this context to ensure phase coherence between the channels), then there is a limit on how low the cross-correlation between the waveforms can be (which depends on the time–bandwidth product). Because their cross-correlation is rather flat, one could use two LFM waveforms, one an up-chirp and the other a down-chirp, on the respective orthogonal antenna elements [396, 397]. Various other coding approaches have been examined, including bias removal of coherent cross-channel coupling [398], pulse-to-pulse phase coding [399], and a frequency-interleaved OFDM structure that minimizes the spectral overlap (the spectral maxima of one waveform coincides with the spectral minima of the other) while maintaining the same general spectral support [400]. It has also recently been experimentally demonstrated [136] that adaptive range-domain processing using knowledge of the two waveforms can separate the copolarized and cross-polarized components, just as well as the time alternating approach (with a higher computational cost).

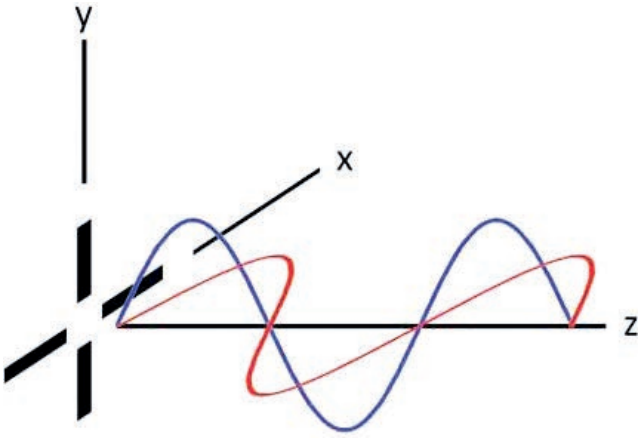

Fig. 36.
Crossed dipoles to enable dual-polarized operation.

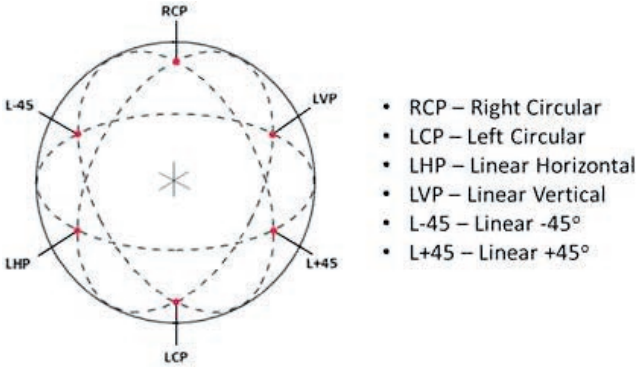

Fig. 37.
Poincaré sphere representing different polarization states.

IV. CONCLUSIONS

WD is an exciting technology that has sparked intense interest from the research community in recent years because of advances in high-fidelity electronic components and high-performance computing. WD is expected to have a profound impact on radar spectrum management, particularly in light of increasing competition for spectrum usage, as well as to facilitate enhanced radar sensitivity and discrimination and perhaps even to enable new sensing modes. As mentioned at the beginning of this tutorial, the definition of WD is clearly broad, but such is to be expected for a topic that continues to evolve.

ACKNOWLEDGMENTS

The authors would like to thank several individuals for their help in preparing this lengthy manuscript. John Jakabosky of the U.S.

Naval Research Laboratory (previously of the University of Kansas) and Patrick McCormick of the University of Kansas provided the figures used throughout. Prof. Hugh Griffiths of University College London generously allowed use of figures on ambiguity functions of illuminators of opportunity. Prof. Chris Allen of the University of Kansas provided useful references on current waveform generation technology.

The individuals participating in the North Atlantic Treaty Organization (NATO) SET-179 and SET-182 research task groups on dynamic waveform diversity and design and radar spectrum engineering and management, respectively, provided different perspectives and research contributions in these last few years. Likewise, the material surveyed in this tutorial would not exist without the continued advancements by a multitude of people in the radar research community.

Dr. Dale Blair and Prof. Maria Greco provided the opportunity to prepare a *Systems Magazine* tutorial summarizing and cataloging the array of contributions in WD. We certainly learned some new things in the process.

Finally, a special thank you goes to Dr. Michael C. Wicks for pointing the radar community down this path. To borrow more from Joe Guerci's Cambrian explosion analogy, it will be interesting to see what emerges next from this primordial radar soup. ◈

REFERENCES

[1] M. Wicks, E. Mokole, S. D. Blunt, V. Amuso, and R. Schneible, eds., *Principles of Waveform Diversity & Design,* Raleigh, NC: SciTech Publishing, 2010.

[2] S. Pillai, K. Y. Li, I. Selesnick, and B. Himed, *Waveform Diversity: Theory & Applications,* New York, NY, USA: McGraw-Hill, 2011.

[3] F. Gini, A. De Maio, and L. K. Patton, *Waveform Design and Diversity for Advanced Radar Systems,* London, UK: IET Press, 2012.

[4] M. C. Wicks, Private communication to R. W. McMillan and E. L. Mokole, Utica, NY, 28 March 2002.

[5] H. Griffiths, L. Cohen, S. Watts, E. Mokole, C. Baker, M. Wicks, and S. Blunt. Radar spectrum engineering and management: Technical and regulatory issues. *Proceedings of the IEEE,* **103**, 1, 85–102 (Jan. 2015).

[6] www.analog.com/media/cn/training-seminars/tutorials/450968421DDS_Tutorial_rev12-2-99.pdf

[7] www.hit.bme.hu/~papay/edu/Lab/33220A_Tutorial.pdf

[8] www.tek.com/dl/76W_30631_0_HR_Letter.pdf

[9] IEEE Standard Radar Definitions, IEEE standard 686-2008, May 2008.

[10] N. Levanon and E. Mozeson, *Radar Signals,* Hoboken, NJ, USA: Wiley–IEEE Press, 2004.

[11] N. J. Willis, *Bistatic Radar,* SciTech, 2005.

[12] M. Cherniakov, ed., *Bistatic Radar: Principles and Practice,* West Sussex, England: Wiley, 2007.

[13] N. J. Willis and H. D. Griffiths, eds., *Advances in Bistatic Radar,* Hoboken, NJ, USA: SciTech, 2007.

[14] M. Cherniakov, ed., *Bistatic Radar: Emerging Technology,* Wiley, 2008.

[15] M. Vespe, G. Jones, and C. J. Baker. Lesson for radar: Waveform diversity in echolocating mammals. *IEEE Signal Processing Magazine,* **26**, 1, 65–75 (Jan. 2009).

[16] T. G. Leighton, S. D. Meers, and P. R. White. Propagation through nonlinear time-dependent bubble clouds and the estimation of bubble populations from measured acoustic characteristics. *Proceedings of the Royal Society of London A,* **460**, 2521–2550 (Sept. 2004).

[17] C. J. Baker, G. E. Smith, A. Balleri, M. Holderied, and H. D. Griffiths. Biomimetic echolocation with application to radar and sonar sensing. *Proceedings of the IEEE,* **102**, 4, 447–458 (Apr. 2014).

[18] H. U. Schnitzler and E. K. V. Kalko. Echolocation by insect-eating bats. *Bioscience,* **51**, 557–569 (2001).

[19] K. Ghose and C. F. Moss. Sonar beam pattern of a flying bat as it tracks tethered insects. *Journal of the Acoustical Society of America,* **114**, 2, 1120–1131 (Aug. 2003).

[20] M. Vespe, G. Jones, and C. J. Baker. Diversity strategies: Lessons from natural systems. In *Principles of Waveform Diversity and Design,* M. Wicks, E. Mokole, S. Blunt, R. Schneible, and V. Amuso, eds., Raleigh, NC, USA: SciTech, 2010, 25–50.

[21] J. R. Potter and E. A. Taylor. On novel reception models for bottlenose dolphin echolocation. *Proceedings of the Institute of Acoustics,* **24**, 2002.

[22] T. G. Leighton, G. H. Chua, and P. R. White. Do dolphins benefit from nonlinear mathematics when processing their sonar returns? *Proceedings of the Royal Society of London A,* **468**, 3517–3532 (2012).

[23] G. H. Chua, P. R. White and T. G. Leighton. Use of clicks resembling those of the Atlantic bottlenose dolphin (*Tursiops truncatus*) to improve target discrimination in bubbly water with biased pulse summation sonar. *IET Radar, Sonar and Navigation,* **6**, 6, 510–515 (July 2012).

[24] W. W. L. Au and S. W. Martin. Why dolphin biosonar performs so well in spite of mediocre "equipment." *IET Radar, Sonar & Navigation,* **6**, 6, 566–575 (July 2012).

[25] T. G. Leighton, *The Acoustic Bubble,* San Diego, CA, USA: Elsevier, 2004.

[26] T. G. Leighton, S. D. Richards, and P. R. White, Marine mammal signals in bubbly water. *Proceedings of the Institute of Acoustics*, 2004.

[27] E. Hüttman, German Patent 768 068, Mar. 22, 1940.

[28] J. R. Klauder, A. C. Price, S. Darlington, and W. J. Albersheim. The theory and design of chirp radars. *The Bell System Technical Journal,* **XXXIX**, 4, 745–808 (July 1960).

[29] R. Manasse. The use of pulse coding to discriminate against clutter. MIT Lincoln Lab Group Report 312-12 (June 1961).

[30] S. Sussman. Least-square synthesis of radar ambiguity functions. *IEEE Transactions on Information Theory,* **8**, 3, 246–254 (Apr. 1962).

[31] L. J. Spafford. Optimum radar receive waveforms in the presence of clutter. General Electric Technical Information Series Report R65EMH14, June 1965.

[32] H. L. Van Trees. Optimum signal design and processing for reverberation-limited environments. *IEEE Transactions on Military Electronics,* **MIL-9**, 3–4, 212–229 (July–Oct. 1965).

[33] M. Ares. Optimum burst waveforms for detection of targets in uniform range-extended clutter. General Electric Technical Information Series Report R66EMH16, Mar. 1966.

[34] W. D. Rummier. Clutter suppression by complex weighting of coherent pulse trains. *IEEE Transactions on Aerospace and Electronics Systems,* **AES-2**, 689–699 (Nov. 1966).

[35] D. DeLong and E. Hofstetter. On the design of optimum radar waveforms for clutter rejection. *IEEE Transactions on Information Theory,* **13**, 3, 454–463 (July 1967).

[36] C. A. Stutt and L. J. Spafford. A "best" mismatched filter response for radar clutter discrimination. *IEEE Transactions on Information Theory,* **IT-14**, 2, 280–287 (Mar. 1968).

[37] R. Turyn. On Barker codes of even length. *Proceedings of the IEEE,* **51**, 9, 1256 (Sept. 1963).

[38] R. L. Frank. Polyphase codes with good non-periodic correlation properties. *IEEE Transactions on Information Theory,* **9**, 1, 43–45 (Jan. 1963).

[39] M. J. E. Golay. Complementary series. *IRE Transactions Information Theory,* **IT-7**, 2, 82–87 (Apr. 1961).

[40] D. A. Huffman. The generation of impulse-equivalent pulse trains. *IRE Transactions Information Theory,* **8**, 10–16 (Sept. 1962).

[41] S. A. Zadoff. Phase coded communication system, U.S. Patent 3 099 796, July 30, 1963.

[42] R. Gold. Optimal binary sequences for spread spectrum multiplexing. *IEEE Transactions on Information Theory,* **13**, 5, 619–621 (Oct. 1967).

[43] D. K. Barton, *Radars Volume 3—Pulse Compression,* Dedham MA, Artech House, 1975.

[44] R. Sivaswamy. Digital and analog sub-complementary sequences for pulse compression. *IEEE Transactions on Aerospace & Electronic Systems,* **AES-14**, 2, 343–350 (Mar. 1978).

[45] B. L. Lewis and F. F. Kretschmer. A new class of polyphase pulse compression codes and techniques. *IEEE Transactions on Aerospace & Electronic Systems,* **AES-17**, 3, 364–372 (May 1981).

[46] J. P. Costas. A study of a class of detection waveforms having nearly ideal range-Doppler ambiguity properties. *Proceedings of the IEEE,* **72**, 8, 996–1009 (Aug. 1984).

[47] J. Guerci, Plenary address. A radar Cambrian explosion? In *Proceedings of the IEEE Conference*, Cincinnati, OH, May 2014.

[48] J. V. DiFranco and W. L. Rubin, *Radar Detection,* Raleigh, NC, USA: SciTech, 2004.

[49] G. Fabrizio, *High Frequency Over-the-Horizon Radar: Fundamental Principles, Signal Processing, and Practical Applications,* New York, NY, USA: McGraw-Hill, 2013.

[50] H. Rohling and M. Kronauge. New radar waveform based on a chirp sequence. In *Proceedings of the International Radar Conference*, Lille, France, Oct. 2014.

[51] L. Shi, C. Allen, M. Ewing, S. Keshmiri, M. Zakharov, F. Florencio, N. Niakan, and R. Knight. Multichannel sense-and-avoid radar for small UAVs. In *Proceedings of the IEEE/AIAA Digital Avionics Systems Conference*, Syracuse, NY, Oct. 2013.

[52] W. J. Caputi. Stretch: A time-transformation technique. *IEEE Transactions on Aerospace & Electronic Systems,* **AES-7**, 2, 269–278 (Mar. 1971).

[53] M. A. Richards, J. A. Scheer, and W. A. Holm, *Principles of Modern Radar, Vol. I: Basic Principles,* Raleigh, NC, USA: SciTech, 2010.

[54] C. E. Cook. A class of nonlinear FM pulse compression signals. *Proceedings of the IEEE,* **52**, 11, 1369–1371 (Nov. 1964).

[55] E. Fowle. The design of FM pulse compression signals. *IEEE Transactions on Information Theory,* **10**, 1, 61–67 (Jan. 1964).

[56] M. Labitt. Obtaining low sidelobes using non-linear FM pulse compression. *MIT Lincoln Lab Project Report,* ATC-223 (Nov. 1994).

[57] I. Gladkova. Design of frequency modulated waveforms via the Zak transform. *IEEE Transactions on Aerospace & Electronic Systems,* **40**, 1, 355–359 (Jan. 2004).

[58] A. W. Doerry. Generating nonlinear FM chirp waveforms for radar. *Sandia Report,* SAND2006-5856 (Sept. 2006).

[59] A. Johnston. Improvements to a pulse compression radar matched filter. *Radio & Electronic Engineer,* **53**, 4, 138–140 (Apr. 1983).

[60] J. A. Johnston and A. C. Fairhead. Waveform design and Doppler sensitivity analysis for nonlinear FM chirp pulses. *IEE Proceedings Communications, Radar & Signal Processing,* **133**, 2, 163–175 (Apr. 1986).

[61] T. Collins and P. Atkins. Nonlinear frequency modulation chirps for active sonar. *IEE Proceedings Radar, Sonar & Navigation,* **146**, 6, 312–316 (Dec. 1999).

[62] E. De Witte and H. D. Griffiths. Improved ultra-low range sidelobe pulse compression waveform design. *Electronics Letters,* **40**, 22, 1448–1450 (Oct. 2004).

[63] R. H. Barker. Group synchronizing of binary digital sequences. *Communication Theory,* W. Jackson, ed., Academic Press, 273–287, 1953.

[64] M. N. Cohen, M. R. Fox, and J. M. Baden. Minimum peak sidelobe pulse compression codes. In *Proceedings of the IEEE International Radar Conference*, Arlington, VA, May 1990.

[65] G. Coxson and J. Russo. Efficient exhaustive search for optimal-peak-sidelobe binary codes. *IEEE Transactions on Aerospace & Electronic Systems,* **41**, 1, 302–308 (Jan. 2005).

[66] C. J. Nunn and G. E. Coxson. Best-known autocorrelation peak sidelobe levels for binary codes of length 71 to 105. *IEEE Transactions on Aerospace & Electronic Systems,* **44**, 1, 392–395 (Jan. 2008).

[67] B. L. Lewis and F. F. Kretschmer. Linear frequency modulation derived polyphase pulse compression codes. *IEEE Transactions on Aerospace & Electronic Systems,* **AES-18**, 5, 637–641 (Sept. 1982).

[68] C. J. Nunn and G. E. Coxson. Polyphase pulse compression codes with optimal peak and integrated sidelobes. *IEEE Transactions on Aerospace & Electronic Systems,* **45**, 2, 775–781 (Apr. 2009).

[69] S. H. Han and J. H. Lee. An overview of peak-to-average power ratio reduction techniques for multicarrier transmission. *IEEE Wireless Communications,* **12**, 2, 56–65 (Apr. 2005).

[70] N. Levanon. Multifrequency complementary phase-coded radar signal. *IEE Proceedings Radar, Sonar & Navigation,* **147**, 6, 276–284 (Dec. 2000).

[71] B. M. Horton. Noise-modulated distance measuring systems. *Proceedings of the IRE,* **47**, 5, 821–828 (May 1959).

[72] X. Xu and R. M. Narayanan. Range sidelobe suppression technique for coherent ultra wide-band random noise radar imaging. *IEEE Transactions on Antennas & Propagation,* **49**, 12, 1836–1842 (Dec. 2001).

[73] S. R. J. Axelsson. Random noise radar/sodar with ultrawideband waveforms. *IEEE Transactions on Geoscience & Remote Sensing,* **45**, 5, 1099–1114 (May 2007).

[74] D. Tarchi, K. Lukin, J. Fortuny-Guasch, A. Mogyla, P. Vyplavin, and A. Sieber. SAR imaging with noise radar. *IEEE Transactions on Aerospace & Electronic Systems,* **46**, 3, 1214–1225 (July 2010).

[75] M. Malanowski and K. Kulpa. Detection of moving targets with continuous-wave noise radar: Theory and measurements. *IEEE Transactions on Geoscience & Remote Science,* **50**, 9, 3502–3509 (Sept. 2012).

[76] P. E. Pace *Detecting and Classifying Low Probability of Intercept Radar,* Norwood, MA, USA: Artech House, 2004.

[77] D. R. Sheen, D. W. Kletzli, N. P. Malinas, T. B. Lewis, and J. F. Roman. Ultrawidebandwidth measurements of foliage transmission

properties at UHF: Measurements systems and results. *Proceedings of the SPIE,* **1631**, 206–218 (May 1992).

[78] H. Hellsten, L. M. H. Ulander, A. Gustavsson, and B. Larsson. Development of VHF CARABAS II SAR. *Proceedings of the SPIE,* **2747**, 48–60 (June 1996).

[79] J. P. Hansen. Environmental measurements of sea scatter using an ultrawideband X-band radar with variable resolution. *Proceedings of the SPIE,* **1631**, 182–193 (May. 1992).

[80] T. R. Witten. Present state-of-the-art in ground penetrating radars for mine detection. *Proceedings of the SPIE,* **3392**, 576–585 (Sept. 1998).

[81] C. C. DeLuca, V. R. Marinelli, M. A. Ressler, and T. T. Ton. Unexploded ordnance detection experiments at extensive, fully ground-truthed test sites at Yuma Proving Ground and Eglin AFB. *Proceedings of the SPIE,* **3710**, 1025–1034 (Aug. 1999).

[82] J. Andrieu, F. Gallais, V. Mallepeyre, V. Bertrand, B. Beillard, B. Jecko, R. Guillerey, and M. Legoff. Land mine detection with an ultra-wideband SAR system. *Proceedings of the SPIE,* **4742**, 237–247 (Aug. 2002).

[83] B. Karlsen, H. B. D. Sørenson, J. Larsen, and K. B. Jakobsen. GPR detection of buried symmetrically shaped mine-like objects using selective independent component analysis. *Proceedings of the SPIE,* **5089**, 375–386 (Sept. 2003).

[84] D. M. Port, P. T. Gardiner, and K. J. Long. Analysis and application of a vehicle mounted ground penetrating radar array. *Proceedings of the SPIE,* **5089**, 348–357 (Sept. 2003).

[85] F. van der Lijn, F. Roth, and M. Verhaegen. Estimating the impulse response of buried objects from ground penetrating radar signals. *Proceedings of the SPIE,* **5089**, 387–394 (Sept. 2003).

[86] S. Crabbe, J. Sachs, P. Peyerl, G. Alli, L. Eng, M. Khalili, J. Busto, and A. Berg. Results of field testing with the multi-sensor DEMAND and BIOSENS technology in Croatia and Bosnia developed in the European Union's 5th framework programme. *Proceedings of the SPIE,* **5415**, 456–467 (Sept. 2004).

[87] W. A. Chamma and S. Kashyap. Detection of targets behind walls using ultra wide band short pulse. *Ultra-Wideband, Short-Pulse Electromagnetics 6,* E. L. Mokole, M. Kragalott, and K. R. Gerlach, eds., New York, NY, USA: Kluwer Academic/Plenum, 493–506, 2003.

[88] R. J. Fontana, E. A. Richley, A. J. Marzullo, L. C. Beard, R. W. T. Mulloy, and E. J. Knight. An ultra wideband radar for micro air vehicle applications. *IEEE Conference Ultra Wideband Systems and Technologies,* Baltimore MD, May 2002.

[89] M. Amin, ed., *Through-the-Wall Radar Imaging,* Boca Raton, FL, USA: CRC Press, 2010.

[90] D. O. North. An analysis of the factors which determine signal/noise discrimination in pulsed-carrier systems. *Proceedings of the IEEE,* **51**, 7, 1016–1027 (July 1963).

[91] P. M. Woodward, *Probability and Information Theory with Applications to Radar,* Oxford, UK: Elsevier Science & Technology, 1953.

[92] L. E. Brennan and I. S. Reed. Optimum processing of unequally spaced radar pulse trains for clutter rejection. *IEEE Transactions on Aerospace & Electronic Systems,* **AES-4**, 3, 474–477 (May 1968).

[93] R. Roy and O. Lowenschuss. Design of MTI detection filters with nonuniform interpulse periods. *IEEE Transactions on Circuit Theory,* **CT-17**, 4, 604–612 (Nov. 1970).

[94] J. J. Kroszczynski. Pulse compression by means of linear-period modulation. *Proceedings of the IEEE,* **57**, 7, 1260–1266 (July 1969).

[95] S. D. Blunt, J. Jakabosky, M. Cook, J. Stiles, S. Seguin, and E. L. Mokole. Polyphase-coded FM (PCFM) radar waveforms, part II: Optimization. *IEEE Transactions on Aerospace & Electronic Systems,* **50**, 3, 2230–2241 (July 2014).

[96] E. R. Billam. Eclipsing effects with high-duty-factor waveforms in long-range radar. *IEE Proceedings F—Communications, Radar & Signal Processing,* **132**, 7, 598–603 (Dec. 1985).

[97] S. D. Blunt, K. Gerlach, and E. Mokole. Pulse compression eclipsing repair. In *Proceedings of the IEEE Radar Conference,* Rome, Italy, May 2008.

[98] B. Manz. Advancing TWTs: The traveling wave tube lives on … and on. *AOC Journal of Electronic Defense,* **32**, 7, 26–30 (July 2009).

[99] H. D. Griffiths, C. J. Baker, and D. Adamy, *Stimson's Introduction to Airborne Radar,* 3rd ed., Raleigh, NC, USA: SciTech, 2014.

[100] B. Levush, D. K. Abe, J. P. Calame, B. G. Danly, K. T. Nguyen, E. J. Dutkowski, R. H. Abrams, and R. K. Parker. Vacuum electronics: Status and trends. *IEEE Aerospace & Electronic Systems Magazine,* **22**, 9, 28–34 (Sept. 2007).

[101] C. M. Armstrong. The quest for the ultimate vacuum tube. *IEEE Spectrum,* **52**, 12, 28–33 and 50–51 (Dec. 2015).

[102] J. C. Pedro and N. B. Carvalho, *Intermodulation Distortion in Microwave and Wireless Circuits,* Norwood, MA, USA: Artech House, 2003.

[103] S. D. Blunt, M. Cook, J. Jakabosky, J. de Graaf, and E. Perrins. Polyphase-coded FM (PCFM) radar waveforms, part I: Implementation. *IEEE Transactions on Aerospace & Electronic Systems,* **50**, 3, 2218–2229 (July 2014).

[104] E. Costa, M. Midrio, and S. Pupolin. Impact of amplifier nonlinearities on OFDM transmission system performance. *IEEE Communications Letters,* **3**, 2, 37–39 (Feb. 1999).

[105] J. Jakabosky, L. Ryan, and S. D. Blunt. Transmitter-in-the-loop optimization of distorted OFDM radar emissions. In *Proceedings of the IEEE Radar Conference,* Ottawa, Canada, Apr./May 2013.

[106] A. M. Klein and M. T. Fujita. Detection performance of hard-limited phase-coded signals. *IEEE Transactions on Aerospace & Electronic Systems,* **AES-15**, 6, 795–802 (Nov. 1979).

[107] J. G. Proakis and D. K. Manolakis, *Digital Signal Processing,* 4th ed., Upper Saddle River, NJ, USA: Prentice Hall, 2006.

[108] M. H. Ackroyd and F. Ghani. Optimum mismatched filters for sidelobe suppression. *IEEE Transactions on Aerospace & Electronic Systems,* **AES-9**, 2, 214–218 (Mar. 1973).

[109] S. D. Blunt, K. Gerlach, and T. Higgins. Aspects of radar range superresolution. In *Proceedings of the IEEE Radar Conference*, Waltham, MA, Apr. 2007.

[110] D. Henke, P. McCormick, S. D. Blunt, and T. Higgins. Practical aspects of optimal mismatch filtering and adaptive pulse compression for FM waveforms. In *Proceedings of the IEEE International Radar Conference*, Arlington, VA, May 2015.

[111] J. E. Cilliers and J. C. Smit. Pulse compression sidelobe reduction by minimization of Lp-norms. *IEEE Transactions on Aerospace & Electronic Systems,* **43**, 3, 1238–1247 (July 2007).

[112] A. De Maio, Y. Huang, M. Piezzo, S. Zhang, and A. Farina. Design of radar receive filters optimized according to Lp-norm based criteria. *IEEE Transactions on Signal Processing,* **59**, 8, 4023–4029 (May 2011).

[113] O. Rabaste and L. Savy. Mismatched filter optimization for radar applications using quadratically constrained quadratic programs. *IEEE*

Transactions on Aerospace & Electronic Systems, **51**, 4, 3107–3122 (Oct. 2015).

[114] T. Aittomaki and V. Koivunen. Mismatched filter design for radar waveforms by semidefinite relaxation. In *Proceedings of the IEEE International Conference on Acoustics, Speech and Signal Processing,* Brisbane, Australia, Apr. 2015.

[115] J. M. Baden and M. N. Cohen. Optimal peak sidelobe filters for biphase pulse compression. In *Proceedings of the IEEE International Radar Conference*, Arlington, VA, May 1990.

[116] B. Zrnic, A. Zejak, A. Petrovic, and I. Simic. Range sidelobe suppression for pulse compression radars utilizing modified RLS algorithm. In *Proceedings of the IEEE International Symposium on Spread Spectrum Techniques & Applications,* Sun City, South Africa, Sept. 1998.

[117] R. C. Daniels and V. Gregers-Hansen. Code inverse filtering for complete sidelobe removal in binary phase coded pulse compression systems. In *Proceedings of the IEEE International Radar Conference*, Arlington, VA, May 2005.

[118] B. L. Lewis. Range-time-sidelobe reduction technique for FM-derived polyphase PC codes. *IEEE Transactions on Aerospace & Electronic Systems,* **29**, 3, 834–840 (July 1993).

[119] R. Sato. Simple mismatched filter for binary pulse compression code with small PSL and small S/N loss. **39**, 2, 711–718 (Apr. 2003).

[120] S. Zoraster. Minimum peak range sidelobe filters for binary phase-coded waveforms. *IEEE Transactions on Aerospace & Electronic Systems,* **AES-16**, 1, 112–115 (Jan. 1980).

[121] S. C. Park and J. F. Doherty. A minimax optimization approach to sidelobe suppression filter design. In *Proceedings of the IEEE International Conference on Acoustics, Speech & Signal Processing,* Atlanta, GA, May 1996.

[122] R. M. Nuthalapati. Design of mismatched filters for long binary codes. In *Proceedings of the IEEE Radar Conference* Rome, Italy, May 2008.

[123] U. C. Doyuran and R. F. Tigrek. M-ary CPM pulse compression filter design for low, flat sidelobes. In *Proceedings of the International Radar Conference*, Lille, France, Oct. 2014.

[124] Y. I. Abramovich. Compensation methods of resolution of wideband signals. *Radio Engineering & Electronic Physics,* **23**, 1, 54–49 (Jan. 1978).

[125] R. Bose, A. Freedman, and B. Steinberg. Sequence CLEAN: A modified deconvolution technique for microwave imaging of contiguous targets. *IEEE Transactions on Aerospace & Electronic Systems,* **38**, 1, 89–97 (Jan. 2002).

[126] H. Deng. Effective CLEAN algorithms for performance-enhanced detection of binary coding radar signals. *IEEE Transactions on Signal Processing,* **52**, 1, 72–78 (Jan. 2004).

[127] S. D. Blunt and K. Gerlach. Adaptive pulse compression via MMSE estimation. *IEEE Transactions on Aerospace & Electronic Systems,* **42**, 2, 572–584 (Apr. 2006).

[128] S. D. Blunt, A. Shackelford, and K. Gerlach. Single pulse imaging. In *Proceedings of the International Waveform Diversity & Design Conference*, Lihue, HI, Jan. 2006.

[129] S. D. Blunt, A. Shackelford, K. Gerlach, and K. J. Smith. Doppler compensation & single pulse imaging via adaptive pulse compression. *IEEE Transactions on Aerospace & Electronic Systems,* **45**, 2, 647–659 (Apr. 2009).

[130] T. Yardibi, J. Li, P. Stoica, M. Xue, and A. B. Baggeroer. Source localization and sensing: A nonparametric iterative adaptive approach based on weighted least squares. *IEEE Transactions on Aerospace & Electronic Systems,* **46**, 1, 425–443 (Jan. 2010).

[131] R. O. Lane. The effects of Doppler and pulse eclipsing on sidelobe reduction techniques. In *Proceedings of the IEEE Radar Conference*, Verona, NY, Apr. 2006.

[132] K. Gerlach and S. D. Blunt. Radar pulse compression repair. *IEEE Transactions on Aerospace & Electronic Systems,* **43**, 3, 1188–1195 (July 2007).

[133] Z. Li, Y. Zhang, S. Wang, L. Li, and M. McLinden. Fast adaptive pulse compression based on matched filter outputs. *IEEE Transactions on Aerospace & Electronic Systems,* **51**, 1, 548–564 (Jan. 2015).

[134] S. D. Blunt and K. Gerlach. Multistatic adaptive pulse compression. *IEEE Transactions on Aerospace & Electronic Systems,* **42**, 3, 1043–1057 (July 2006).

[135] S. D. Blunt, W. Dower, and K. Gerlach. Hybrid interference suppression for multistatic radar. *IET Radar, Sonar & Navigation,* **2**, 5, 323–333 (Oct. 2008).

[136] P. McCormick, J. Jakabosky, S. D. Blunt, C. Allen, and B. Himed. Joint polarization/waveform design and adaptive receive processing. In *Proceedings of the IEEE International Radar Conference*, Arlington, VA, May 2015.

[137] S. D. Blunt and T. Higgins. Dimensionality reduction techniques for efficient adaptive radar pulse compression. *IEEE Transactions on Aerospace & Electronic Systems,* **46**, 1, 349–362 (Jan. 2010).

[138] P. M. McCormick, S. D. Blunt, and T. Higgins. A gradient descent implementation of adaptive pulse compression. In *Proceedings of the IEEE Radar Conference*, Philadelphia, PA, May 2016.

[139] R. A. Scholtz. How do you define bandwidth? In *Proceedings of the International Telemetering Conference*, Los Angeles, CA, Oct. 1972.

[140] F. Sabath, E. L. Mokole, and S. N. Samaddar. Definition and classification of ultra-wideband signals and devices. *URSI Radio Science Bulletin,* 313, 12–26, June 2005.

[141] American National Standards Institute (ANSI, ANSI C63.14-1998, *American National Standards Dictionary for Technologies of Electromagnetic Compatibility (EMC, Electromagnetic Pulse (EMP, and Electromagnetic Discharge (ESD),* Oct. 1998.

[142] IEEE Standard 145-2013, *IEEE Standard Definitions of Terms for Antennas,* Mar. 2014.

[143] OSD/DARPA Ultra-Wideband Radar Review Panel. Assessment of Ultra Wide-Band (UWB) Technology. Defense Advanced Research Projects Agency (DARPA), Report R-6280, 1990.

[144] International Electrotechnical Commission (IEC). Electromagnetic compatibility (EMC)—Part 2: Environment. Section 9: Description of HEMP environment-radiated disturbance. EMC Publication 61000-2-9, Feb. 1996.

[145] Title 47 (Telecommunication, Chapter I (Federal Communications Commission, Subchapter A, Part 15 (Radio Frequency Devices, Subpart F (Ultra-Wideband Operation, *Electronic Code of Federal Regulations (ECFR) for the United States,* Mar. 2016.

[146] A. W. Rihaczek, *Principles of High-Resolution Radar,* New York, NY, USA: McGraw-Hill, 1969.

[147] S. N. Samaddar and E. L. Mokole. Some basic properties of antennas associated with ultrawideband radiation. *Ultra-Wideband, Short-Pulse Electromagnetics 3,* C. E. Baum, L. Carin, and A. P. Stone, eds., New York, NY, USA: Plenum Press, 1997.

[148] H. F. Engler. System considerations for large percent-bandwidth radar. In *Proceedings of the IEEE National Telesystems Conference*, Atlanta, GA, Mar. 1991.

[149] H. Urkowitz, C. A. Hauer, and J. F. Koval. Generalized resolution in radar systems. *Proceedings of the IEEE,* **50**, 10, 2093–2105 (Oct. 1962).

[150] M. A. Richards, *Fundamentals of Radar Signal Processing,* 2nd ed., New York, NY, USA: McGraw-Hill, 2014.

[151] A. L. Drozd, C. K. Mohan, P. K. Varshney, and D. D. Weiner. Multiobjective joint optimization and frequency diversity for efficient utilization of the RF transmission hyperspace. In *Proceedings of the International Waveform Diversity & Design Conference*, Edinburgh, United Kingdom, Nov. 2004.

[152] H. H. Faust, B. Connolly, T. M. Firestone, R. C. Chen, B. H. Cantrell, and E. Mokole. A spectrally clean transmitting system for solid-state phased-array radars. In *Proceedings of the IEEE Radar Conference*, Philadelphia, PA, Apr. 2004.

[153] J. W. Taylor and H. J. Blinchikoff. Quadriphase code—A radar pulse compression signal with unique characteristics. *IEEE Transactions on Aerospace & Electronic Systems,* **24**, 2, 156–170 (May 1988).

[154] S. Blunt, M. Cook, E. Perrins, and J. de Graaf. CPM-based radar waveforms for efficiently bandlimiting a transmitted spectrum. In *Proceedings of the IEEE Radar Conference*, Pasadena, CA, May 2009.

[155] J. B. Anderson, T. Aulin, and C.-E. Sundberg, *Digital Phase Modulation,* Plenum Press, New York, NY, 1986.

[156] *IRIG Standard 106-00: Telemetry Standards,* Range Commanders Council Telemetry Group, Range Commanders Council, White Sands Missile Range, New Mexico.

[157] *Bandwidth-Efficient Modulations: Summary of Definitions, Implementation, and Performance,* Report Concerning Space Data System Standards, Informational Report CCSDS 413.0-G-2.

[158] *Specifications of the Bluetooth System,* Bluetooth Special Interest Group, ver. 1.2, Nov. 2003.

[159] P. S. Tan, J. Jakabosky, J. M. Stiles, and S. D. Blunt. On higher-order representations of polyphase-coded FM radar waveforms. In *Proceedings of the IEEE International Radar Conference*, Arlington, VA, May 2015.

[160] J. Jakabosky, S. D. Blunt, and B. Himed. Optimization of "over-coded" radar waveforms. In *Proceedings of the IEEE Radar Conference*, Cincinnati, OH, May 2014.

[161] J. Kurdzo, B. L. Cheong, R. Palmer, and G. Zhang. Optimized NLFM pulse compression waveforms for high-sensitivity radar observations. In *Proceedings of the International Radar Conference*, Lille, France, Oct. 2014.

[162] J. Jakabosky, S. D. Blunt, and T. Higgins. Ultra-low sidelobe waveform design via spectral shaping and LINC transmit architecture. In *Proceedings of the IEEE International Radar Conference*, Arlington, VA, May 2015.

[163] F. H. Raab, P. Asbeck, S. Cripps, P. B. Kenington, Z. B. Popovic, N. Pothecary, J. F. Sevic, and N. O. Sokal. Power amplifiers and transmitters for RF and microwave. *IEEE Transactions on Microwave Theory & Techniques,* **50**, 3, 814–826 (Mar. 2002).

[164] F. M. Ghannouchi and O. Hammi. Behavioral modeling and predistortion. *IEEE Microwave Magazine,* 52–64 (Dec. 2009).

[165] H. Griffiths, S. Blunt, L. Cohen, and L. Savy. Challenge problems in spectrum engineering and waveform diversity. In *Proceedings of the IEEE Radar Conference*, Ottawa, Canada, Apr./May 2013.

[166] J. G. Andrews, S. Buzzi, W. Choi, S. V. Hanly, A. Lozano, A. C. K. Soong, and J. C. Zhang. What will 5G be? *IEEE Journal on Selected Areas in Communications,* **32**, 6, 1065–1082 (June 2014).

[167] L. Ryan, J. Jakabosky, S. D. Blunt, C. Allen, and L. Cohen. Optimizing polyphase-coded FM waveforms within a LINC transmit architecture. In *Proceedings of the IEEE Radar Conference*, Cincinnati, OH, May 2014.

[168] M. Fellows, M. Flachsbart, J. Barlow, J. Barkate, C. Baylis, L. Cohen, R. J. Marks. Optimization of power-amplifier load impedance and waveform bandwidth for real-time reconfigurable radar. *IEEE Transactions on Aerospace & Electronic Systems,* **51**, 3, 1961–1971 (July 2015).

[169] C. Blum and A. Roli. Metaheuristics in combinatorial optimization: Overview and conceptual comparison. *ACM Computing Surveys,* **35**, 3, 268–308 (Sept. 2003).

[170] L. S. Wang, J. P. McGeehan, J. P. Williams, and A. Doufexi. Application of cooperative sensing in radar-communications coexistence. *IET Communications,* **2**, 6, 856–868 (July 2008).

[171] C. Sturm and W. Wiesbeck. Waveform design and signal processing aspects for fusion of wireless communications and radar sensing. *Proceedings of the IEEE,* **99**, 7, 1236–1259 (July 2011).

[172] H. Deng and B. Himed. Interference mitigation processing for spectrum-sharing between radar and wireless communication systems. *IEEE Transactions on Aerospace & Electronic Systems,* **49**, 3, 1911–1919 (July 2013).

[173] B. Fell, G. Jacyna, and D. McLemore. A high-level overview of fundamental limits studies for the DARPA SSPARC program. In *Proceedings of the IEEE Radar Conference*, Philadelphia, PA, May 2016.

[174] M. J. Marcus. Spectrum policy for radio spectrum access. *Proceedings of the IEEE,* **100**, 1685–1691 (May 2012).

[175] F. H. Sanders, R. L. Sole, B. L. Bedford, D. Franc, and T. Pawlowitz. Effects of RF interference on radar receivers. *NTIA Tech Rep.,* TR-06-444, Feb. 2006.

[176] A. Ghasemi and E. S. Sousa. Spectrum sensing in cognitive radio networks: Requirements, challenges and design trade-offs. *IEEE Communications Magazine,* **46**, 4, 32–39 (Apr. 2008).

[177] A. Martone, K. Sherbondy, K. Ranney, and T. Dogaru. Passive sensing for adaptable radar bandwidth. In *Proceedings of the IEEE International Radar Conference*, Arlington, VA, May 2015.

[178] J. R. Guerci, *Cognitive Radar: The Knowledge-Aided Fully Adaptive Approach,* Norwood, MA, USA: Artech House, 2010.

[179] S. Haykin, *Cognitive Dynamic Systems: Perception–Action Cycle, Radar and Radio,* New York, NY, USA: Cambridge University Press, 2012.

[180] M. E. Davis, *Foliage Penetration Radar: Detection and Characterization of Objects Under Trees,* Raleigh, NC, USA: SciTech, 2012.

[181] D. J. Daniels, *Ground Penetrating Radar,* 2nd ed., London, UK: The Institution of Engineering and Technology, 2007.

[182] B. H. Ferrell and W. C. Woody. Notched-spectrum swept-frequency generator and method therefore, U.S. Patent 5 852 418, Dec. 1998.

[183] K. Gerlach. Thinned spectrum ultrawideband waveforms using stepped-frequency polyphase codes. *IEEE Transactions on Aerospace & Electronic Systems,* **34**, 4, 1356–1361 (Oct. 1998).

[184] M. J. Lindenfeld. Sparse frequency transmit and receive waveform design. *IEEE Transactions on Aerospace & Electronic Systems,* **40**, 3, 851–861 (July 2004).

[185] M. R. Cook, T. Higgins, and A. K. Shackelford. Thinned spectrum radar waveforms. In *Proceedings of the International Waveform Diversity & Design Conference*, Niagara Falls, ON, Canada, Aug. 2010.

[186] K. Gerlach, M. R. Frey, M. J. Steiner, and A. Shackelford. Spectral nulling on transmit via nonlinear FM radar waveforms. *IEEE Transactions on Aerospace & Electronic Systems,* **47**, 2, 1507–1515 (Apr. 2011).

[187] I. W. Selesnick and S. U. Pillai. Chirp-like transmit waveforms with multiple frequency-notches. In *Proceedings of the IEEE Radar Conference*, Kansas City, MO, May 2011.

[188] L. K. Patton, C. A. Bryant, and B. Himed. Radar-centric design of waveforms with disjoint spectral support. In *Proceedings of the IEEE Radar Conference*, Atlanta, GA, May 2012..

[189] L. K. Patton, D. E. Hack, and B. Himed. Adaptive pulse design for space–time adaptive processing. In *Proceedings of the IEEE Sensor Array and Multichannel Signal Processing Workshop,* Hoboken, NJ, June 2012.

[190] L. K. Patton and B. D. Rigling. Phase retrieval for radar waveform optimization. *IEEE Transactions on Aerospace & Electronic Systems,* **48**, 4, 3287–3302 (Oct. 2012).

[191] C. Nunn and L. R. Moyer. Spectrally-compliant waveforms for wideband radar. *IEEE Aerospace & Electronic Systems Magazine,* **27**, 8, 11–15 (Aug. 2012).

[192] A. Aubry, A. De Maio, Y. Huang, M. Piezzo, and A. Farina. A new radar waveform design algorithm with improved feasibility for spectral coexistence. *IEEE Transactions on Aerospace & Electronic Systems,* **51**, 2, 1029–1038 (Apr. 2015).

[193] J. Jakabosky, B. Ravenscroft, S. D. Blunt, and A. Martone. Gapped spectrum shaping for tandem-hopped radar/communications & cognitive sensing. In *Proceedings of the IEEE Radar Conference*, Philadelphia, PA, May 2016.

[194] S. W. Frost and B. Rigling. Sidelobe predictions for spectrally-disjoint radar waveforms. In *Proceedings of the IEEE Radar Conference*, Atlanta, GA, May 2012..

[195] M. Greenspan. Potential pitfalls of cognitive radars. In *Proceedings of the IEEE Radar Conference*, Cincinnati, OH, May 2014.

[196] M. R. Bell. Information theory and radar waveform design. *IEEE Transactions on Information Theory,* **39**, 5, 1578–1597 (Sept. 1993).

[197] D. T. Gjessing. Adaptive techniques for radar detection and identification of objects in an ocean environment. *IEEE Journal of Oceanic Engineering,* **OE-6**, 1, 5–17 (Jan. 1981).

[198] D. T. Gjessing, J. Hjelmstad, and T. Lund. A multifrequency adaptive radar for detection and identification of objects: Results on preliminary experiments on aircraft against a sea-clutter background. *IEEE Transactions on Antennas & Propagation,* **AP-30**, 3, 351–365 (May 1982).

[199] S. U. Pillai, H. S. Oh, D. C. Youla, and J. R. Guerci. Optimal transmit–receiver design in the presence of signal-dependent interference and channel noise. *IEEE Transactions on Information Theory,* **46**, 2, 577–584 (Mar. 2000).

[200] S. M. Sowelam and A. H. Tewfik. Waveform selection in radar target classification. *IEEE Transactions on Information Theory,* **46**, 3, 1014–1029 (May 2000).

[201] D. A. Garren, M. K. Osborn, A. C. Odom, J. S. Goldstein, S. U. Pillai, and J. R. Guerci. Enhanced target detection and identification via optimized radar transmission pulse shape. *IEE Proceedings Radar, Sonar & Navigation,* **148**, 3, 130–138 (June 2001).

[202] D. A. Garren, A. C. Odom, M. K. Osborn, J. S. Goldstein, S. U. Pillai, and J. R. Guerci. Full-polarization matched-illumination for target detection and identification. *IEEE Transactions on Aerospace & Electronic Systems,* **38**, 3, 824–837 (July 2002).

[203] S. Kay. Optimal signal design for detection of Gaussian point targets in stationary Gaussian clutter/reverberation. *IEEE Journal of Selected Topics in Signal Processing,* **1**, 1, 31–41 (June 2007).

[204] A. Leshem, O. Naparstek, and A. Nehorai. Information theoretic adaptive radar waveform design for multiple extended targets. *IEEE Journal of Selected Topics in Signal Processing,* **1**, 1, 42–55 (June 2007).

[205] S. P. Sira, D. Cochran, A. Papandreou-Suppappola, D. Morrell, W. Moran, S. D. Howard, and R. Calderbank. Adaptive waveform design for improved detection of low-RCS targets in heavy sea clutter. *IEEE Journal of Selected Topics in Signal Processing,* **1**, 1, 56–66 (June 2007).

[206] N. A. Goodman, P. R. Venkata, and M. A. Neifeld. Adaptive waveform design and sequential hypothesis testing for target recognition with active sensors. *IEEE Journal of Selected Topics in Signal Processing,* **1**, 1, 105–113 (June 2007).

[207] F. Ahmad and M. G. Amin. Matched-illumination waveform design for a multistatic through-the-wall radar systems. *IEEE Journal of Selected Topics in Signal Processing,* **4**, 1, 177–186 (Feb. 2010).

[208] R. A. Romero, J. Bae, and N. A. Goodman. Theory and application of SNR and mutual information matched illumination waveforms. *IEEE Transactions on Aerospace & Electronic Systems,* **47**, 2, 912–927 (Apr. 2011).

[209] L. K. Patton and B. D. Rigling. Autocorrelation constraints in radar waveform optimization for detection. *IEEE Transactions on Aerospace & Electronic Systems,* **48**, 2, 951–968 (Apr. 2012).

[210] Y. Chen, Y. Nijsure, C. Yuen, Y. H. Chew, Z. Ding, and S. Boussakta. Adaptive distributed MIMO radar waveform optimization based on mutual information. *IEEE Transactions on Aerospace & Electronic System,* **49**, 2, 1374–1385 (Apr. 2013).

[211] A. J. Devaney. Time reversal imaging of obscured targets from multistatic data. *IEEE Transactions on Antennas & Propagation,* **53**, 5, 1600–1610 (May 2005).

[212] D. Liu, G. Kang, L. Li, Y. Chen, S. Vasudevan, W. Joines, Q. H. Liu, J. Krolik, and L. Carin. Electromagnetic time-reversal imaging of a target in a cluttered environment. *IEEE Transactions on Antennas & Propagation,* **53**, 9, 3058–3066 (Sept. 2005).

[213] Y. Jin, J. M. F. Moura, Y. Jiang, D. D. Stancil, and A. G. Cepni. Time reversal detection in clutter: Additional experimental results. *IEEE Transactions on Aerospace & Electronic Systems,* **47**, 1, 140–154 (Jan. 2011).

[214] W. M. G. Dyab, T. K. Sarkar, A. Garcia-Lamperez, M. Salazar-Palma, and M. A. Lagunas. A critical look at the principles of electromagnetic time reversal and its consequences. *IEEE Antennas & Propagation Magazine,* **55**, 5, 28–62 (Oct. 2013).

[215] R. O. Harger. Harmonic radar systems for near-ground in-foliage nonlinear scatterers. *IEEE Transactions on Aerospace & Electronic Systems,* **AES-12**, 2, 230–245 (Mar. 1976).

[216] B. G. Colpitts and G. Boiteau. Harmonic radar transceiver design: Miniature tags for insect tracking. *IEEE Transactions on Antennas & Propagation,* **52**, 11, 2825–2832 (Nov. 2004).

[217] G. J. Mazzaro, A. F. Martone, and D. M. McNamara. Detection of RF electronics by multitone harmonic radar. *IEEE Transactions on Aerospace & Electronic Systems,* **50**, 1, 477–490 (Jan. 2014).

[218] K. A. Gallagher, R. M. Narayanan, G. J. Mazzaro, and K. D. Sherbondy. Linearization of a harmonic radar transmitter by feed-forward filter reflection. In *Proceedings of the IEEE Radar Conference*, Cincinnati, OH, May 2014.

[219] K. A. Gallagher, R. M. Narayanan, G. J. Mazzaro, K. I. Ranney, A. F. Martone, and K. D. Sherbondy. Moving target indication with nonlinear radar. In *Proceedings of the IEEE International Radar Conference*, Arlington, VA, May 2015.

[220] H. Aniktar, D. Baran, E. Karav, E. Akkaya, Y. S. Birecik, and M. Sezgin. Getting the bugs out: A portable harmonic radar system for electronic countersurveillance applications. *IEEE Microwave Magazine,* **15**, 10, 40–52 (Nov. 2015).

[221] J. A. Kosinski, W. D. Palmer, and M. B. Steer. Unified understanding of RF remote probing. *IEEE Sensors Journal,* **11**, 12, 3055–3063 (Dec. 2011).

[222] C. Stagner, A. Conrad, C. Osterwise, D. G. Beetner, and S. Grant. A practical superheterodyne-receiver detector using stimulated emissions. *IEEE Transactions on Instrumentation & Measurement,* **60**, 4, 1461–1468 (Apr. 2011).

[223] R. G. Lyons. Signal and interference output of a bandpass nonlinearity. *IEEE Transactions on Communications,* **COM-27**, 6, 888–891 (June 1979).

[224] A. Martone, D. McNamara, G. Mazzaro, and A. Hedden. Cognitive nonlinear radar. *Army Research Lab Tech Rep.,* ARL-MR-0837 (Jan. 2013).

[225] R. M. Axline, G. R. Sloan, and R. E. Spalding. Radar transponder apparatus and signal processing technique. US Patent 5,486,830 (Jan. 1996).

[226] D. Hounam and K. H. Wagel. A technique for the identification and localization of SAR targets using encoding transponders. *IEEE Transactions on Geoscience & Remote Sensing,* **39**, 1, 3–7 (Jan. 2001).

[227] D. L. Richardson, S. A. Stratmoen, G. A. Bendor, H. E. Lee, and M. J. Decker. Tag communication protocol and system. US Patent 6,329,944 (Dec. 2001).

[228] S. V. Vanjari, J. V. Krogmeier, and M. R. Bell. Remote data sensing using SAR and harmonic reradiators. *IEEE Transactions on Aerospace & Electronic Systems,* **43**, 4, 1426–1440 (Oct. 2007).

[229] S. D. Blunt, P. Yatham, and J. Stiles. Intrapulse radar-embedded communications. *IEEE Transactions on Aerospace & Electronic Systems,* **46**, 3, 1185–1200 (July 2010).

[230] S. D. Blunt, J. G. Metcalf, C. R. Biggs, and E. Perrins. Performance characteristics and metrics for intra-pulse radar-embedded communications. *IEEE Journal on Selected Areas in Communications,* **29**, 10, 2057–2066 (Dec. 2011).

[231] J. G. Metcalf, C. Sahin, S. D. Blunt, and M. Rangaswamy. Analysis of symbol-design strategies for intrapulse radar-embedded communications. *IEEE Transactions on Aerospace & Electronic Systems,* **51**, 4, 2914–2931 (Oct. 2015).

[232] D. Ciuonzo, A. De Maio, G. Foglia, and M. Piezzo. Intrapulse radar-embedded communications via multiobjective optimization. *IEEE Transactions on Aerospace & Electronic Systems,* **51**, 4, 2960–2974 (Oct. 2015).

[233] *Sandia Lab News,* 1 and 4 (Nov. 2005).

[234] G. J. Foschini and M. J. Gans. On limits of wireless communications in a fading environment when using multiple antennas. *Wireless Personal Communications,* **6**, 3, 311–335 (1998).

[235] I. E. Telatar. Capacity of multi-antenna Gaussian channels. *European Transactions Communications,* **10**, 6, 585–595 (Nov. 1999).

[236] D. J. Rabideau and P. Parker. Ubiquitous MIMO multifunction digital array radar. In *Proceedings of the 37th Asilomar Conference on Signals, Systems & Computers,* Asilomar, CA, Nov. 2003.

[237] D. W. Bliss and K. W. Forsythe. Multiple-input multiple-output (MIMO) radar and imaging: Degrees of freedom and resolution. In *Proceedings of the 37th Asilomar Conference on Signals, Systems & Computers,* Asilomar, CA, Nov. 2003.

[238] D. J. Rabideau and P. A. Parker. Ubiquitous MIMO multifunction digital array radar … and the role of time–energy management in radar. *MIT Lincoln Lab Tech Rep.,* Project Report DAR-4 ESC-TR-2003-059, Dec. 2003.

[239] M. Skolnik. Systems aspects of digital beam forming ubiquitous radar. *NRL Tech Rep.,* NRL/MR/5007-02-8625, June 2002.

[240] E. Fishler, A. Haimovich, R. Blum, D. Chizhik, L. Cimini, and R. Valenzuela. MIMO radar: An idea whose time has come. In *Proceedings of the IEEE Radar Conference*, Philadelphia, PA, May 2004.

[241] G. V. Trunk and P. K. Hughes. Multi-beam phased arrays using dual apertures. In *Proceedings of the IEEE International Symposium on Phased Array Systems & Technology,* Boston, MA, Oct. 1996.

[242] G. C. Tavik, C. L. Hilterbrick, J. B. Evins, J. J. Alter, J. G. Crnkovich, J. W. de Graaf, W. Habicht, G. P. Hrin, S. A. Lessin, D. C. Wu, and S. M. Hagewood. The advanced multifunction RF concept. *IEEE Transactions on Microwave Theory & Techniques,* **53**, 3, 1009–1020 (Mar. 2005).

[243] P. Calvary and D. Janer. Spatio-temporal coding for radar array processing. In *Proceedings of the IEEE International Conference on Acoustics, Speech & Signal Processing,* Seattle, WA, May 1998.

[244] J. Dorey, Y. Blanchard, and F. Christophe. Le projet RIAS, une approche nouvelle du radar de surveillance aérienne. In *Proceedings of the IEEE Colloque International dur le Radar,* Versailles, France, 1984.

[245] J. Dorey, G. Garnier, and G. Auvray, RIAS, synthetic impulse and antenna radar. In *Proceedings of the International Radar Conference*, Paris, France, Apr. 1989.

[246] A. S. Luce, H. Molina, D. Muller, and V. Thirard. Experimental results on RIAS digital beamforming radar. In *Proceedings of the IET International Radar Conference*, Brighton, United Kingdom, Oct. 1992.

[247] J. Li and P. Stoica, eds., *MIMO Radar Signal Processing,* John Wiley & Sons, Inc., Hoboken, NJ, 2009.

[248] K. M. Cuomo, S. D. Coutts, J. C. McHarg, N. B. Pulsone, and F. C. Robey. Wideband aperture coherence processing for next generation radar (NexGen). *Lincoln Lab Tech Report,* ESC-TR-2004-087, July 2004.

[249] S. Coutts, K. Cuomo, J. McHarg, F. Robey, and D. Weikle. Distributed coherent aperture measurements for next generation BMD radar. In *Proceedings of the IEEE Sensor Array & Multichannel Processing Workshop,* Waltham, MA, July 2006.

[250] J. Bergin, S. McNeil, L. Fomundam, and P. A. Zulch. MIMO phased-array for SMTI radar. In *Proceedings of the IEEE Aerospace Conference*, Big Sky, MT, Mar. 2008.

[251] D. R. Fuhrmann, J. P. Browning, and M. Rangaswamy. Signaling strategies for the hybrid MIMO phased-array radar. *IEEE Journal of Selected Topics in Signal Processing,* **4**, 1, 66–78 (Jan. 2010).

[252] H. Li and B. Himed. Transmit subaperaturing for MIMO radar with co-located antennas. *IEEE Journal of Selected Topics in Signal Processing,* **4**, 1, 55–65 (Jan. 2010).

[253] F. Daum and J. Huang. MIMO radar: Snake oil or good idea? *IEEE Aerospace & Electronic Systems Magazine,* **24**, 5, 8–12 (May 2009).

[254] E. Brookner. MIMO radar demystified and where it makes sense to use. In *Proceedings of the IEEE Radar Conference*, Cincinnati, OH, May 2014.

[255] F. C. Robey, S. Coutts, D. Weikle, J. C. McHarg, and K. Cuomo. MIMO radar theory and experimental results. In *Proceedings of the 38th Asilomar Conference on Signals, Systems & Computers,* Asilomar, CA, Nov. 2004.

[256] G. Krieger. MIMO-SAR: Opportunities and pitfalls. *IEEE Transactions on Geoscience & Remote Sensing,* **52**, 5, 2628–2645 (May 2014).

[257] T. K. Sarkar, S. Burintramart, N. Yilmazer, S. Hwang, Y. Zhang, A. De, and M. Salazar-Palma. A discussion about some of the principles/practices of wireless communication under a Maxwellian framework. *IEEE Transactions on Antennas & Propagation,* **54**, 12, 3727–3745 (Dec. 2006).

[258] G. J. Frazer, Y. I. Abramovich, and B. A. Johnson. Spatially waveform diverse radar: Perspectives for high frequency OTHR. In *Proceedings of the IEEE Radar Conference*, Boston, MA, Apr. 2007.

[259] G. J. Frazer, Y. I. Abramovich, and B. A. Johnson. Use of adaptive non-causal transmit beamforming in OTHR: Experimental results. In *Proceedings of the IEEE International Radar Conference*, Adelaide, Australia, Sept. 2008.

[260] H. L. Van Trees, *Optimum Array Processing,* New York, NY, USA: John Wiley & Sons, 2002.

[261] G. San Antonio, D. R. Fuhrmann, and F. C. Robey. MIMO radar ambiguity functions. *IEEE Journal of Selected Topics in Signal Processing,* **1**, 1, 167–177 (June 2007).

[262] C.-Y. Chen and P. P. Vaidyanathan. Properties of the MIMO radar ambiguity function. In *Proceedings of the IEEE International Conference on Acoustics, Speech & Signal Processing,* Las Vegas, NV, Mar./Apr. 2008.

[263] B. Friedlander. On signal models for MIMO radar. *IEEE Transactions on Aerospace & Electronic Systems,* **48**, 4, 3655–3660 (Oct. 2012).

[264] W. L. Melvin. A STAP overview. *IEEE Aerospace & Electronic Systems Magazine,* **19**, 1, 19–35 (Jan. 2004).

[265] T. Higgins, T. Webster, and A. K. Shackelford. Mitigating interference via spatial and spectral nulling. *IET Radar, Sonar & Navigation,* **8**, 2, 84–93 (Feb. 2014).

[266] T. Webster, T. Higgins, A. K. Shackelford, J. Jakabosky, and P. McCormick. Phase-only adaptive spatial transmit nulling. In *Proceedings of the IEEE International Radar Conference*, Arlington, VA, May 2015.

[267] B. Cordill, J. Metcalf, S. A. Seguin, D. Chatterjee, and S. D. Blunt. The impact of mutual coupling on MIMO radar emissions. In *Proceedings of the IEEE International Conference on Electromagnetics in Advanced Applications,* Torino, Italy, Sept. 2011.

[268] G. Babur, P. J. Aubry, and F. Le Chevalier. Antenna coupling effects for space–time radar waveforms: Analysis and calibration. *IEEE Transactions on Antennas & Propagation,* **62**, 5, 2572–2586 (May 2014).

[269] W.-Q. Wang, *Multi-Antenna Synthetic Aperture Radar,* Boca Raton, FL, USA: CRC Press, 2013.

[270] P. F. Sammartino, D. Tarchi, J. Fortuny-Guasch, F. Oliveri, and R. Giuliani. Phase compensation and processing in multiple-input-multiple-output radars. *IET Radar, Sonar & Navigation,* **6**, 4, 222–232 (Apr. 2012).

[271] J. D. Taylor, *Introduction to Ultra-Wideband Radar Systems,* Boca Raton, FL, USA: CRC Press, 1994.

[272] P. M. McCormick, S. D. Blunt, and J. Metcalf. Joint spectrum/beampattern design of wideband MIMO radar emissions. In *Proceedings of the IEEE Radar Conference*, Philadelphia, PA, May 2016.

[273] P. Antonik, M. C. Wicks, H. D. Griffiths, and C. J. Baker. Frequency diverse array radars. In *Proceedings of the IEEE Radar Conference*, Verona, NY, Apr. 2006.

[274] M. Secmen, S. Demir, A. Hizal, and T. Eker. Frequency diverse array antenna with periodic time modulated pattern in range and angle. In *Proceedings of the IEEE Radar Conference*, Waltham, MA, Apr. 2007.

[275] T. Higgins and S. Blunt. Analysis of range-angle coupled beamforming with frequency-diverse chirps. In *Proceedings of the International Waveform Diversity & Design Conference*, Orlando, FL, Feb. 2009.

[276] P. F. Sammartino, C. J. Baker, and H. D. Griffiths. Frequency diverse MIMO techniques for radar. *IEEE Transactions on Aerospace & Electronic Systems,* **49**, 1, 201–222 (Jan. 2013).

[277] W.-Q. Wang. Range-angle dependent transmit beampattern synthesis for linear frequency diverse arrays. *IEEE Transactions on Antennas & Propagation,* **61**, 8, 4073–4081 (Aug. 2013).

[278] G. Babur, P. Aubry, and F. LeChevalier. Space–time radar waveforms: Circulating codes. *Journal of Electrical & Computer Engineering*, 2013.

[279] K. Roussel, G. Babur, and F. Le Chevalier. Optimization of low sidelobes radar waveforms: Circulating codes. In *Proceedings of the International Radar Conference*, Lille, France, Oct. 2014.

[280] M. Rolfs. Microsaccades: Small steps on a long way. *Vision Research,* **49**, 2415–2441 (2009).

[281] E. Ahissar and A. Arieli. Seeing via miniature eye movements: A dynamic hypothesis for vision. *Frontiers in Computational Neuroscience,* **6**, 89 (Nov. 2012).

[282] S. D. Blunt, P. McCormick, T. Higgins, and M. Rangaswamy. Physical emission of spatially-modulated radar. *IET Radar, Sonar & Navigation,* **8**, 12, 1234–1246 (Dec. 2014).

[283] P. McCormick and S. D. Blunt. Fast-time 2-D spatial modulation of physical radar emissions. In *Proceedings of the International Radar Symposium*, Dresden, Germany, June 2015.

[284] C.-Y. Chen and P. P. Vaidyanathan. MIMO radar space–time adaptive processing using prolate spheroidal wave functions. *IEEE Transactions on Signal Processing,* **56**, 2, 623–635 (Feb. 2008).

[285] Y. I. Abramovich, G. J. Frazer, and B. A. Johnson. Iterative adaptive Kronecker MIMO radar beamformer: Description and convergence analysis. *IEEE Transactions on Signal Processing,* **58**, 7, 3681–3691 (July 2010).

[286] W. Roberts, P. Stoica, J. Li, T. Yardibi, and F. A. Sadjadi. Iterative adaptive approaches to MIMO radar imaging. *IEEE Journal of Selected Topics in Signal Processing,* **4**, 1, 5–20 (Jan. 2010).

[287] J. Yu and J. Krolik. MIMO adaptive beamforming for nonseparable multipath clutter mitigation. *IEEE Transactions on Aerospace & Electronic Systems,* **50**, 4, 2604–2618 (Oct. 2014).

[288] P. M. McCormick, T. Higgins, S. D. Blunt, and M. Rangaswamy. Adaptive receive processing of spatially modulated physical radar emissions. *IEEE Journal of Selected Topics in Signal Processing,* **9**, 8, 1415–1426 (Dec. 2015).

[289] S. D. Blunt, J. Metcalf, J. Jakabosky, J. Stiles, and B. Himed. Multiwaveform space–time adaptive processing. to appear in *IEEE Transactions on Aerospace & Electronic Systems*.

[290] H. D. Griffiths, M. C. Wicks, D. Weiner, R. Adve, P. A. Antonik, and I. Fotinopoulos. Denial of bistatic hosting by spatial–temporal waveform design. *IEE Proceedings Radar, Sonar & Navigation,* **152**, 2, 81–88 (Apr. 2005).

[291] E. B. Baruch and A. Leshem. Overcoming spatial denial in non-cooperative bistatic radar. In *Proceedings of the IEEE Sensor Array & Multichannel Signal Processing Workshop,* Hoboken, NJ, June 2012.

[292] J. Euziere, R. Guinvarc'h, M. Lesturgie, B. Uguen, and R. Gillard. Dual function radar communication time-modulated array. In *Proceedings of the International Radar Conference*, Lille, France, Oct. 2014.

[293] A. Hassanien, M. G. Amin, Y. D. Zhang, and F. Ahmad. Dual-function radar-communications: Information embedding using sidelobe control and waveform diversity. to appear in *IEEE Transactions on Signal Processing.*

[294] A. Hassanien, M. G. Amin, Y. D. Zhang, and F. Ahmad. Phase-modulation based dual-function radar-communications. to appear in *IET Radar, Sonar & Navigation.*

[295] A. L. Hume and C. J. Baker. Netted radar sensing. In *Proceedings of the IEEE Radar Conference*, Atlanta, GA, May 2001.

[296] H. Deng. Orthogonal netted radar systems. *IEEE Aerospace & Electronic Systems Magazine,* **27**, 5, 28–35 (May 2012).

[297] E. Fishler, A. Haimovich, R. Blum, L. Cimini, D. Chizhik, and R. Valenzuela. Spatial diversity in radars—Models and detection performance. *IEEE Transactions on Signal Processing,* **54**, 823–838 (Mar. 2006).

[298] A. M. Haimovich, R. S. Blum, and L. J. Cimini. MIMO radar with widely separated antennas. *IEEE Signal Processing Magazine,* **25**, 1, 116–129 (Jan. 2008).

[299] H. Godrich, A. M. Haimovich, and R. S. Blum. Target localization accuracy gain in MIMO radar-based systems. *IEEE Transactions on Information Theory,* **56**, 6, 2783–2803 (June 2010).

[300] K. Milne. Principles and concepts of multistatic surveillance radars. In *Proceedings of the IET International Radar Conference*, London, United Kingdom, Oct. 1977.

[301] E. Conte, E. D'Addio, A. Farina, and M. Longo. Multistatic radar detection: Synthesis and comparison of optimum and suboptimum receivers. *IEE Proceedings F—Communications, Radar & Signal Processing,* **130**, 6, 484–494 (Oct. 1983).

[302] E. Hanle. Survey of bistatic and multistatic radar. *IEE Proceedings F—Communications, Radar & Signal Processing,* **133**, 7, 613–623 (Dec. 1986).

[303] E. D'Addio and A. Farina. Overview of detection theory in multistatic radar. *IEE Proceedings F—Communications, Radar & Signal Processing,* **133**, 7, 587–595 (Dec. 1986).

[304] V. S. Chernyak, *Fundamentals of Multisite Radar Systems: Multistatic Radars and Multistatic Radar Systems,* Amsterdam, The Netherlands: CRC Press, 1998. (Russian version in 1993).

[305] V. S. Chernyak. On the concept of MIMO radar. In *Proceedings of the IEEE International Radar Conference*, Arlington, VA, May 2010.

[306] Y. Yang and R. S. Blum. Phase synchronization for coherent MIMO radar: Algorithms and their analysis. *IEEE Transactions on Signal Processing,* **59**, 11, 5538–5557 (Nov. 2011).

[307] M. R. Inggs, J. S. Sandenbergh, and S. A. C. Lewis. Investigation of white rabbit for synchronization and timing of netted radar. In *Proceedings of the IEEE Radar Conference*, Johannesburg, South Africa, Oct. 2015.

[308] P. Swerling. Probability of detection for fluctuating targets. *IRE Transactions Information Theory,* **IT-6**, 2, 269–308 (Apr. 1960).

[309] W. P. Birkemeier and N. D. Wallace. Radar tracking accuracy improvement by means of pulse-to-pulse frequency modulation. *AIEE Transactions Communication & Electronics,* **81**, 6, 571–575 (Jan. 1963).

[310] R. J. Sims and E. R. Graf. Reduction of radar glint by diversity techniques. *IEEE Transactions on Antennas & Propagation,* **AP-19**, 4. 462–468 (July 1971).

[311] V. Vannicola. Detection of slow fluctuating targets with frequency diversity channels. *IEEE Transactions on Aerospace & Electronic Systems,* **AES-10**, 1, 43–52 (Jan. 1974).

[312] J. M. Loomis and E. R. Graf. Frequency-agility processing to reduce radar glint pointing error. *IEEE Transactions on Aerospace & Electronic Systems,* **AES-10**, 6, 811–820 (Nov. 1974).

[313] M. C. Jackson. The geometry of bistatic radar systems. *IEE Proceedings F—Communications, Radar, & Signal Processing,* **133**, 7, 604–612 (Dec. 1986).

[314] T. Tsao, M. Slamani, P. Varshney, D. Weiner, and H. Schwarzlander. Ambiguity function for a bistatic radar. *IEEE Transactions on Aerospace & Electronic Systems,* **33**, 3, 1041–1051 (July 1997).

[315] P. Howland, ed., Special issue on Passive Radar Systems, *IEE Proceedings Radar, Sonar & Navigation,* **152**, 3 (June 2005).

[316] H. D. Griffiths and C. J. Baker. Measurement and analysis of ambiguity functions of passive radar transmissions. In *Proceedings of the IEEE International Radar Conference*, Arlington, VA, May 2005.

[317] C. J. Baker, H. D. Griffiths, and I. Papoutsis. Passive coherent location radar systems. Part 2: Waveform properties. *IEE Proceedings Radar, Sonar & Navigation,* **152**, 3, 160–168 (June 2005).

[318] I. Bradaric, G. Capraro, D. Weiner, and M. Wicks. Multistatic radar systems signal processing. In *Proceedings of the IEEE Radar Conference*, Verona, NY, Apr. 2006.

[319] T. Derham, S. Doughty, C. Baker, and K. Woodbridge. Ambiguity functions for spatially coherent and incoherent multistatic radar. *IEEE Transactions on Aerospace & Electronic Systems,* **46**, 1, 230–245 (Jan. 2010).

[320] T. Webster, J. Kim, I. Bradaric, and M. Cheney. Deterministic and statistical models for multistatic ambiguity functions. In *Proceedings of the IEEE Radar Conference*, Atlanta, GA, May 2012..

[321] M. S. Greco, P. Stinco, F. Gini, and A. Farina. Cramer-Rao bounds and selection of bistatic channels for multistatic radar systems. *IEEE Transactions on Aerospace & Electronic Systems,* **47**, 4, 2934–2948 (Oct. 2011).

[322] S. R. Stevens and J. A. Jackson. Emitter selection criteria for passive multistatic synthetic aperture radar imaging. *IET Radar, Sonar & Navigation,* **8**, 9, 1267–1279 (Dec. 2014).

[323] T. Webster, M. Cheney, E. L. Mokole. Multistatic polarimetric radar data modeling and imaging of moving targets. *Inverse Problems,* **30**, 3 (Feb. 2014).

[324] S. Brisken. Multistatic ISAR—Chances and challenges. In *Proceedings of the International Radar Conference*, Lille, France, Oct. 2014.

[325] T. Higgins, T. Webster, and E. L. Mokole. Passive multistatic radar experiment using WiMAX signals of opportunity. Part 1: Signal processing. *IET Radar, Sonar & Navigation,* **10**, 2, 238–247 (Feb. 2016).

[326] T. Webster, T. Higgins, and E. L. Mokole. Passive multistatic radar experiment using WiMAX signals of opportunity. Part 2: Multistatic velocity backprojection. *IET Radar, Sonar & Navigation,* **10**, 2, 248–255 (Feb. 2016).

[327] L. Lo Monte, D. Erricolo, F. Soldovieri, and M. C. Wicks. Radio frequency tomography for tunnel detection. *IEEE Transactions on Geoscience & Remote Sensing,* **48**, 3, 1128–1137 (Mar. 2010).

[328] J. Brown, K. Woodbridge, H. Griffiths, and A. Stove. Passive bistatic radar experiments from an airborne platform. *IEEE Aerospace & Electronic Systems Magazine,* **27**, 11, 50–55 (Nov. 2012).

[329] D. J. Sego and H. Griffiths. Tomography using digital broadcast television. In *Proceedings of the IEEE Radar Conference*, Cincinnati, OH, May 2014.

[330] T. M. Tran, A. J. Terzuoli, G. J. Scalzi, and L. Lo Monte. Toward passive RF tomography: Signal processing and experimental validation. In *Proceedings of the IEEE Radar Conference,* Cincinnati, OH, May 2014.

[331] C. C. Tseng and C. L. Liu. Complementary sets of sequences. *IEEE Transactions on Information Theory,* **IT-18**, 5, 644–652 (Sept. 1972).

[332] R. Sivaswamy. Multiphase complementary codes. *IEEE Transactions on Information Theory,* **IT-24**, 5, 546–552 (Sept. 1978).

[333] R. L. Frank. Polyphase complementary codes. *IEEE Transactions on Information Theory,* **IT-26**, 6, 641–647 (Oct. 1980).

[334] F. F. Kretschmer and K. Gerlach. Low sidelobe radar waveforms derived from orthogonal matrices. *IEEE Transactions on Aerospace & Electronic Systems,* **27**, 1, 92–102 (Jan. 1991).

[335] A. Pezeshki, A. R. Calderbank, W. Moran, and S. D. Howard. Doppler resilient Golay complementary waveforms. *IEEE Transactions on Information Theory,* **54**, 9, 4254–4266 (Sept. 2008).

[336] E. Mozeson and N. Levanon. Removing autocorrelation sidelobes by overlaying orthogonal coding on any train of identical pulses. *IEEE Transactions on Aerospace & Electronic Systems,* **39**, 2, 583–603 (Apr. 2003).

[337] S. J. Searle, S. D. Howard, and W. Moran. Formation of ambiguity functions with frequency-separated Golay coded pulses. *IEEE Transactions on Aerospace & Electronic Systems,* **45**, 4, 1580–1597 (Oct. 2009).

[338] R. C. Chen and T. Higgins. Doppler tolerant time separated Golay waveforms. In *Proceedings of the International Waveform Diversity & Design Conference*, Lihue, HI, Jan. 2012.

[339] D. R. Wehner, *High-Resolution Radar,* 2nd ed., Artech House, 1995.

[340] D. E. Maron. Frequency-jumped burst waveforms with stretch processing. In *Proceedings of the IEEE Radar Conference*, Arlington, VA, May 1990.

[341] D. J. Rabideau. Nonlinear synthetic wideband waveforms. In *Proceedings of the IEEE Radar Conference*, Los Angeles, CA, May 2002.

[342] N. Levanon. Stepped-frequency pulse-train radar signal. *IEE Proceedings Radar, Sonar & Navigation,* **149**, 6, 297–309 (Dec. 2002).

[343] N. Levanon and E. Mozeson. Nullifying ACF grating lobes in stepped-frequency train of LFM pulses. *IEEE Transactions on Aerospace & Electronic Systems,* **39**, 2, 694–703 (Apr. 2003).

[344] I. Gladkova and D. Chebanov. Grating lobes suppression in stepped-frequency pulse train. *IEEE Transactions on Aerospace & Electronic Systems,* **44**, 4, 1265–1275 (Oct. 2008).

[345] I. Gladkova. Analysis of stepped-frequency pulse train design. *IEEE Transactions on Aerospace & Electronic Systems,* **45**, 4, 1251–1261 (Oct. 2009).

[346] W. L. Melvin and J. A. Scheer, eds., *Principles of Modern Radar, Vol. II: Advanced Techniques,* Raleigh, NC, USA: SciTech, 2013.

[347] J. M. Anderson, M. A. Temple, W. M. Brown, and B. L. Crossley. A nonlinear suppression technique for range ambiguity resolution in pulse Doppler radars. In *Proceedings of the IEEE Radar Conference*, Atlanta, GA, May 2001.

[348] J. D. Jenshak and J. M. Stiles. Transmit coding with a range ambiguity. In *Proceedings of the International Waveform Diversity & Design Conference*, Orlando, FL, Feb. 2009.

[349] S. Blunt, M. Cook, and J. Stiles. Embedding information into radar emissions via waveform implementation. In *Proceedings of the International Waveform Diversity & Design Conference*, Niagara Falls, Canada, Aug. 2010.

[350] T. G. Leighton, G. H. Chua, P. R. White, K. F. Tong, and H. D. Griffiths. Radar clutter suppression and target discrimination using twin inverted pulses. *Proceedings of the Royal Society of London A,* **469** (Oct. 2013).

[351] T. G. Leighton, D. C. Finfer, P. R. White, G. H. Chua, and J. K. Dix. Clutter suppression and classification using Twin Inverted Pulse Sonar (TWIPS). *Proceedings of the Royal Society of London A,* **466**, 3453–3478 (Dec. 2010).

[352] T. G. Leighton, D. C. Finfer, G. H. Chua, P. R. White, and J. K. Dix. Clutter suppression and classification using Twin Inverted Pulse Sonar in ship wakes. *Journal of the Acoustical Society of America,* **130**, 3431–3437 (Nov. 2011).

[353] B. G. Laird. On ambiguity resolution by random phase processing. In *Proceedings of the International Conference on Radar Meteorology,* Boston, MA, 1981.

[354] S. Carlsson. MTI-filtering for multiple time around clutter suppression in coherent on receive radars. In *Proceedings of the IET International Radar Conference*, London, United Kingdom, Oct. 1982.

[355] M. Sachidananda and D. S. Zrnic. Recovery of spectral moments from overlaid echoes in a Doppler weather radar. *IEEE Transactions on Geoscience & Remote Sensing,* **GE-24**, 5, 751–764 (Sept. 1986).

[356] F. Lin and M. Steiner. New techniques for radar coherent range ambiguity resolution. In *Proceedings of the IEEE Radar Conference*, Atlanta, GA, May 2001.

[357] N. Levanon. Mitigating range ambiguity in high PRF radar using inter-pulse binary coding. *IEEE Transactions on Aerospace & Electronic Systems,* **45**, 2, 687–697 (Apr. 2009).

[358] M. Cook, S. D. Blunt, and J. Jakabosky. Optimization of waveform diversity and performance for pulse-agile radar. In *Proceedings of the IEEE Radar Conference*, Kansas City, MO, May 2011.

[359] A. O'Connor, J. Kantor, and J. Jakabosky. Joint equalization filters that mitigate waveform-diversity modulation of clutter. In *Proceedings of the IEEE Radar Conference*, Philadelphia, PA, May 2016.

[360] D. P. Scholnik. Range-ambiguous clutter suppression with pulse-diverse waveforms. In *Proceedings of the IEEE Radar Conference*, Kansas City, MO, May 2011.

[361] T. Higgins, S. Blunt, and A. Shackelford. Time-range adaptive processing for pulse agile radar. In *Proceedings of the International Waveform Diversity & Design Conference*, Niagara Falls, Canada, Aug. 2010.

[362] T. Higgins, K. Gerlach, A. Shackelford, and S. Blunt. Aspects of non-identical multiple pulse compression. In *Proceedings of the IEEE Radar Conference*, Kansas City, MO, May 2011.

[363] A. O'Connor, J. Kantor, and J. Jakabosky. Space–time adaptive mismatch processing. In *Proceedings of the IEEE Radar Conference*, Philadelphia, PA, May 2016.

[364] H. R. Ward. Doppler processor rejection of range ambiguous clutter. **AES-11**, 2, 519–522 (July 1975).

[365] J. P. Reilly. Clutter rejection limitations from ambiguous range clutter. In *Proceedings of the IEEE International Radar Conference*, Arlington, VA, May 1990.

[366] F. E. Nathanson, J. P. Reilly, and M. N. Cohen, *Radar Design Principles,* 2nd ed., SciTech, 1999.

[367] B. C. Flores, E. A. Solis, and G. Thomas. Assessment of chaos-based FM signals for range-Doppler imaging. *IEE Proceedings Radar, Sonar & Navigation,* **150**, 4, 313–322 (Aug. 2003).

[368] E. Gambi, F. Chiaraluce, and S. Spinsante. Chaos-based radars for automotive applications: Theoretical issues and numerical simulation. *IEEE Transactions on Vehicular Technology,* **57**, 6, 3858–3863 (Nov. 2008).

[369] Q. Yang, Y. Zhang, and X. Gu. Design of ultralow sidelobe chaotic radar signal by modulating group delay method. *IEEE Transactions on Aerospace & Electronic Systems,* **51**, 4, 3023–3035 (Oct. 2015).

[370] J. Jakabosky, S. D. Blunt, and B. Himed. Waveform design and receive processing for nonrecurrent nonlinear FMCW radar. In *Proceedings of the IEEE International Radar Conference*, Arlington, VA, May 2015.

[371] J. Jakabosky, S. D. Blunt, and B. Himed. Spectral-shape optimized FM noise radar for pulse agility. In *Proceedings of the IEEE Radar Conference*, Philadelphia, PA, May 2016.

[372] D. Giuli. Polarization diversity in radars. *IEE Proceedings,* **74**, 2, 245–269 (Feb. 1986).

[373] G. A. Ioannidis and D. E. Hammers. Optimum antenna polarizations for target discrimination in clutter. *IEEE Transactions on Antennas & Propagation,* **AP-27**, 3, 357–363 (May 1979).

[374] E. R. Ferrara and T. M. Parks. Direction finding with an array of antennas having diverse polarizations. *IEEE Transactions on Antennas & Propagation,* **AP-31**, 2, 231–236 (Mar. 1983).

[375] N. E. Chamberlain, E. K. Walton, and F. D. Garber. Radar target identification of aircraft using polarization-diverse features. *IEEE Transactions on Aerospace & Electronic Systems,* **27**, 1, 58–67 (Jan. 1991).

[376] L. M. Novak, M. C. Burl, and W. W. Irving. Optimal polarimetric processing for enhanced target detection. *IEEE Transactions on Aerospace & Electronic Systems,* **29**, 1, 234–244 (Jan. 1993).

[377] F. Sadjadi. Improved target classification using optimum polarimetric SAR signatures. *IEEE Transactions on Aerospace & Electronic Systems,* **38**, 1, 38–49 (Jan. 2002).

[378] F. Aldhubaib, and N. V. Shuley. Radar target recognition based on modified characteristic polarization states. *IEEE Transactions on Aerospace & Electronic Systems,* **46**, 4, 1921–1933 (Oct. 2010).

[379] M. Martorella, E. Giusti, L. Demi, Z. Zhou, A. Cacciamano, F. Berizzi, and B. Bates. Target recognition by means of polarimetric ISAR images. *IEEE Transactions on Aerospace & Electronic Systems,* **47**, 1, 225–239 (Jan. 2011).

[380] R. Touzi, J. Hurley, and P. W. Vachon. Optimization of the degree of polarization for enhanced ship detection using polarimetric RADARSAT-2. *IEEE Transactions on Geoscience & Remote Sensing,* **53**, 10, 5403–5424 (Oct. 2015).

[381] T. A. Seliga and V. N. Bringi. Potential use of radar differential reflectivity measurements of orthogonal polarizations for measuring precipitation. *Journal of Applied Meteorology & Climatology,* **15**, 1, 67–76 (Jan. 1976).

[382] F. K. Schwering, E. J. Violette, and R. H. Espeland. Millimeter-wave propagation in vegetation: Experiments and theory. *IEEE Transactions on Geoscience & Remote Sensing,* **26**, 3, 355–367 (May 1988).

[383] V. N. Bringi and V. Chandrasekar, *Polarimetric Doppler Weather Radar: Principles and Applications,* Cambridge, United Kingdom: Cambridge Univ. Press, 2001.

[384] S. Lim, V. Chandrasekar, and V. N. Bringi. Hydrometeor classification system using dual-polarization radar measurements: Mode improvements and in situ verification. *IEEE Transactions on Geoscience & Remote Sensing,* **43**, 4, 792–801 (Apr. 2005).

[385] J. P. Fritz and V. Chandrasekar. A fully polarimetric characterization of the impact of precipitation on short wavelength synthetic aperture radar. *IEEE Transactions on Geoscience & Remote Sensing,* **50**, 5, 2037–2048 (May 2012).

[386] M. Hurtado and A. Nehorai. Polarimetric detection of targets in heavy inhomogeneous clutter. *IEEE Transactions on Signal Processing,* **56**, 4, 1349–1361 (Apr. 2008).

[387] S. R. Cloude and K. P. Papathanassiou. Polarimetric SAR interferometry. *IEEE Transactions on Geoscience & Remote Sensing,* **36**, 5, 1551–1565 (Sept. 1998).

[388] J. J. van Zyl and Y. Kim, *Synthetic Aperture Radar Polarimetry,* Hoboken, NJ, USA: John Wiley & Sons, 2011.

[389] J. L. Eaves and B. C. Appling. Intrapulse polarization agile radar system (IPAR), U.S. Patent 4 472 717, Sept. 18, 1984.

[390] E. M. Kennaugh, *Polarization Properties of Radar Reflection,* M. S. thesis, Electrical Engineering Dept., Ohio State University, Mar. 1952.

[391] J. R. Huynen. Phenomenological theory of radar targets. Ph.D. dissertation, Technical University of Delft, The Netherlands, 1970.

[392] W. M. Boerner, M. B. El-Arini, C. Y. Chan, and P. M. Mastoris. Polarization dependence in electromagnetic inverse problems. *IEEE Transactions on Antennas & Propagation,* **AP-29**, 2, 262–271 (Mar. 1981).

[393] S. R. Cloude and E. Pottier. A review of target decomposition theorems in radar polarimetry. *IEEE Transactions on Geoscience & Remote Sensing,* **34**, 2, 498–518 (Mar. 1996).

[394] A. Y. Nashashibi, K. Sarabandi, P. Frantzis, R. D. De Roo, and F. T. Ulaby. An ultrafast wide-band millimeter-wave (MMW) polarimetric radar for remote sensing applications. *IEEE Transactions on Geoscience & Remote Sensing,* **40**, 8, 1777–1786 (Aug. 2002).

[395] J. Dall, S. S. Kristensen, V. Krozer, C. C. Hernandez, J. Vidkjaer, A. Kusk, J. Balling, N. Skou, S. S. Søbjaerg, and E. L. Christensen. ESA's Polarimetric airborne radar ice sounder (POLARIS): Design and first results. *IET Radar, Sonar & Navigation,* **4**, 3, 488–496 (June 2010).

[396] D. Giuli, L. Facheris, M. Fossi, and A. Rossettini. Simultaneous scattering matrix measurement through signal coding. In *Proceedings of the IEEE International Radar Conference*, Arlington, VA, May 1990.

[397] D. Giuli, M. Fossi, and L. Facheris. Radar target scattering matrix measurement through orthogonal signals. *IEE Proceedings F: Radar and Signal Processing,* **140**, 4, 233–242 (Aug. 1993).

[398] M. Galletti, D. S. Zrnic, F. Gekat, and P. Goelz. Eigenvalue signal processing for weather radar polarimetry: Removing the bias induced by antenna coherent cross-channel coupling. *IEEE Transactions on Geoscience & Remote Sensing,* **52**, 12, 7695–7707 (Dec. 2014).

[399] I. R. Ivic, and R. J. Doviak. Evaluation of phase coding to mitigate differential reflectivity bias in polarimetric PAR. *IEEE Transactions on Geoscience & Remote Sensing,* **54**, 1, 431–451 (Jan. 2016).

[400] Z. Wang, F. Tigrek, O. Krasnov, F. Van Der Zwan, P. Van Genderen, and P. Yarovoy. Interleaved OFDM radar signals for simultaneous polarimetric measurements. *IEEE Transactions on Aerospace & Electronic Systems,* **48**, 3, 2085–2099 (July 2012).

BIO

Shannon D. Blunt (S'96—M'02—SM'07—F'16) received the Ph.D. degree in electrical engineering from the University of Missouri in 2002. From 2002 to 2005 he was with the Radar Division of the Naval Research Laboratory in Washington, D.C. Since 2005 he has been with the Department of Electrical Engineering and Computer Science at the University of Kansas where he is currently a Professor and Director of the Radar Systems & Remote Sensing Lab (RSL).

In 2012 Prof. Blunt received the IEEE/AESS Nathanson Memorial Radar Award and in 2008 received the AFOSR Young Investigator Award. He has over 120 refereed journal and conference publications, 11 patents, 7 book chapters, and co-edited the book Principles of Waveform Diversity & Design.

He is a member of the IEEE/AESS Radar Systems Panel where he is currently Chair of the Conferences Committee and the Nathanson Award Committee. He is an Associate Editor for IEEE Transactions on Aerospace & Electronic Systems and is on the Editorial Board for IET Radar, Sonar & Navigation. He was General Chair of the 2011 IEEE Radar Conference in Kansas City and is a member of the Program Committee for the MSS Tri-Service Radar Symposium series. He was Chair of the NATO SET-179 research task group on "Dynamic Waveform Diversity & Design" and a member of SET-182 on "Radar Spectrum Engineering & Management" and SET-227 on "Cognitive Radar". He is a Fellow of IEEE.

Eric L. Mokole (F'11) received the B.S. degree in applied mathematics from New York University (New York, NY) in 1971, the M.S. degree in mathematics from Northern Illinois University (DeKalb, IL) in 1973, the M.S. degrees in physics and applied mathematics in 1976 and 1978, respectively, and the Ph.D. degree in mathematics in 1982 from the Georgia Institute of Technology (Atlanta, GA).

Dr. Mokole retired from the US Naval Research Laboratory (NRL) in 2014 after 32 years of experience in conducting and leading radar-related R&D and system analyses for existing and proposed US Navy radar programs on spaceborne, airborne, shipboard, expeditionary-based, and ultrawideband platforms. These efforts involved: radar waveform diversity and design; radar spectrum theory and engineering; system simulation/modeling; data analysis; information extraction; non-Gaussian detection theory; electronic-warfare and electronic-protection modeling; RF propagation aboard naval ships; tropospheric/ionospheric propagation; pulsed propagation for dispersive media; layered-media propagation; RF scattering from the sea, atmosphere, land, and human-made structures; sensing through the earth and man-made structures; and antenna theory and development. From 1983 to 1986 he held a position in the Electronic Warfare Division of the Naval Intelligence Support Center (now the Office of Naval Intelligence) in Washington, DC. From 1986-2014, he was employed in various roles by the NRL Radar Division. From 2001-2005, he was Head of the NRL Surveillance Technology Branch. After a period as Acting Superintendent of NRL Radar from 2005-2008, he resumed Branch-Head duties until his retirement in 2014. Currently, he is an independent consultant.

He has over 85 conference/journal articles, book chapters, and reports and is co-editor/co-author of 5 books (Ultra-Wideband, Short-Pulse Electromagnetics 6, 7, and 10; Physics of Multiantenna Systems and Broadband Processing; Principles of Waveform Diversity and Design). He has presented over 150 talks and tutorials. Currently, Dr. Mokole is a Member of IEEE AES-S Radar Systems Panel and Member of its Conference, Waveform Diversity, and Radar Standards Committees, Chair of the IEEE AP-S Standing Committee on New Technology Directions, Co-Chair of the AP-S committee on the Special Interest Group on Humanitarian Technology (SIGHT), Member of the AP-S Standards Committee, Chair of the AP-S RCS Measurements Standard Revision (Std. 1502), Member of the AP-S Strategic Planning Committee, and Member of the AP-S Member and Geographic Activities Committee (2015-present). He is also Government Liaison to USNC-URSI where he is a Member of Commissions A/B/C/E and Secretary and Vice-Chair of C. He has served as the US Member, Vice Chair, and Chair of NATO's Sensors and Electronics Technology Panel, as the US Navy Lead for the MSS Tri-Service Radar Symposia, and as a Committee Member of the MSS National Symposia), as well as being on the MSS Executive Committee. He was a Panel Member and Subject Matter Expert for the US Office of Secretary of Defense's Radar Spectrum and Technology Working Group, a Founding Member of Tri-Service Waveform Diversity Working Group, and is a Member of the AMEREM/EUROEM High-Power Electromagnetics Committee. He is an MSS Fellow and a Fellow if the IEEE.

IEEE Aerospace and Electronic Systems Magazine *
(AES-M)

IEEE Aerospace & Electronic Systems Magazine

ISSN: 0885-8985/Coden: IESMEA
PUBID: 62
Vo1. 1, no. 1-(Jan. 1986-Present)
AES-M

IEEE Aerospace and Electronic Systems Society Newsletter*
OCLC: 12814086
Vol. 10, no. 1-Vol. 20, no. 12 (Jan 1975–Dec 1985)

[NOTE: Not in IEEE Xplore]

S -AES Newsletter
[Aerospace & Electronic Systems Society Newsletter]
Vol. 8, no. 3–Vol. 9, no.12 (Mar 1973–Dec 1974)
[NOTE: Not in IEEE Xplore]

Note: These newsletters did not carry articles. They carried announcements, news, and membership information.

The IEEE changed groups to societies effective Jan. 1, 1973.

G-AES Newsletter
[Group on Aerospace & Electronics Systems]
Vol. 1, no. 1–Vol. 8, no. 2 (July 1965–Feb 1973)
[NOTE: Not in IEEE Xplore]

Effective July 1, 1965, the Aerospace and Electronic Systems (AES) Group was formed by the merger of the Military Electronics (MIL), Aerospace & Navigational Electronics (ANE), Space Electronics & Telemetry (SET) and Aerospace (AS) Groups.

MIL-E-GRAM

Monthly newsletter of the Military Electronics Group of the Institute of Electrical and Electronics Engineers
(Vol. 5, no.1 - Vol. 7, no. 10 (Jan 1963–June 1965)

The Institute of Radio Engineers (IRE) and the American Institute of Electrical Engineers (AIEE) joined to form the Institute of Electrical and Electronic Engineers (IEEE) (January 1, 1963)

Monthly newsletter of the Military Electronics Group of the Institute of Radio Engineers
(Vol. 1, no.1-12 – Vol. 4, no. 10 (Oct 1955 – Dec 1962)
[NOTE: Not in IEEE Xplore]

Sources:
- David B. Dobson (LSM), Amin. Editor, IEEE AESS
- IEEE Aerospace and Systems Society: IEEE Transactions on Aerospace and Electronic Systems 50 Year Cumulative Index of the Archival Periodical Publications, (Vol 36, No 3, Pt 2, Jul 2000),

Compiled by: E. Moscara, Sr. Information Analyst, IEEE
Last updated: 15-December 2005

* At the present time, information about newsletters of the Aerospace & Navigational Electronics and Space Electronics & Telemetry Groups prior to the July 1, 1965 merger is not available. The Aerospace Group included its News & Information within its Transactions, which are referenced in the *50 Year Cumulative Index* (vol. 36, no. 3, July 2000, Part 2).